

Chapter 4

Massive Stars and their Supernovae

Friedrich-Karl Thielemann¹, Raphael Hirschi², Matthias Liebendörfer³, and Roland Diehl⁴

4.1 Cosmic Significance of Massive Stars

Our understanding of stellar evolution and the final explosive endpoints such as supernovae or hypernovae or gamma-ray bursts relies on the combination of

- a) (magneto-)hydrodynamics
- b) energy generation due to nuclear reactions accompanying composition changes
- c) radiation transport
- d) thermodynamic properties (such as the equation of state of stellar matter).

Hydrodynamics is essentially embedded within the numerical schemes which implement the physics of processes (b) to (d). In early phases of stellar evolution, hydrodynamical processes can be approximated by a *hydrostatic* treatment. Nuclear energy production (b) includes all nuclear reactions triggered during stellar evolution and explosive end stages, also among unstable isotopes produced on the way. Radiation transport (c) covers atomic physics (e.g. opacities) for photon transport, but also nuclear physics and neutrino nucleon/nucleus interactions in late phases and core collapse. The thermodynamical treatment (d) addresses the mixture of *ideal gases* of photons, electrons/positrons and nuclei/ions. These are fermions and bosons, in dilute media or at high temperatures their energies can often be approximated by Maxwell-Boltzmann distributions. At very high densities, the *nuclear* equation of state is required to relate pressure and density. It exhibits a complex behavior, with transitions from individual nuclei to clusters of nucleons with a background neutron bath, homogeneous phases of nucleons, the emergence of hyperons and pions up to a possible hadron-quark phase transition.

The detailed treatment of all these ingredients and their combined application is discussed in more depth in textbooks (Kippenhahn and Weigert, 1994; Maeder,

¹ University of Basel, 4056 Basel, Switzerland (f-k.thielemann@unibas.ch)

² University of Keele, Keele, ST5 5BG, United Kingdom

³ University of Basel, 4056 Basel, Switzerland

⁴ Max Planck Institut für extraterrestrische Physik, 85748 Garching, Germany

2009; Arnett, 1996; Iliadis, 2007), and/or the preceding Chapter (3), where the evolution of low and intermediate mass stars is addressed. That chapter also includes the stellar structure equations in spherical symmetry and a discussion of opacities for photon transport. Ch. 8 and 9 (tools for modeling objects and their processes) go into more detail with regard to modeling *hydrodynamics*, (convective) instabilities and energy transport as well as the energy generation due to nuclear reactions and the determination of the latter. Here we want to focus on the astrophysical aspects, i.e. a description of the evolution of massive stars and their endpoints with a special emphasis on the composition of their ejecta (in form of stellar winds during the evolution or of explosive ejecta). Low and intermediate mass stars end their evolution as AGB stars, finally blowing off a planetary nebula via wind losses and leaving a white dwarf with an unburned C and O composition. Massive stars evolve beyond this point and experience all stellar burning stages from H over He, C, Ne, O and Si-burning up to core collapse and explosive endstages. In this chapter we want to discuss the nucleosynthesis processes involved and the production of radioactive nuclei⁵ in more detail. This includes all hydrostatic nuclear-burning stages experienced by massive stars, and explosive burning stages when a shock wave moves outward after a successful explosion was initiated, but also final wind ejecta from the hot proto-neutron star which emerged in the collapse and explosion phase. All these ejecta will enter the interstellar medium in galaxies, initially appearing as gas and dust in wind bubbles and supernova remnants, later determining the evolution of the larger-scale gas composition. The interstellar gas composition will evolve with time, and the composition of newly formed stars will witness this composition at the time of their formation.

Massive stars play an important role as contributors to the gas composition of the interstellar medium via wind losses or explosions. In astronomical terms they are the progenitors of blue supergiants (BSG), red supergiants (RSG), Wolf-Rayet (WR) and luminous blue variable (LBV) stars (Maeder and Meynet, 2010). At the end of their life, they explode as core collapse supernovae (ccSNe), observed as SNe of type II or Ib,c (Woosley and Bloom, 2006) and also as long soft gamma-ray bursts (GRBs Piran (2004)). After collapse, their cores become neutron stars or black holes. They are one of the main sites for nucleosynthesis, which takes place during both pre-SN (hydrostatic) burning stages and during explosive burning. A weak *s* process occurs during core He- (and C-) burning (The et al, 2007; El Eid et al, 2009) and the *r* process probably occurs during the explosion (Qian and Woosley, 1996). These *s*(low) and *r*(apid) neutron capture processes are mainly responsible for the heavy nuclei beyond the Fe-group. Radioactive isotopes like ²⁶Al and ⁶⁰Fe detected by the INTEGRAL satellite are produced by massive stars, plus many more radioactivities from the final explosive ejecta (like e.g. ⁴⁴Ti, ⁵⁶Ni, ⁵⁶Co etc., see Sect. 4.4.2 and 4.5). Ch. 2 and 3 discussed also many long-lived heavy nuclei beyond Fe with half-lives larger than 10⁷ and up to 10¹¹ years. As massive stars are probably not the origin of heavy *s*-process nuclei (see Ch. 3), we will address here those nuclei which are clearly identified with the *r* process (²³²Th, 1.4 × 10¹⁰y, ²³⁵U,

⁵ We focus especially on long-lived radioactivities which can be observed with gamma-ray satellites, and refractory isotopes which can be observed in dust condensations included in meteorites.

$7 \times 10^8 \text{y}$, ^{236}U , $2.3 \times 10^7 \text{y}$, ^{238}U , $4.5 \times 10^9 \text{y}$, ^{244}Pu , $8 \times 10^7 \text{y}$, ^{247}Cm , $1.6 \times 10^7 \text{y}$) and where especially ^{232}Th and ^{238}U , with half-lives comparable to the age of the Galaxy/Universe, can also serve as chronometers.

Massive stars, even though they are much less numerous than low mass stars, contribute significantly (about two thirds) to the integrated luminosity of galaxies. At high redshifts z , or low metallicities Z , they are even more important drivers of characteristic phenomena and evolution. The first stars formed are thought to be all massive or even very massive, and to be the cause of the re-ionisation of the universe. As discussed above, if the final core collapse leads to a black hole, the endpoint of this evolution can be the origin of the subset of (long, soft) gamma ray bursts (GRBs). GRBs are the new *standard candles* for cosmology at high redshifts. They are visible from higher redshifts than usual SNe (of type I or II) are, and thus will impose tighter constraints on cosmological models. Massive stars with their large energy output can be seen out to significant (cosmological) distances – either directly through their thermal photospheric emission, or indirectly through the impact on their surroundings (ionization, or heated dust). In their *collapsar* and GRB extremes, emission is beamed into a jet, which makes them visible even at greater distances. This can also give us information on the star formation history at a very early age of the universe ($z > 10$) beyond the reach of galaxy observations. Closer to home, recent surveys of metal poor halo stars provide a rich variety of constraints for the early chemical evolution of our Galaxy and thus the nucleosynthesis ejecta (*astro-archeology*).

4.2 Hydrostatic and Explosive Burning in Massive Stars

Following the motivation for studying massive stars in the previous section, we now discuss the ingredients for their modeling. Thermonuclear energy generation is one of the key aspects: It shapes the interior structure of the star, thus its evolutionary time scales, and the generation of new chemical elements and nuclei. Without understanding these, the *feedback* from massive stars *as it determines the evolution of galaxies* cannot be understood in astrophysical terms.⁶ Thermonuclear burning, nuclear energy generation and resulting nuclear abundances are determined by thermonuclear reactions and weak interactions. The treatment of the required nuclear/plasma physics, and a detailed technical description of reaction rates, their determination and the essential features of composition changes and reaction networks is presented in Ch. 9. Here we want to discuss which types of reactions are involved specifically in the evolution of massive stars and their catastrophic end stages. Nuclear burning can in general be classified into two categories:

- (1) hydrostatic burning stages on timescales dictated by stellar energy loss
- (2) explosive burning due to hydrodynamics of the specific event.

⁶ Empirical descriptions from observations of a multitude of galaxies are often utilized to substitute such astrophysical models in cosmological simulations.

Massive stars (as opposed to low and intermediate mass stars) are the ones which experience explosive burning (2) as a natural outcome at the end of their evolution and they undergo more extended hydrostatic burning stages (1) than their low- and intermediate-mass cousins. Therefore, we want to address some of these features here in a general way, before describing the evolution and explosion in more detail.

The important ingredients for describing nuclear burning and the resulting composition changes (i.e. nucleosynthesis) are (i) strong-interaction cross sections and photodisintegrations, (ii) weak interactions related to decay half-lives, electron or positron captures, and finally (iii) neutrino-induced reactions. They will now be discussed⁷.

4.2.1 Nuclear Burning During Hydrostatic Stellar Evolution

Hydrostatic burning stages are characterized by temperature thresholds, permitting thermal Maxwell-Boltzmann distributions of (charged) particles (nuclei) to penetrate increasingly larger Coulomb barriers of electrostatic repulsion. These are (two body) reactions as discussed in Equ. 9.6 and 9.9 of Ch. 9, representing terms of the type $i\hat{r}_j$ in the network equation (9.1). H-burning converts ^1H into ^4He via pp-chains or the CNO-cycles. The simplest pp-chain is initiated by $^1\text{H}(p, e^+ \nu)^2\text{H}(p, \gamma)^3\text{He}$ and completed by $^3\text{He}(^3\text{He}, 2p)^4\text{He}$. The dominant CNO-cycle chain $^{12}\text{C}(p, \gamma)^{13}\text{N}(e^+ \nu)^{13}\text{C}(p, \gamma)^{14}\text{N}(p, \gamma)^{15}\text{O}(e^+ \nu)^{15}\text{N}(p, \alpha)^{12}\text{C}$ is controlled by the slowest reaction $^{14}\text{N}(p, \gamma)^{15}\text{O}$. The major reactions in He-burning are the 3α - reaction $^4\text{He}(2\alpha, \gamma)^{12}\text{C}$ and $^{12}\text{C}(\alpha, \gamma)^{16}\text{O}$. The 3α - reaction, being essentially a sequence of two two-body reactions with an extremely short-lived intermediate nucleus ^8Be , is an example for the term $i\hat{r}_j$ in Equ. 9.1, which includes the product of three abundances. The H- and He-burning stages are also encountered in low and intermediate mass stars, leaving white dwarfs as central objects. They are discussed in much more detail with all minor reaction pathways in Ch. 3. Massive stars, the subject of the present Chapter, undergo further burning stages up to those involving the production of Fe-group nuclei. Table 4.1 lists these burning stages and their typical central densities and temperatures, their duration and the typical luminosity in photons (from Woosley and Weaver (1995)), which involve the reaction types given below. For further details see Sect. 4.3.

- *Heavy-ion fusion reactions:* In C-burning the reaction $^{12}\text{C}(^{12}\text{C}, \alpha)^{20}\text{Ne}$ dominates, in O-burning it is $^{16}\text{O}(^{16}\text{O}, \alpha)^{28}\text{Si}$. The corresponding reaction rates $i\hat{r}_j$ (after integrating over a Maxwell-Boltzmann distribution of targets and projectiles) have the form given in Equ. 9.9 of Ch. 9 and contribute to the second term in Equ. 9.1. Reactions going beyond these key reactions are provided in tables 4.2 and 4.3. Further features as well as the status of nuclear cross sections are

⁷ A review of the sources for this microphysics input is given for (i) in Ch. 9 and for (iii) in Ch. 8. We will review some of the required weak interaction rates (ii) in the subsections on late phases of stellar evolution / core collapse and the description of the explosion.

Table 4.1 Burning stages of a $20M_{\odot}$ star

	ρ_c	T_c	τ	L_{phot}
Fuel (g cm^{-3})	(10^9 K)	(yr)	(yr)	(erg s^{-1})
Hydrogen	5.6(0)	0.04	1.0(7)	2.7(38)
Helium	9.4(2)	0.19	9.5(5)	5.3(38)
Carbon	2.7(5)	0.81	3.0(2)	4.3(38)
Neon	4.0(6)	1.70	3.8(-1)	4.4(38)
Oxygen	6.0(6)	2.10	5.0(-1)	4.4(38)
Silicon	4.9(7)	3.70	2 days	4.4(38)

Table 4.2 Major Reactions in Carbon Burning

(a) basic energy generation
$^{12}\text{C}(^{12}\text{C}, \alpha)^{20}\text{Ne}$ $^{12}\text{C}(^{12}\text{C}, \text{p})^{23}\text{Na}$
$^{23}\text{Na}(\text{p}, \alpha)^{20}\text{Ne}$ $^{23}\text{Na}(\text{p}, \gamma)^{24}\text{Mg}$ $^{12}\text{C}(\alpha, \gamma)^{16}\text{O}$
(b) fluxes $> 10^{-2} \times$ (a)
$^{20}\text{Ne}(\alpha, \gamma)^{24}\text{Mg}$ $^{23}\text{Na}(\alpha, \text{p})^{26}\text{Mg}(\text{p}, \gamma)^{27}\text{Al}$
$^{20}\text{Ne}(\text{n}, \gamma)^{21}\text{Ne}(\text{p}, \gamma)^{22}\text{Na}$ $(e^+ \nu)^{22}\text{Ne}(\alpha, \text{n})^{25}\text{Mg}(\text{n}, \gamma)^{26}\text{Mg}$
$^{21}\text{Ne}(\alpha, \text{n})^{24}\text{Mg}$ $^{22}\text{Ne}(\text{p}, \gamma)^{23}\text{Na}$ $^{25}\text{Mg}(\text{p}, \gamma)^{26}\text{Al}(e^+ \nu)^{26}\text{Mg}$
(c) low temperature, high density burning
$^{12}\text{C}(\text{p}, \gamma)^{13}\text{N}(e^+ \nu)^{13}\text{C}(\alpha, \text{n})^{16}\text{O}(\alpha, \gamma)^{20}\text{Ne}$
$^{24}\text{Mg}(\text{p}, \gamma)^{25}\text{Al}(e^+ \nu)^{25}\text{Mg}$
$^{21}\text{Ne}(\text{n}, \gamma)^{22}\text{Ne}(\text{n}, \gamma)^{23}\text{Ne}(e^- \bar{\nu})^{23}\text{Na}(\text{n}, \gamma)^{24}\text{Na}(e^- \nu)^{24}\text{Mg} + s \text{ processing}$

discussed in recent reviews on hydrostatic burning stages (Haxton et al, 2006; Buchmann and Barnes, 2006; Costantini et al, 2009; Wiescher et al, 2010) and Ch. 9.

- *Photo-disintegrations:* The alternative to fusion reactions are photodisintegrations which start to play a role at sufficiently high temperatures T when $30kT \approx Q$ (the Q -value or energy release of the inverse capture reaction). This ensures the existence of photons with energies $> Q$ in the Planck distribution and leads to Ne-Burning [$^{20}\text{Ne}(\gamma, \alpha)^{16}\text{O}$, $^{20}\text{Ne}(\alpha, \gamma)^{24}\text{Mg}$] at $T > 1.5 \times 10^9$ K (preceding O-burning) due to a small Q -value of ≈ 4 MeV and Si-burning at temperatures in excess of 3×10^9 K [initiated like Ne-burning by photodisintegrations]. Such photodisintegrations (after integrating over a thermal (Planck) distribution of photons at temperature T) have the form given in equation (9.4) of Ch. 9 and act similar to decays with a temperature-dependent decay constant, contributing (like decays) to the first term $i\lambda_j$ in equation (9.1). In table 4.4 we provide some of the main reactions of Ne-burning, which is initiated by the photodisintegration of Ne.
- *Electron capture reactions:* Massive stellar cores eventually lead to electron-gas degeneracy, i.e. the Pauli exclusion principle for fermions determines the population of energy states rather than the Boltzmann statistics, valid only for low densities / high temperatures. The Fermi energy of electrons is

Table 4.3 Major Reactions in Oxygen Burning

(a) basic energy generation
$^{16}\text{O}(^{16}\text{O}, \alpha)^{28}\text{Si}$ $^{16}\text{O}(^{12}\text{O}, \text{p})^{31}\text{P}$ $^{16}\text{O}(^{16}\text{O}, \text{n})^{31}\text{S}(e^+ \nu)^{31}\text{P}$
$^{31}\text{P}(\text{p}, \alpha)^{28}\text{Si}(\alpha, \gamma)^{32}\text{S}$
$^{28}\text{Si}(\gamma, \alpha)^{24}\text{Mg}(\alpha, \text{p})^{27}\text{Al}(\alpha, \text{p})^{30}\text{Si}$
$^{32}\text{S}(\text{n}, \gamma)^{33}\text{S}(\text{n}, \alpha)^{30}\text{Si}(\alpha, \gamma)^{34}\text{S}$
$^{28}\text{Si}(\text{n}, \gamma)^{29}\text{Si}(\alpha, \text{n})^{32}\text{S}(\alpha, \text{p})^{35}\text{Cl}$
$^{29}\text{Si}(\text{p}, \gamma)^{30}\text{P}(e^+ \nu)^{30}\text{Si}$
electron captures
$^{33}\text{S}(e^-, \nu)^{33}\text{P}(\text{p}, \text{n})^{33}\text{S}$
$^{35}\text{Cl}(e^-, \nu)^{35}\text{S}(\text{p}, \text{n})^{35}\text{Cl}$
(b) high temperature burning
$^{32}\text{S}(\alpha, \gamma)^{36}\text{Ar}(\alpha, \text{p})^{39}\text{K}$
$^{36}\text{Ar}(\text{n}, \gamma)^{37}\text{Ar}(e^+ \nu)^{37}\text{Cl}$
$^{35}\text{Cl}(\gamma, \text{p})^{34}\text{S}(\alpha, \gamma)^{38}\text{Ar}(\text{p}, \gamma)^{39}\text{K}(\text{p}, \gamma)^{40}\text{Ca}$
$^{35}\text{Cl}(e^-, \nu)^{35}\text{S}(\gamma, \text{p})^{34}\text{S}$
$^{38}\text{Ar}(\alpha, \gamma)^{42}\text{Ca}(\alpha, \gamma)^{46}\text{Ti}$
$^{42}\text{Ca}(\alpha, \text{p})^{45}\text{Sc}(\text{p}, \gamma)^{46}\text{Ti}$
(c) low temperature, high density burning
$^{31}\text{P}(e^- \nu)^{31}\text{S}$ $^{31}\text{P}(\text{n}, \gamma)^{32}\text{P}$
$^{32}\text{S}(e^-, \nu)^{32}\text{P}(\text{p}, \text{n})^{32}\text{S}$
$^{33}\text{P}(\text{p}, \alpha)^{30}\text{Si}$

Table 4.4 Major Reactions in Neon Burning

(a) basic energy generation
$^{20}\text{Ne}(\gamma, \alpha)^{16}\text{O}$ $^{20}\text{Ne}(\alpha, \gamma)^{24}\text{Mg}(\alpha, \gamma)^{28}\text{Si}$
(b) fluxes $> 10^{-2} \times$ (a)
$^{23}\text{Na}(\text{p}, \alpha)^{20}\text{Ne}$ $^{23}\text{Na}(\alpha, \text{p})^{26}\text{Mg}(\alpha, \text{n})^{29}\text{Si}$
$^{20}\text{Ne}(\text{n}, \gamma)^{21}\text{Ne}(\alpha, \text{n})^{24}\text{Mg}(\text{n}, \gamma)^{25}\text{Mg}(\alpha, \text{n})^{28}\text{Si}$
$^{28}\text{Si}(\text{n}, \gamma)^{29}\text{Si}(\text{n}, \gamma)^{30}\text{Si}$
$^{24}\text{Mg}(\alpha, \text{p})^{27}\text{Al}(\alpha, \text{p})^{30}\text{Si}$
$^{26}\text{Mg}(\text{p}, \gamma)^{27}\text{Al}(\text{n}, \gamma)^{28}\text{Al}(e^- \bar{\nu})^{28}\text{Si}$
(c) low temperature, high density burning
$^{22}\text{Ne}(\alpha, \text{n})^{25}\text{Mg}(\text{n}, \gamma)^{26}\text{Mg}(\text{n}, \gamma)^{27}\text{Mg}(e^- \bar{\nu})^{27}\text{Al}$
^{22}Ne left from prior neutron-rich carbon burning

$$E_F = \hbar^2/2m_e(3\pi^2)^{2/3}n_e^{2/3} \quad (4.1)$$

Here n_e is the density of the electron gas $n_e = \rho N_A Y_e$, ρ denotes the matter density and N_A Avogadro's number. In late stages of O-burning, in Si-burning (and during the later collapse stage) this Fermi energy of (degenerate) electrons, increases to the level of nuclear energies (MeV). In a neutral, completely ionized plasma, the electron abundance Y_e is equal to the total proton abundance $Y_e = \sum_i Z_i Y_i$ (summing over all abundances of nuclei, including protons/hydrogen) and limited by the extreme values 0 (only neutrons) and 1 (only protons) with typical values during stellar evolution close to 0.5 or slightly below. Such conditions permit electron captures on protons and nuclei, if the negative Q-value of the reaction can be overcome by the electron (Fermi) energy. The general features for typical conditions are presented in table 4.5, example reactions were already given in table 4.3. Thus, at sufficiently high densities, electron captures - which

Table 4.5 Electron Capture

$p + e^- \rightarrow \nu_e + n$ or $p(e^-, \nu_e)n$
$(A, Z) + e^- \rightarrow \nu_e + (A, Z-1)$ or ${}^A Z(e^-, \nu_e)^A Z-1$
$E_F(\rho Y_e = 10^7 \text{ gcm}^{-3}) = 0.75 \text{ MeV}$
$E_F(\rho Y_e = 10^9 \text{ gcm}^{-3}) = 4.70 \text{ MeV}$

are energetically prohibited - can become possible and lead to an enhanced *neutronization* of the astrophysical plasma, in addition to the role of beta-decays and electron captures with positive Q-values (Nomoto and Hashimoto, 1988). In degenerate Ne-O-Mg cores (after core C-burning of stars with $8 < M/M_\odot < 10$), electron captures on ${}^{20}\text{Ne}$ and ${}^{24}\text{Mg}$ cause a loss of degeneracy pressure support and introduce a collapse rather than only a contraction, which combines all further burning stages on a short collapse time scale (Nomoto, 1987). In Si-burning of more massive stars, electron capture on intermediate mass and Fe-group nuclei becomes highly important and determines the neutronization (Y_e) of the central core. As discussed in Ch. 9, such rates contribute to the one-body reaction terms ${}_i \lambda_j$ in Equ. 9.1 with the effective decay constants in Equ. 9.5 being a function of T and $n_e = \rho N_A Y_e$, the electron number density.

Table 4.6 Neutrino Reactions

$\nu_e + n \leftrightarrow p + e^-$ or $n(\nu_e, e^-)p$
$\bar{\nu}_e + p \leftrightarrow n + e^+$ or $p(\bar{\nu}_e, e^+)n$
$\nu_e + (Z, A) \leftrightarrow (Z+1, A) + e^-$ or ${}^A Z(\nu_e, e^-)^A Z+1$
$\bar{\nu}_e + (Z, A) \leftrightarrow (Z-1, A) + e^+$ or ${}^A Z(\bar{\nu}_e, e^+)^A Z-1$
$(Z, A) + \nu \leftrightarrow \nu + (Z, A)^*$

Neutrino cross section on nucleons, nuclei and electrons are minute, by comparison to above reactions. It therefore requires high densities of the order $\rho > 10^{12} \text{ g cm}^{-3}$ that also the inverse process to electron/positron capture (neutrino capture) can occur on relevant timescales. The same is true for other processes such as e.g. inelastic scattering, leaving a nucleus in an excited state which can emit nucleons and alpha particles. Such neutrino-induced reactions can be expressed in a similar way as photon and electron captures, integrating now over the corresponding neutrino distribution. The latter is, however, not necessarily in thermal equilibrium and not just a function of temperature and neutrino densities. Neutrino distributions are rather determined by (neutrino) radiation transport calculations (see Ch. 8, where also other neutrino scattering processes are discussed).

All the reactions presented above and occurring at different times in the sequence of burning stages, contribute to the three types of terms in the reaction network equation (Equ.9.1 in Ch. 9). If one is interested to show how nuclear abundances Y_i enter in this set of equations, it can also be written in the form⁸

$$\frac{dY_i}{dt} = \sum_j P_j^i \lambda_j Y_j + \sum_{j,k} P_{j,k}^i \rho N_A <j,k> Y_j Y_k + \sum_{j,k,l} P_{j,k,l}^i \rho^2 N_A^2 <j,k,l> Y_j Y_k Y_l. \quad (4.2)$$

Core Si-burning, the final burning stage during stellar evolution, which is initiated by the photodisintegration $^{28}\text{Si}(\gamma, \alpha)^{24}\text{Mg}$ close to $3 \times 10^9 \text{ K}$ - and followed by a large number of fusion and photodisintegration reactions - ends with nuclear reactions in a complete *chemical equilibrium*⁹ (nuclear statistical equilibrium, NSE) and an abundance distribution centered around Fe (as discussed in Ch. 9, Equ. 9.14 and 9.15). These temperatures permit photodisintegrations with typical Q-values of 8-10 MeV as well as the penetration of Coulomb barriers in capture reaction. In such an NSE the abundance of each nucleus Y_i is only dependent on temperature T , density ρ , its nuclear binding energy B_i , and via charge conservation on $\sum_i Z_i Y_i = Y_e$. Y_e is altered by weak interactions on longer timescales. A *quasi-equilibrium (QSE)* can occur, if localized nuclear mass regions are in equilibrium with the background of free neutrons, protons and α particles, but offset from other regions of nuclei and thus their NSE values (Hix and Thielemann, 1996, 1999b; Hix et al, 2007). Different quasi-equilibrium regions are usually separated from each other by slow reactions

⁸ The formal difference to Equ. 9.1 is that one does not sum here over the reactions but rather over all reaction partners (see also the equation following Table 3.2 in Ch. 3). However, in total, all the terms which appear are identical. Due to the different summation indices, the P's have a slightly different notation, λ 's denote decay rates called L in Ch. 9, and $<j,k>$ correspond to $<\sigma^*v>$ of reactions between nuclei j and k , while $<j,k,l>$ includes a similar expression for three-body reactions (Nomoto et al, 1985). A survey of computational methods to solve nuclear networks is given in Hix and Thielemann (1999a); Timmes (1999). (Like for electron abundances Y_e , the abundances Y_i in Eq.(4.2) are related to number densities $n_i = \rho N_A Y_i$ and mass fractions of the corresponding nuclei via $X_i = A_i Y_i$, where A_i is the mass number of nucleus i and $\sum X_i = 1$.)

⁹ all strong (thermonuclear) and photodisintegration reactions are equilibrated, while weak interaction reactions, changing Y_e , may occur on longer timescales.

with typically small Q -values. Such boundaries between QSE groups, which are due to slow reactions, can be related to neutron or proton shell closures, like e.g. $Z = N = 20$, separating the Si- and Fe-groups in early phases of Si-burning.

All reactions discussed above, occurring during all stellar burning stages, are essentially related to nuclei from H to the Fe-group, and not much beyond.

- *Neutron capture processes:* Through neutron capture reactions, also during regular stellar evolution, there is a chance to produce heavier nuclei. During core and shell He-burning specific α -induced reactions can liberate neutrons which are responsible for the slow neutron capture process (s process). A major neutron source is the reaction $^{22}\text{Ne}(\alpha, n)^{25}\text{Mg}$, with ^{22}Ne being produced via successive α -captures on the H-burning CNO product $^{14}\text{N}(\alpha, \gamma)^{18}\text{F}(\beta^+)^{18}\text{O}(\alpha, \gamma)^{22}\text{Ne}$. If occurring, the mixing of ^{12}C into H-burning shells can produce an even stronger neutron source $^{13}\text{C}(\alpha, n)^{16}\text{O}$ via $^{12}\text{C}(p, \gamma)^{13}\text{N}(\beta^+)^{13}\text{C}$. In massive, rotating, low metallicity stars, mixing can lead to the production of *primary* ^{14}N and ^{22}Ne , i.e. a neutron source which does not reflect the initial metallicity of ^{14}N in the CNO-cycle, and can thus be much stronger. Ch. 3 discusses in full detail the strong s process via a combination of ^{13}C and ^{22}Ne in He-shell flashes of low and intermediate mass stars. In a similar way mixing processes can also occur in massive stars due to rotation or convective instabilities. Without such mixing processes only *secondary* (metallicity-dependent) ^{22}Ne is available for $^{22}\text{Ne}(\alpha, n)^{25}\text{Mg}$ and core He-burning as well as shell C-burning lead to a weak s process (The et al, 2007). The s process can in principle form elements up to Pb and Bi through a series of neutron captures and β^- -decays, starting on existing heavy nuclei around Fe (Käppeler and Mengoni, 2006). Weak s processing, based on *secondary* ^{22}Ne , does not proceed beyond mass numbers of $A = 80 - 90$. The production of heavier nuclei is possible in massive stars if *primary* ^{14}N and ^{22}Ne are available.

4.2.2 Explosive Burning

Many of the hydrostatic nuclear-burning processes occur also under explosive conditions at higher temperatures and on shorter timescales (see Fig.4.1), when often the β -decay half-lives are longer than the explosive timescales, producing significant abundances of unstable isotopes as burning proceeds. This requires in general the additional knowledge of nuclear reactions for and among unstable nuclei. The fuels for explosive nucleosynthesis consist mainly of $N=Z$ nuclei like ^{12}C , ^{16}O , ^{20}Ne , ^{24}Mg , or ^{28}Si (the ashes of prior hydrostatic burning), resulting in heavier nuclei, again with $N \approx Z$. At high densities also electron captures on nuclei $e^- + {}^A_Z \rightarrow {}^A_{Z-1} + \nu$ can occur at substantial rates due to energetic, degenerate electrons when Fermi energies are high, as already discussed for late hydrostatic burning stages.

Explosive Si-burning differs strongly from its hydrostatic counterpart and can be divided into three different regimes: (i) incomplete Si-burning and complete Si-burning with either (ii) a normal (high density, low entropy) or (iii) an α -rich (low

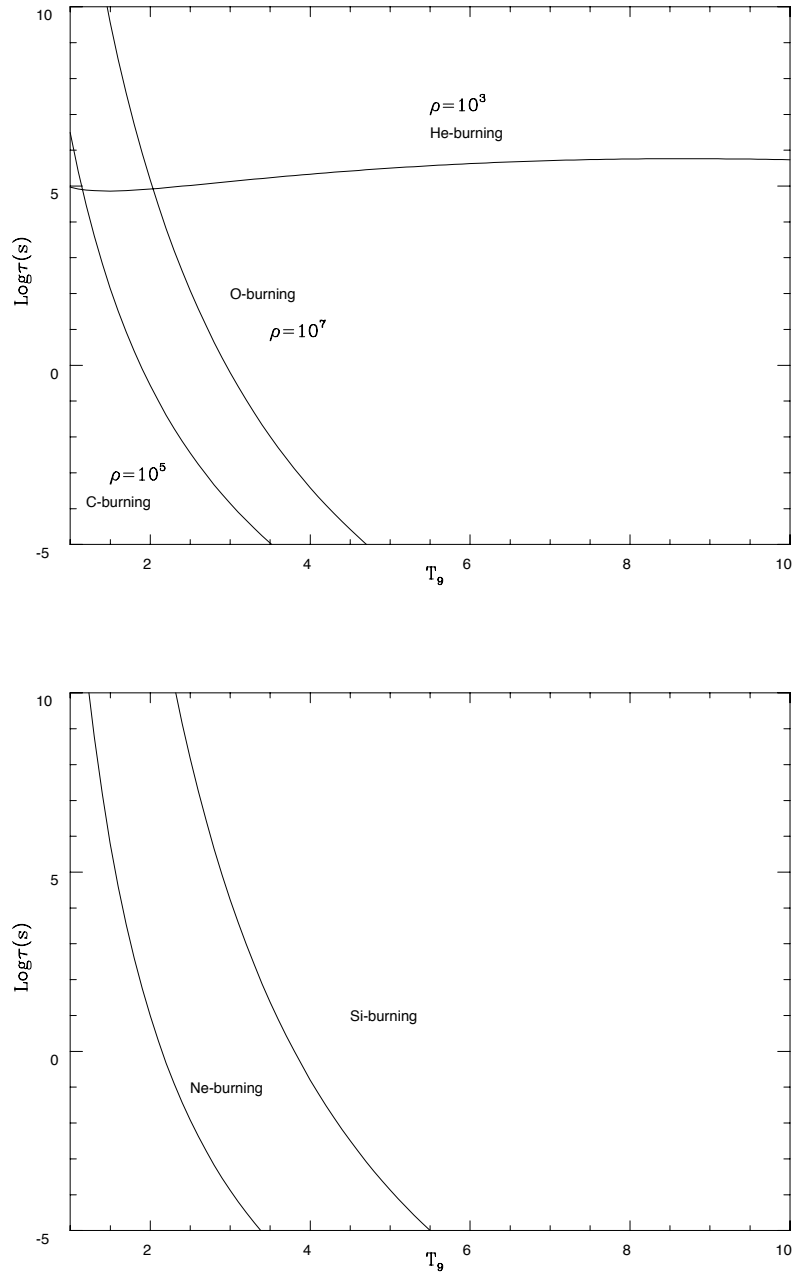


Fig. 4.1 Burning timescales in (\log_{10}) seconds for fuel exhaustion of He-, C-, and O-burning (top) and Ne- and Si-burning (bottom), as a function of temperature. Density-dependent timescales are labeled with a chosen typical density (in g cm $^{-3}$). They scale with $1/\rho$ for C- and O-burning and $1/\rho^2$ for He-burning. Ne- and Si-burning, initiated by photodisintegrations, are not density-dependent. The almost constant He-burning timescale beyond $T_9 = T/10^9 \text{ K} = 1$ permits efficient destruction on explosive timescales only for high densities.

density, high entropy) freeze-out of charged-particle reactions during cooling from NSE. At initially-high temperatures or during a *normal* freeze-out, the abundances remain in a full NSE. The full NSE can break up in smaller equilibrium clusters (quasi-equilibrium, QSE), for a detailed discussion see Hix and Thielemann (1996, 1999b); Hix et al (2007). An example for such QSE-behavior is an α -rich freeze-out, caused by the inability of the 3α - reaction ${}^4\text{He}(2\alpha, \gamma){}^{12}\text{C}$, and the ${}^4\text{He}(\alpha n, \gamma){}^9\text{Be}$ reaction to keep light nuclei like n, p, and ${}^4\text{He}$, and nuclei beyond $A=12$ in an NSE during declining temperatures, when densities are low. This causes a large α -particle abundance after freeze-out of nuclear reactions. This effect, most pronounced for core collapse supernovae, depends on the entropy of the reaction environment, being proportional to T^3/ρ in a radiation dominated plasma (see Fig. 4.2).

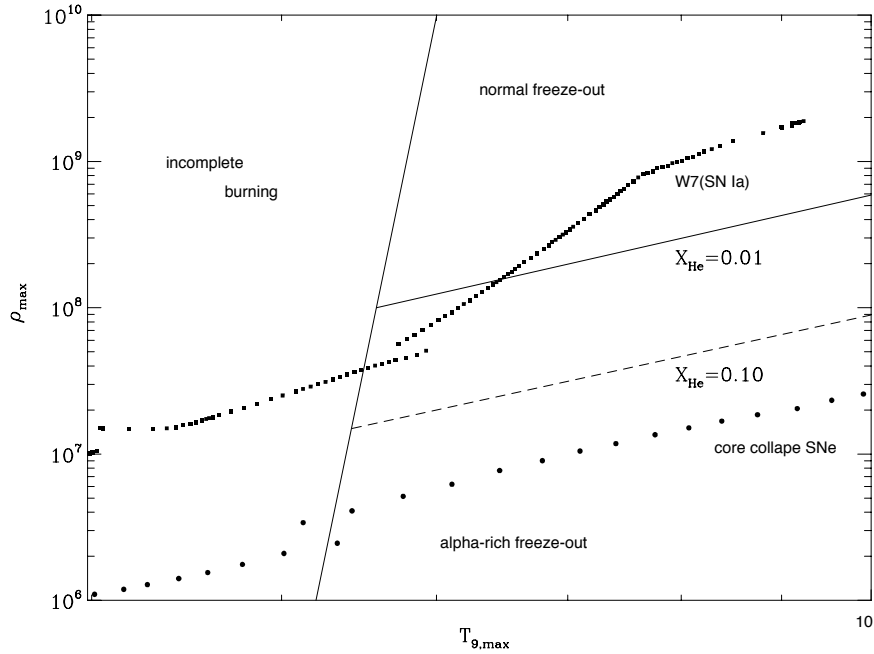


Fig. 4.2 Final results of explosive Si-burning as a function of maximum temperatures and densities attained in explosions before adiabatic expansion. For temperatures in excess of $5 \times 10^9 \text{ K}$ any fuel previously existing is photodisintegrated into nucleons and α particles before re-assembling in the expansion. For high densities this is described by a full NSE with an Fe-group composition, favoring nuclei with maximum binding energies and proton/nucleon ratios equal to Y_e . For lower densities the NSE breaks into local equilibrium groups (quasi-equilibrium, QSE) with group boundaries determined by reactions with an insufficiently fast reaction stream. Alpha-rich freeze-out (insufficient conversion of α particles into nuclei beyond carbon) is such a QSE-behavior. Lines with 1% and 10% remaining α -particle mass fraction are indicated as well as typical conditions for mass zones in type Ia and core-collapse supernovae.

r -process nucleosynthesis (*rapid* neutron capture) relates to environments of explosive Si-burning, either with low or high entropies, where matter experiences a normal or α -rich freeze-out. The requirement of a neutron to seed-nuclei ratio of 10 to 150 after freeze-out of charged particle reactions¹⁰ translates into $Y_e=0.12-0.3$ for a normal freeze-out. For a moderate $Y_e>0.40$ an extremely α -rich freeze-out is needed (see the discussion in Section 4.4). Under these conditions the large mass fraction in ${}^4\text{He}$ (with $N = Z$) permits ratios of remaining free neutrons to (small) abundances of heavier seed nuclei, which are sufficiently high to attain r -process conditions. In many cases QSE-groups of neutron captures and photodisintegrations are formed in the isotopic chains of heavy elements during the operation of the r process.

4.3 Evolution of Massive Stars up to Core Collapse

In Section 4.2 we have discussed nuclear burning processes in detail, including also individual reactions which are of relevance during the evolution of massive stars. This relates to the main focus of this book, the production of (radioactive) nuclei in astrophysical environments. In the present section we will discuss the physics of stellar evolution and major related observational features; but we refer to review articles or textbooks for technical descriptions of treatments of mass, energy, and momentum conservations equations as well as energy transport (via radiation or convective motions) (Maeder, 2009; Maeder and Meynet, 2010; Heger et al, 2003; Limongi et al, 2000; Limongi and Chieffi, 2003, 2006; Ohkubo et al, 2008; El Eid et al, 2009) (but see also the hydrostatic stellar structure / evolution equations in spherical symmetry, as presented in Ch. 3). Stellar-evolution calculations as discussed here are based on the *Geneva code* of A. Maeder and G. Meynet and their students (Maeder, 2009; Maeder and Meynet, 2010). This numerical implementation of stellar evolution includes (i) an adaptative reaction network for the advanced burning stages, which is capable to follow the detailed evolution of Y_e and a large set of nuclei; (ii) a discretization of the stellar-structure equations, modified in order to damp instabilities occurring during the advanced stages of evolution; (iii) the treatment of dynamical shear in addition to the other mixing processes (such as, e.g., horizontal turbulence, secular shear and meridional circulation); and (iv) the treatment of convection as a diffusive process from O-burning onwards. This allows to follow the evolution of massive stars from their birth until the stage of Si-burning, including all nuclear burning stages discussed in Sect. 4.2, for a wide range of initial masses, metallicities and stellar rotation. Here the treatment of rotation and mixing effects still utilizes methods based on spherical symmetry. Full multi-dimensional calculations of mixing processes during stellar evolution have recently been established (Meakin and Arnett, 2007; Arnett et al, 2009) and might open up a new era for our understanding of the evolution of stars.

¹⁰ Such neutron/seed ratio is required in order to produce all, including the heaviest, r -process nuclei via neutron capture from seed nuclei at their abundances before freeze-out.

4.3.1 *Stellar Evolution with Rotation*

The evolution of all stars (including massive stars discussed here) is initiated by core H-burning, during which the star is found on the so-called main sequence (MS) in the Hertzsprung-Russell (HR) diagram, which relates the stellar luminosity to the stellar surface temperature (color). The observational appearance of a star after the completion of core H-burning is affected by the fact that the H-burning region continues to move outward as a burning shell. The He-core contracts and ignites core He-burning in the center, which produces mainly C and O. The star's trajectory in the HR diagram leaves the main sequence, and its radius increases due to the increased radiation pressure. Depending on the resulting surface temperature it becomes a blue or red supergiant (BSG or RSG). Radiation pressure can rise to such extreme values that stars (more massive than $20\text{--}30\,M_{\odot}$) blow off their outer parts through strong *stellar winds* of velocities up to $2000\,\text{km s}^{-1}$, exposing the more-interior parts of the star, the helium (or in some cases, the carbon) shell. Such a Wolf-Rayet (WR) star loses between 10^{-6} and a few times $10^{-5}\,M_{\odot}$ per year, in comparison to our Sun losing 10^{-14} of its M_{\odot} per year through its solar wind. For non-rotating stars, the transition to the WR phase appears through the so-called Luminous Blue Variable stars (LBVs). LBVs are massive, intrinsically bright stars which display different scales of light and color variability, ranging from rapid microvariations to rare outbreaks of catastrophic mass loss. They represent a very short-lived (perhaps as little as 40,000 years) strongly mass-losing phase in the evolution of massive stars, during which they undergo deep erosion of the outer layers before they enter the Wolf-Rayet phase. For rotating stars, the WR phase may start before the star ends its main sequence, since rotation enhances mass loss and rotation-induced mixing further reduces the hydrogen content at the surface (Meynet and Maeder, 2003, 2005). In the following we discuss how these evolutionary phases depend on the initial properties of a star. Late burning phases progress much more rapidly than the H burning of the main sequence state. This is because the carriers of the star's energy loss, which drives the evolution of a star, change from photons to neutrinos, which escape immediately at the densities discussed here, while photons undergo a multitude of scattering processes until they finally escape at the photosphere¹¹. The characteristics of late-burning stages are essentially identified by the size of a star's C+O-core after core He-burning.

The evolution of stars is governed mainly by three initial parameters: (1) its mass M , (2) its metallicity (Z , i.e. the mass fraction of pre-existing elements heavier than He from earlier stellar generations), and (3) the rotation rate or surface rotation velocity v_{rot} . Solar metallicity corresponds to¹² $Z = 0.02$. The evolution can also be influenced by interior magnetic fields, and by a close binary companion. Rotation significantly affects the pre-supernova state, through the impact it has on the

¹¹ It takes a photon about 10^5 years to reach the surface, after it has been launched in the hot core of, e.g., our Sun.

¹² The current value of solar metallicity is believed to be $Z=0.014$, see Ch. 1; the value of $Z=0.02$, which had been established before and was in common use till~2005, remains a reference for comparisons, though.

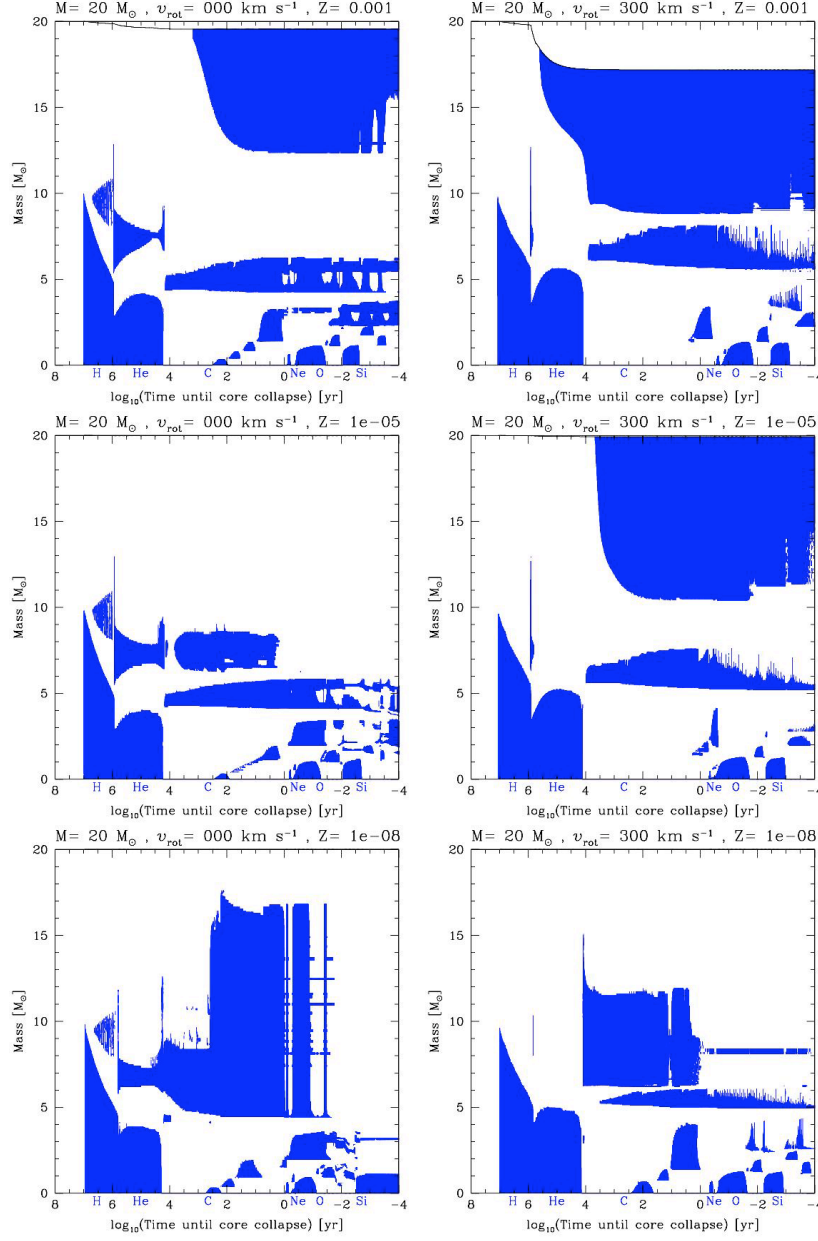


Fig. 4.3 Stellar structure (Kippenhahn) diagrams, which show the evolution of the structure as a function of the time left until the core collapses after the completion of core Si-burning. The initial parameters of the models are given on the top of each plot. Coloring (shading) marks convective zones, and the burning stages are denoted below the time axis. Non-rotating and moderately rotating $20 M_{\odot}$ star models are shown, for different metallicities Z . v_{rot} indicates the rotation velocity at the surface of the star.

H and He-burning evolution. Two mass groups are distinguishable: Either rotationally induced mixing dominates (for $M < 30 M_{\odot}$), or rotationally increased mass loss dominates (for $M > 30 M_{\odot}$). For massive stars around solar metallicity, mass loss plays a crucial role, in some cases removing more than half of the initial mass. Internal mixing, induced mainly by convection and rotation, also has a significant effect on the evolution of stars. An important result is the production of primary ^{14}N (via the CNO-cycle) and ^{22}Ne (via α -captures in He-burning), due to mixing of burning products (such as ^{12}C) with hydrogen or α 's, respectively (see the discussion in Sect. 4.2).

The general impact of metallicity can be summarized in the following way: Lower metallicity implies a (slightly) lower luminosity due to the lack of CNO-cycling in hydrogen burning, which leads to slightly smaller convective cores. A lower metallicity also implies a lower opacity due to the lack of heavier elements with their many spectral lines, reducing therefore also radiation pressure and hence mass loss (as long as the chemical composition has not been changed by burning or mixing in the part of the star under consideration). This results in lower metallicity stars being more compact and experiencing less mass loss. Prescriptions for mass loss as used in the Geneva stellar evolution code are described in detail in Meynet and Maeder (2005). Mass loss rates depend on metallicity as $dM/dt \propto (Z/Z_{\odot})^{0.5 \dots 0.86}$, where Z is the mass fraction of heavy elements at the surface of the star. The effects can be seen in Fig. 4.3 which shows the interior structure of stars through so-called *Kippenhahn diagrams* of $20 M_{\odot}$ models for different metallicities and rotation velocities of the stars. These diagrams indicate regions (in radial mass coordinates) where matter is unstable against convection; here the energy transport is dominated by transporting hot matter rather than through the propagation of photons. The implications of such a behavior have already been described in Ch. 3, the evolution of low and intermediate mass stars, and the physical origin and treatment of these effects are addressed in Ch. 8.

With the exception of the outer convection zone, convective regions in most cases indicate *burning zones*, such as *core H-burning*, *core He-burning*, *core C-burning* etc.. They testify also the ignition of outward moving burning shells of the same nuclear burning stages. When comparing models for decreasing metallicities (without rotation, left column of Fig. 4.3) one notices only minute reductions of the core sizes, but it is clearly seen that the outer (H-)burning shell moves further in towards smaller radial mass zones. In the third figure in this column we see merging of the H- and He-burning shells due to this effect, which leads to a largely-increased energy generation and extension of these combined burning zones.

How does rotation change this picture, and how do rotation-induced processes vary with metallicity? At all metallicities, rotation usually increases the core sizes via rotational mixing. The supply of more H-fuel leads to more energy generation and therefore a higher luminosity. The higher luminosity increases the radiation pressure and stellar mass loss. The effect of increased core sizes (and smaller density gradients) can be viewed in all models with $v_{\text{rot}} = 300 \text{ km s}^{-1}$ in the second column of Fig. 4.3. Clearly the convective core sizes are increased and the shell burning zones have moved outward. In the lowest metallicity case, the H/He-layers are sep-

arated again. In the intermediate metallicity case $Z = 10^{-5}$, the outer convection zone reaches the surface, and the star becomes a red supergiant. For metallicities $Z = 0.001$ (top row), the increased luminosity causes a sufficient increase in radiation pressure so that the mass loss is substantially enhanced (see the decrease of the stellar mass indicated by the top line). Mass loss becomes gradually unimportant for decreasing metallicities. For the rotating $20 M_{\odot}$ models the stellar fraction lost is more than 50% for solar metallicities, 13% at $Z = 0.001$, less than 3% for $Z = 10^{-5}$, and less than 0.3% for $Z = 10^{-8}$.

This can be different for more massive stars (Meynet et al, 2006). In Fig.4.4, we show results for low metallicity stars with $Z = 10^{-8}$ and fast rotation (500-800 km s $^{-1}$) from 9 to 85 M_{\odot} . The surface layers of massive stars usually accelerate due to internal transport of angular momentum from the core to the envelope. Since at low Z , stellar winds are weak, this angular momentum dredged up by meridional circulation remains inside the star, and the star reaches critical rotation more easily. At the critical limit, matter can be launched into a Keplerian disk which probably dissipates under the action of the strong radiation pressure of the star. Such an effect can be seen for the 85 M_{\odot} star, which loses in total more than 75% of its initial mass, and initially about 10% due to critical rotation. The remaining mass loss occurs during the red supergiant phase after rotation and convection have enriched the surface in primary CNO elements. We can also see that this effect becomes vanishingly small for stars with masses $M < 30 M_{\odot}$. The two $20 M_{\odot}$ models with varying metallicities and degrees of rotation again indicate the influence of metallicity and rotation on the compactness and mass loss of stars. In both cases the mass loss is negligible.

We have not shown here the evolution of extremely low metallicity stars. Below a metallicity of about $Z = 10^{-10}$, the CNO cycle cannot operate when H-burning starts after the star has been formed. The star therefore contracts until He-burning ignites, because the energy generation rate of H burning through the pp-chains cannot balance the effect of the gravitational force. Once enough C and O is produced, the CNO cycle can operate, and the star behaves like stars with $Z > 10^{-10}$ for the rest of the main sequence. Metal-free stellar evolution models are presented in Chi-efi and Limongi (2004); Heger and Woosley (2002); Umeda and Nomoto (2005); Ekström et al (2008).

Including the effects of both mass loss and rotation, massive star models reproduce many observables of stars with metallicities around solar Z . For example, models with rotation allow chemical surface enrichments already on the main sequence of core hydrogen burning (MS), whereas without the inclusion of rotation, self-enrichment is only possible during advanced burning evolution such as the red supergiant RSG stage (Heger and Langer, 2000; Meynet and Maeder, 2000). Rotating star models also better reproduce the ratio of star types, for the ones which retain their hydrogen surface layer (O stars), which lose the hydrogen layer completely (WR stars), and which even lose their helium layer. The latter affects also the appearance of later core collapse supernova explosions of massive stars. Indeed, rotation changes the supernova type due to the mass loss of the hydrogen envelope (turning such an event in optical observations from a type II supernova with a strong

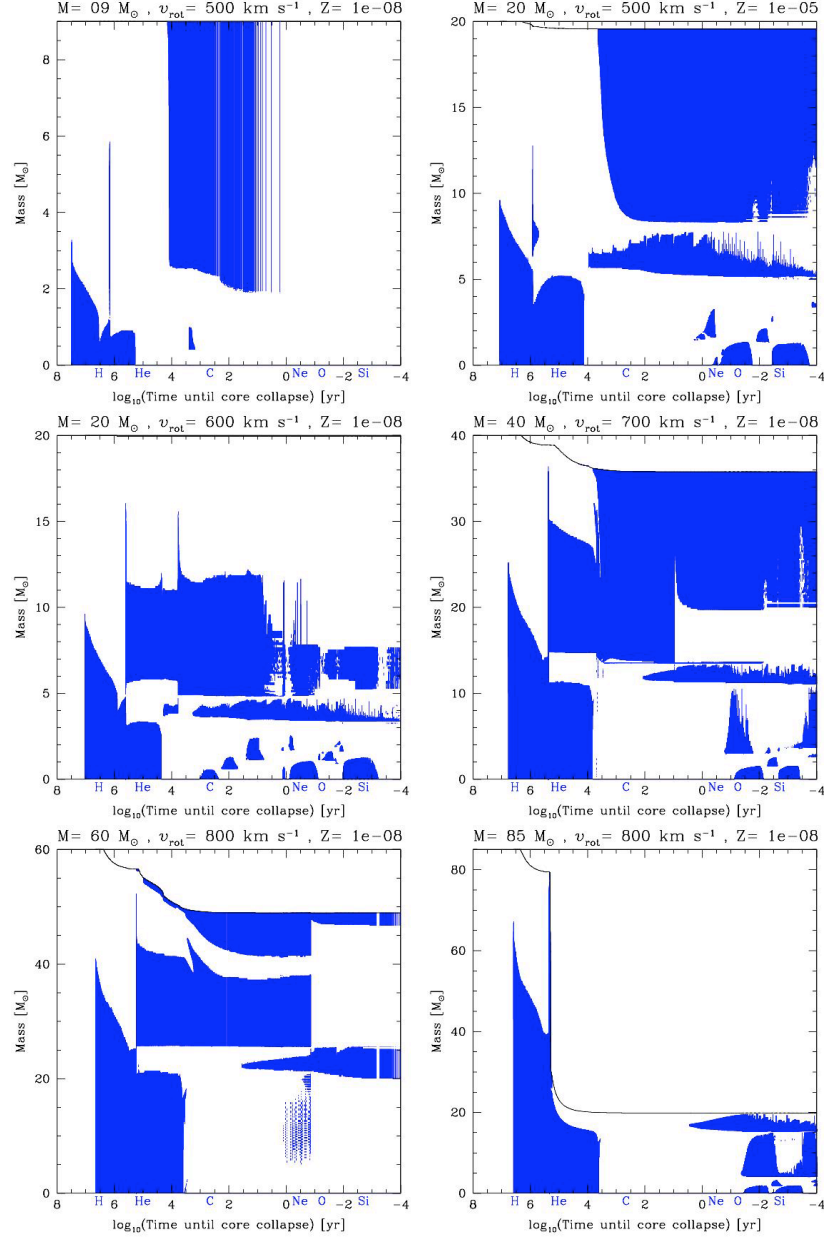


Fig. 4.4 The same as Fig. 4.3. Stellar structure diagrams for rapidly rotating stars of metallicity $Z = 10^{-8}$, over a mass range from 9 to 85 M_{\odot} . We see the drastically increasing amount of mass loss with increasing mass (enhancing mixing of burning products to the surface, and increasing opacities, i.e. acting like increased metallicities, plus some mass loss from critical rotation for the most massive stars). The two metallicity cases shown for the 20 M_{\odot} star show again that stars are less compact and show more and enhanced mass loss for higher metallicities (becoming a RSG which leads to the appearance of a large convective envelope).

plateau phase to a IIb event with a smaller plateau, or even a Ib event for the case of complete loss of the hydrogen envelope, and a Ic event with the additional loss of the He-envelope). This is discussed in more detail in Sect. 4.4. Both aspects, the chemical surface enrichment in MS stars as well as the ratio of type Ib+Ic to type II supernovae, as a function of metallicity, are drastically changed compared to non-rotating models, which underestimate these ratios (Georgy et al, 2009; Meynet and Maeder, 2005). The value of 300 km s^{-1} , used as the initial rotation velocity at solar metallicity, corresponds to an average velocity of about 220 km s^{-1} on the main sequence (MS), which is close to the average observed value (Fukuda, 1982; Meynet et al, 2008). Observed ratios of stars of different types in the Magellanic clouds, as compared to our Galaxy (Maeder et al, 1999; Martayan et al, 2007), point to stars rotating faster at lower metallicities. Fast initial rotation velocities in the range of $600 - 800 \text{ km s}^{-1}$ (Hirschi et al, 2005) are supported by observations of very low- Z stars (Chiappini et al, 2006).

Rotation affects all burning stages and the resulting Fe-core (we will discuss this issue further in the next subsection, see also Fig. 4.6). The size of the Fe-core in turn determines the final fate, whether a supernova explosion with neutron star formation or the collapse to a black hole occurs. The effects of rotation on pre-supernova models are most spectacular for stars between 15 and $25 M_{\odot}$. It changes the total size/radius of progenitors (leading to blue instead of red supergiants) and the helium and CO core (bigger by a factor of ~ 1.5 in rotating models). The history of convective zones (in particular the convective zones associated with shell H-burning and core He-burning) is strongly affected by rotation induced mixing (Hirschi et al, 2005). The most important rotation induced mixing takes place at low Z while He is burning inside a convective core. Primary C and O are mixed from the convective core into the H-burning shell. Once the enrichment is strong enough, the H-burning shell is boosted (the CNO cycle depends strongly on the C and O mixing at such low initial metallicities). The shell becomes convective and leads to an important primary ^{14}N production while the convective core mass decreases, leading to a less massive CO-core after He-burning than in non-rotating models. Convective and rotational mixing brings the primary CNO to the surface with interesting consequences for the stellar yields. The yield of ^{16}O , being closely correlated with the mass of the CO-core, is reduced. At the same time the C yield is slightly increased (Hirschi et al, 2005), both due to the slightly lower temperatures in core He-burning. This is one possible explanation for the high [C/O] ratio observed in the most metal-poor halo stars (see Fig. 14 in Spite et al (2005) and Fabbian et al (2009)) and in damped Lyman- α systems DLAs (Pettini et al, 2008).

The fate of rotating stars at very low Z is therefore probably the following: $M < 30 - 40 M_{\odot}$: Mass loss is insignificant and matter is only ejected into the ISM during the SN explosion. $30-40 M_{\odot} < M < 60 M_{\odot}$: Mass loss (at critical rotation and in the RSG stage) removes 10-20% of the initial mass of the star. The star probably dies as a black hole without a SN explosion and therefore the feedback into the ISM is only due to stellar winds. $M > 60 M_{\odot}$: A strong mass loss removes a significant amount of mass and the stars enter the WR phase. These stars therefore end as type Ib/c SNe and possibly as GRBs. This behavior

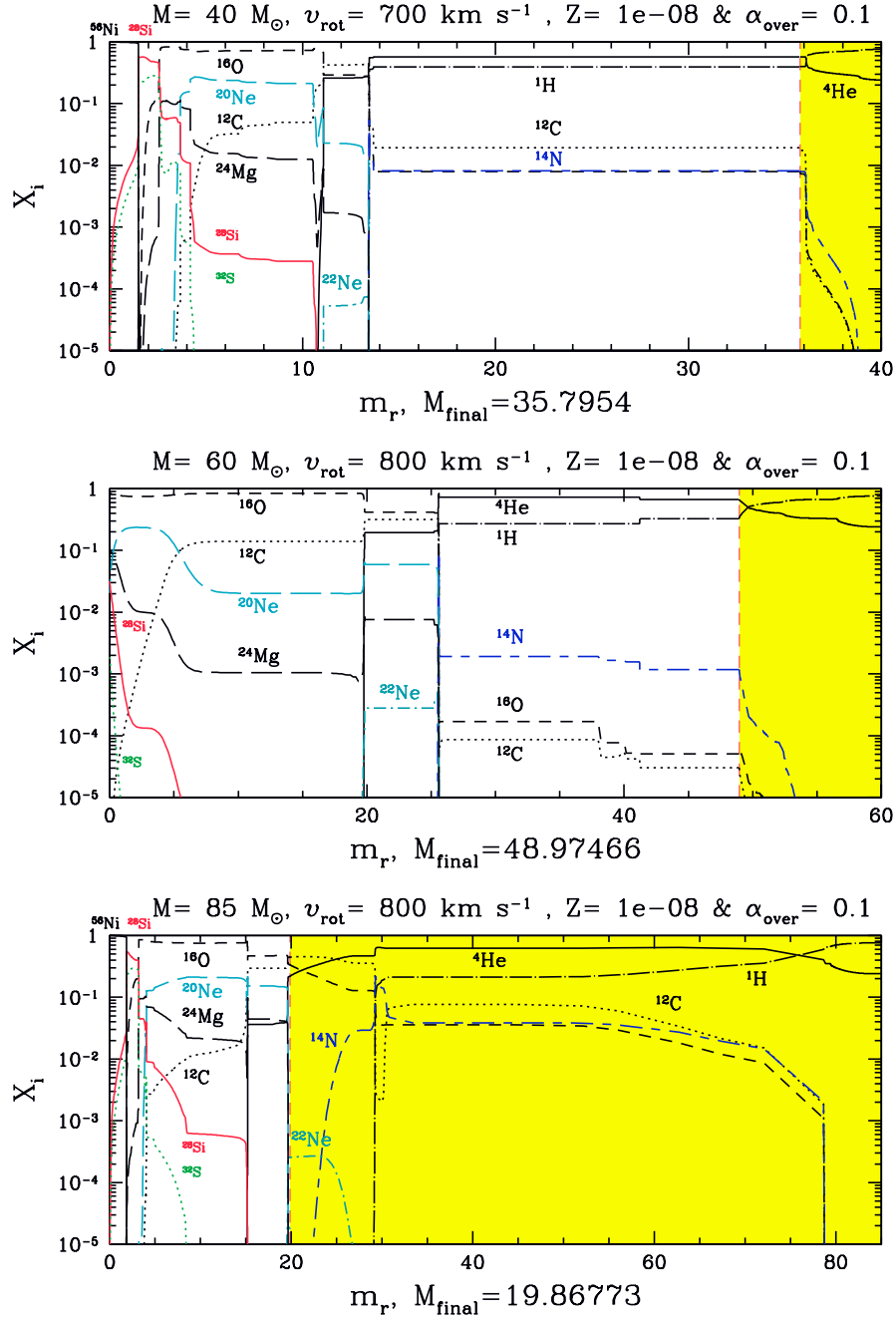


Fig. 4.5 Abundance profiles for the 40 (*top*), 60 (*middle*) and 85 (*bottom*) M_{\odot} models. The pre-SN and wind (yellow shaded area) chemical compositions are separated by a vertical dashed line located at the pre-SN total mass (M_{final}), given below each plot.

Table 4.7 Stellar Properties (Limongi & Chieffi 2006)

M_{ini}/M_{\odot}	M_{fin}/M_{\odot}	M_{He}/M_{\odot}	M_{CO}/M_{\odot}
11	10.56	3.47	1.75
15	13.49	5.29	2.72
20	16.31	7.64	4.35
30	12.91	12.68	8.01
40	12.52	16.49	8.98
60	17.08	25.17	12.62
80	22.62	34.71	17.41

is displayed in Fig. 4.5. At a metallicity $Z = 10^{-8}$, corresponding to an Fe/H ratio $\log_{10}[(\text{Fe}/H)/(\text{Fe}/H)_{\odot}] = [\text{Fe}/H] \sim -6.6$, C and O are shown in models to be mixed into the H-burning shell during He-burning. This raises the importance of the shell, and leads to a reduction of the CO-core size. Later in the evolution, the H-shell deepens and produces large amounts of primary nitrogen. For the most massive stars ($M > 60 M_{\odot}$), significant mass loss occurs during the red supergiant stage, caused by the surface enrichment in CNO elements from rotational and convective mixing.

The properties of non-rotating low- Z stars are presented in Heger et al (2003); Hirschi et al (2008), and several groups have calculated their stellar yields (Heger and Woosley, 2002; Chieffi and Limongi, 2004; Tominaga et al, 2007). All results for the non-rotating stars (whether at solar metallicity or for low- Z models) are consistent among these calculations, differences are understood from the treatments of convection and the rates used for $^{12}\text{C}(\alpha, \gamma)^{16}\text{O}$. The combined contributions to stellar yields by the wind and the later supernova explosion (see Sect. 4.4) will be provided separately. The results for stellar models with metallicities Z close to solar can be described as follows: Rotating stars have larger yields in their stellar winds than the non-rotating ones, because of the extra mass loss and mixing due to rotation, for masses below $\sim 30 M_{\odot}$. The ^{12}C and ^{16}O yields are increased by a factor 1.5–2.5 by rotation. At high mass loss rates (above $\sim 30 M_{\odot}$), the rotating and non-rotating models show similar yield values. When the wind and explosive contributions are added, the total metal production of rotating stars is larger by a factor 1.5–2.5 (see Sect. 4.4). For very massive stars, the situation varies due to the extreme mass loss, as shown in Fig.4.5.

In order to give a quantitative impression of the influence of initial mass, metallicity and rotation on the evolution of stars, we present in Tables 4.7 and 4.8 results for (a) non-rotating solar metallicity stars (Limongi and Chieffi, 2006) and (b) rotating stars for varying metallicities (Hirschi, 2007). Table 4.8 corresponds to the models shown in Figs. 4.3, 4.4, and 4.5. Given are the initial and final mass (in order to give an impression of the mass loss), as well as the core size after central H-burning (the He-core) and after central He-burning (the CO-core), and in table 4.8 also the metallicity Z and initial rotational surface velocity in km s^{-1} . As all burning stages after He-burning occur on significantly shorter timescales than the earlier burning phases, the CO-core size is the important quantity in order to determine the final outcome/fate of the star.

Table 4.8 Stellar Properties (Hirschi et al. 2007)

M_{ini}/M_{\odot}	Z	v_{rot}	M_{fin}/M_{\odot}	M_{He}/M_{\odot}	M_{CO}/M_{\odot}
9	1×10^{-8}	500	9.00	1.90	1.34
20	2×10^{-2}	300	8.76	8.66	6.59
20	1×10^{-3}	0	19.56	6.58	4.39
20	1×10^{-3}	300	17.19	8.32	6.24
20	1×10^{-5}	300	19.93	7.90	5.68
20	1×10^{-5}	500	19.57	7.85	5.91
20	1×10^{-8}	300	20.00	6.17	5.18
20	1×10^{-8}	600	19.59	4.83	4.36
40	1×10^{-8}	700	35.80	13.50	12.80
60	1×10^{-8}	800	48.97	25.60	24.00
85	1×10^{-8}	800	19.87	19.90	18.80

After this general discussion of stellar evolution, as it varies with initial mass, metallicity and rotation, we now focus on two long-lived isotopes ^{26}Al and ^{60}Fe , which have important contributions from the earlier burning stages in explosion ejecta.

^{26}Al

Long-lived ^{26}Al is produced in core and shell H-burning via the NaMgAl-cycle (see Ch. 3) in the $^{25}\text{Mg}(p, \gamma)^{26}\text{Al}$ reaction and will be eventually ejected in the stellar wind during the WR-phase. Gamma-ray observations of the 1.809 MeV decay line of ^{26}Al in systems like the Wolf-Rayet binary system $\gamma 2$ Vel, being the closest known Wolf-Rayet (WR) star, serve as a constraint to nucleosynthesis in Wolf-Rayet stars. From observations of the $\gamma 2$ Vel binary system including a WR star, Oberlack et al (2000) claimed that such WR stars must emit of the order $6 \times 10^{-5} M_{\odot}$ of ^{26}Al by stellar winds. The amount of ^{26}Al ejected into the interstellar medium is very sensitive to metallicity, initial stellar mass, rotation and mass loss rate, related to one or more of the physical effects discussed above. Results of detailed calculations can be found in Langer et al (1995); Meynet et al (1997); Palacios et al (2005); Limongi and Chieffi (2006); Tur et al (2009). Limongi and Chieffi (2006) provide an extended overview for the contribution from 11 to 120 M_{\odot} stars. The dominant source for the ^{26}Al production during stellar evolution is the $^{25}\text{Mg}(p, \gamma)^{26}\text{Al}$ reaction. Therefore the resulting abundance depends (i) on this reaction rate converting ^{25}Mg into ^{26}Al , (ii) on the amount of ^{25}Mg available, i.e. the total amount of matter in the NeNaMgAl-cycle (either in terms of the abundance/metallicity or in terms of the H-core size), and finally (iii) on the amount of ^{26}Al destruction. In the part of the He-core (after H-burning) which undergoes He-burning, neutrons are produced via (α, n) -reactions which destroy ^{26}Al via $^{26}\text{Al}(n, p)^{26}\text{Mg}$ and $^{26}\text{Al}(n, \alpha)^{23}\text{Na}$. A further question is related to the amount of matter being ejected in winds (i.e. mass

loss) during stellar evolution before ^{26}Al can decay inside the star via β^+ -decay with a half-life of 7.17×10^5 y.

He-burning, with its neutrons released, is destructive for ^{26}Al , but shell C-burning is again a source of ^{26}Al , also via $^{25}\text{Mg}(p, \gamma)^{26}\text{Al}$, which is effective due to protons released in $^{12}\text{C}(^{12}\text{C}, p)^{23}\text{Na}$ (see table 4.2 in Sect. 4.2). Convection in the C-burning shell brings in fresh ^{12}C fuel and ^{25}Mg which has been also produced in prior He-burning in the $^{22}\text{Ne}(\alpha, n)^{25}\text{Mg}$ reaction. ^{26}Al production may be effective also in Ne-burning, based on ^{25}Mg left over from C-burning and protons released via $^{23}\text{Na}(\alpha, p)^{26}\text{Mg}$ (see table 4.4). This ^{26}Al only survives if rapidly convected outwards to lower temperature environments (^{26}Al may decay rapidly in hot regions due to thermal population of its short-lived isomeric state; see Fig. 1.3 in Ch. 1).

A fraction of the ^{26}Al produced during stellar evolution will again be destroyed, when a shock front is released in a supernova explosion and propagates through the stellar envelope; in particular, material from C and Ne-burning, being close to the Fe-core, will be affected. But there are also source processes for explosive ^{26}Al production. The total yields, hydrostatic-evolution yields combined with the destruction and contribution from explosive burning, are given in Sect. 4.5.

^{60}Fe

^{60}Fe is produced by neutron captures on ^{59}Fe , and destroyed again via $^{60}\text{Fe}(n, \gamma)^{61}\text{Fe}$, i.e. during the *s* process. Generally, slow capture of neutrons released from the $^{22}\text{Ne}(\alpha, n)^{25}\text{Mg}$ reaction in core He-burning leads to the so-called *weak s* process, producing nuclei up to nuclear mass numbers of around $A=90$. ^{59}Fe is beta-unstable, thus in order for neutron capture to compete with this reaction branching (equating the neutron capture and beta-decay rates) requires a typical neutron density of about $3 \times 10^{10} \text{cm}^{-3}$. These are relatively high neutron densities for an *s* process, which also ensure that the destruction of ^{60}Fe via neutron captures dominates over its decay with its half-life of 2.6×10^6 y (Fig. 7.22 in Ch. 7, Rugel et al (2009)). Core He-burning will not provide sufficiently high-temperatures for the $^{22}\text{Ne}(\alpha, n)^{25}\text{Mg}$ reaction to produce such high neutron densities. It requires the conditions in shell He-burning to do so. Apparently conditions are most favorable during shell He-burning at late evolutionary times when central O-burning has already active and a C-burning shell is existent as well (see Woosley and Weaver, 1995; Rauscher et al, 2002; Limongi and Chieffi, 2006; Tur et al, 2009). ^{60}Fe yields are very sensitive to uncertainties in He-destruction reactions (such as the 3α -rate and $^{12}\text{C}(\alpha, \gamma)^{16}\text{O}$) which compete with the neutron source reaction $^{22}\text{Ne}(\alpha, n)^{25}\text{Mg}$ and neutron(-capture) *poisons* which compete with the production and destruction rates of ^{60}Fe via neutron captures (Rauscher et al, 2002; Tur et al, 2009; Giron et al, 2010; Uberseder et al, 2009). Such uncertainties amount to factors of up to 5 from present rate uncertainties. Another possible effect which has not really been looked into, yet, is the amount of ^{22}Ne available in He-burning. An important effect in low metallicity stars is the production of primary ^{14}N (not inherited from CNO of previous stellar generations, but produced inside the star due to mixing of He-burning

products with H). This causes the production of ^{22}Ne in He-burning and can at low metallicities (with small seed abundances of Fe) permit sizable s processing, affecting again the abundance of ^{60}Fe .

4.3.2 Late Burning Stages and the Onset of Core Collapse

Stars more massive than about $8 M_{\odot}$ will, after finishing core and shell H- and He-burning, lead to CO-cores which exceed the maximum stable mass of white dwarfs (the Chandrasekhar mass). For later burning stages, when the partial or full degeneracy of the electron gas is important, this critical limit $M_{Ch}(\rho Y_e, T)$ decides upon further contraction and the central ignition of subsequent burning stages, i.e. C-, Ne-, O- and Si-burning. Dependent on the Fermi energy of the degenerate electron gas, electron capture on the C-burning products ^{20}Ne and ^{24}Mg can initiate a collapse, leading directly via nuclear statistical equilibrium to a central Fe-core. This evolution path occurs for stars in the range $8\text{--}10 M_{\odot}$ (Nomoto, 1987). More massive stars will proceed through all burning stages until Si-burning will finally produce an Fe-core. All burning stages after core H- and He-burning proceed on timescales which are shorter by orders of magnitude. The reason is that the energy carried away by freely escaping neutrinos dominates over radiation losses by photons which undergo a cascade of scattering processes before their final escape. Most of these neutrinos are created when central densities and temperatures permit neutrino production via new particle reactions, different from beta-decay or electron capture on nuclei. Following neutrino production reactions are relevant: (i) $e^- + e^+$ -pair annihilation (*pair neutrinos*), (ii) electron-photon scattering with neutrino-antineutrino pair creation (photo neutrinos), and (iii) neutrino-antineutrino pair creation from plasma oscillations (*plasmon neutrinos*). Neutrinos dominate the energy loss in stellar evolution from this point on, and lead to increasingly shorter burning timescales, although the photon radiation luminosity of the star remains roughly constant. The timescales for the individual burning stages are given in table 4.1 in section 4.2; these values refer to a $20 M_{\odot}$ star with solar metallicity and no mass loss (Weaver and Woosley, 1993). Effects of mass loss, rotation and metallicity can change these timescales somewhat (up to 20%). Due to the large difference in evolution timescales, the dominant mass loss by stellar winds occurs during H- and He-burning, and the final outcome of stellar evolution is determined by the CO-core size after He-burning. Therefore, given all dependencies of stellar evolution via initial metallicities and rotation, the initial main sequence mass of a star is less indicative for the final outcome than the size of its CO-core.

In the late phases of O- and Si-burning (discussed in Sect. 4.2), electrons are moderately to strongly degenerate, dependent on the initial stellar mass, and will be characterized by increasing Fermi energies. This will allow for electron captures on burning products, and will make matter more neutron-rich, i.e. decrease Y_e , the electron or proton to nucleon (neutrons plus protons) ratio. In high density O-burning ($\rho > 2 \times 10^7 \text{ g cm}^{-3}$) two electron capture reactions become important and lead

to a decrease in Y_e , $^{33}\text{S}(e^-, \nu)^{33}\text{P}$ and $^{35}\text{Cl}((e^-, \nu)^{35}\text{S}$. Such effects become more extensive at even higher densities in Si-burning and a large range of nuclei has been identified to be of major importance $^{55-68}\text{Co}$, $^{56-69}\text{Ni}$, $^{53-62}\text{Fe}$, $^{53-63}\text{Mn}$, $^{64-74}\text{Cu}$, $^{49-54}\text{Sc}$, $^{50-58}\text{V}$, $^{52-59}\text{Cr}$, $^{49-54}\text{Ti}$, $^{74-80}\text{Ga}$, $^{77-80}\text{Ge}$, ^{83}Se , $^{80-83}\text{As}$, $^{50-58}\text{V}$, and ^{75}Zn (Aufderheide et al, 1994). The amount of electron capture and the resulting Y_e has consequences for core sizes. (The core sizes of the late burning stages are shown in Figs. 4.3 and 4.4). The final size of the inner Fe-core represents the maximum mass which can be supported by the pressure of the degenerate electron gas. It is a function of Y_e , but also reflects temperature effects if the electron gas is not completely degenerate (Bethe, 1990), with S_e being the entropy in electrons per baryon

$$M_{Ch}(Y_e, S_e) = 1.44(2Y_e)^2 \left[1 + \left(\frac{S_e}{\pi Y_e} \right)^2 \right] M_\odot. \quad (4.3)$$

Stars with masses exceeding roughly $10 M_\odot$ reach a point in their evolution where their Si-burning core (which will turn eventually into their Fe-core) exceeds this critical mass. At this point they collapse and bounce, if not too massive, to explode in spectacular core collapse events known as type II or Ib/c supernovae. These explosions create a neutron star or black hole at the end of the life of a star. They play a preeminent role in the nucleosynthesis and chemical evolution of a galaxy.

The collapse is initiated by the capture of degenerate electrons on nuclei, which reduces the dominant contribution of the pressure (i.e. the one from the degenerate electron gas). Alternatively, for lower densities and higher temperatures (in more massive stars), the pressure supporting the core is reduced by endoergic photodisintegrations of nuclei, reducing the thermal energy. The evolution in the core is determined by the competition of gravity (that causes the collapse of the core) and weak interaction (that determines the rate at which electrons are captured and the rate at which neutrinos are trapped during the collapse).

The early phases of this final stage of stellar evolution are known as *presupernova evolution*. They follow the late-stage stellar evolution, and proceed until core densities of about $10^{10} \text{ g cm}^{-3}$ and temperatures between 5 and $10 \times 10^9 \text{ K}$ are reached. Until this point, modeling stellar evolution requires the consideration of extensive nuclear reaction networks, but is simplified by the fact that neutrinos need only be treated as a sink of energy and lepton number (due to their immediate escape). At later time and towards the collapse, this is no longer valid: As the weak interaction rates increase with the increasing density, the neutrino mean free paths shorten, so that the neutrinos eventually proceed from phases of free streaming, towards diffusion, and trapping. An adequate handling of the transitions between these transport regimes necessitates a detailed time- and space-dependent bookkeeping of the neutrino distributions in the core (see Ch. 8). During collapse, electron capture, accompanied by ν_e neutrino emission, dominates over electron antineutrino emission because the positron abundance is very low under electron-degenerate conditions. Later in the evolution the electron degeneracy is partially lifted, and in addition to the electron flavor neutrinos, also heavy neutrinos, ν_μ and ν_τ and their antiparti-

cles, are usually included in numerical simulations of core collapse and postbounce evolution.

Advantageously, the temperature during the collapse and explosion are high enough that the matter composition is given by nuclear statistical equilibrium (NSE), i.e. without the need of reaction networks for the strong and electromagnetic interactions. The transition from a rather complex global nuclear reaction network, involving many neutron, proton and α fusion reactions and their inverses, to a quasi-statistical equilibrium, in which reactions are fast enough to bring constrained regions of the nuclear chart into equilibrium, to final and global nuclear statistical equilibrium is extensively discussed by Hix and Thielemann (1996, 1999b); Hix et al (2007). In the late stages of Si-burning and the early collapse phase, weak interactions are dominated by electron captures on protons and nuclei. These are important equally in controlling the neutronization of matter Y_e and, in a large portion, also the stellar energy loss. Due to their strong energy dependence $\propto E_e^5$, the electron capture rates increase rapidly during the collapse while the density and the temperature increase (the electron Fermi energy E_F scales with $\rho^{2/3}$, see 4.2).

The main weak interaction processes during the final evolution of a massive star are electron capture and β -decays. Their determination requires the calculation of Fermi and Gamow-Teller (GT) transitions. While the treatment of Fermi transitions (important only for β -decays) is straightforward, a correct description of the GT transitions is a difficult problem in nuclear structure physics. In astrophysical environments, nuclei are fully ionized. Therefore, electron capture occurs from the continuum of the degenerate electron plasma, and energies of the electrons are high enough to induce transitions to the Gamow-Teller resonance. Shortly after the discovery of this collective excitation, Bethe et al (1979) recognized its importance for stellar electron capture. β^- -decay converts a neutron inside the nucleus into a proton and emits an electron. In a degenerate electron gas, with fully populated levels up to the Fermi energy E_F , all decays which would produce electrons with smaller energies than E_F are not possible (*blocked*). Then, the decay rate of a given nuclear state is greatly reduced or even completely blocked at high densities. However, there is another pathway, as high temperatures populate a distribution of nuclear states: If an excited and thermally populated state of the decaying nucleus is connected by large GT transition probabilities to low-lying states in the daughter nucleus, producing electrons above the Fermi energy, such transition path can contribute significantly to the stellar β -decay rates. The importance of these states in the parent nucleus for β -decay in astrophysical environments was first recognized by Fuller et al (1980, 1982, 1985).

Recent experimental data on GT distributions in iron group nuclei, measured in charge exchange reactions, show that the GT strength is strongly *quenched* (reduced), compared to the *independent-particle-model* value, and fragmented over many states in the daughter nucleus. An accurate understanding of these effects is essential for a reliable evaluation of the stellar weak-interaction rates, particularly for the stellar electron-capture rates (Fuller et al, 1980; Langanke and Martínez-Pinedo, 2000). The nuclear *shell-model* is the only known tool to reliably describe GT distributions in nuclei. When comparing the shell-model based rates (by Lan-

ganke and Martinez-Pinedo) with the those from Fuller et al., one finds that the shell-model based rates are almost always smaller at the relevant temperatures and densities, caused by the above mentioned quenching of the Gamow-Teller strength, and by a systematic misplacement of the energy of the Gamow-Teller resonance.

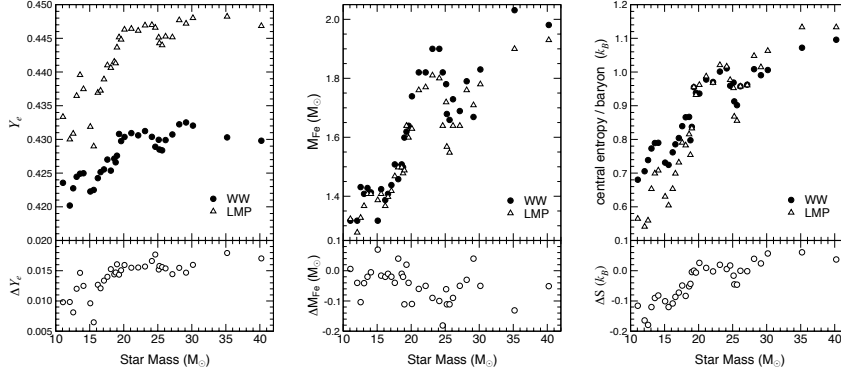


Fig. 4.6 Comparison of the center values of Y_e (left), the iron core sizes (middle) and the central entropy (right) for 11–40 M_\odot stars between the WW models and the ones using the shell model weak interaction rates (LMP) (Heger et al, 2001a). The lower parts define the changes in the 3 quantities between the LMP and WW models.

The influence of these shell-model rates on the late-stage evolution of massive stars has been investigated by Heger et al (2001a,b), and compared to earlier calculations (Woosley and Weaver, 1995). Fig. 4.6 illustrates the consequences of the shell model weak interaction rates for presupernova models in terms of the three decisive quantities: the central electron or proton to nucleon ratio Y_e , the entropy, and the iron core mass. The central values of Y_e at the onset of core collapse increased by 0.01–0.015 for the new rates. This is a significant effect. For example, a change from $Y_e = 0.43$ in the Woosley & Weaver model for a 20 M_\odot star to $Y_e = 0.445$ in the new models increases the respective Chandrasekhar mass by about 0.075 M_\odot (see Equ.4.3). The new models also result in lower core entropies for stars with $M < 20 M_\odot$, while for $M > 20 M_\odot$, the new models actually have a slightly larger entropy. The Fe-core masses are generally smaller, where the effect is larger for more massive stars ($M > 20 M_\odot$), while for the most common supernovae ($M < 20 M_\odot$) the reduction is by about 0.05 M_\odot (the Fe-core is here defined as the mass interior to the point where the composition is dominated by more than 50% of Fe-group elements with $A \geq 48$). This reduction seems opposite to the expected effect due to slower electron capture rates in the new models. It is, however, related to changes in the entropy profile during shell Si-burning which reduces the growth of the iron core just prior to collapse.

The evolution of Y_e during the presupernova phase is plotted in Fig. 4.7. Weak processes become particularly important in reducing Y_e below 0.5 after oxygen depletion ($\approx 10^7$ s and 10^6 s before core collapse for the 15 M and 25 M stars, respectively) and Y_e begins a decline, which becomes precipitous during Si-burning.

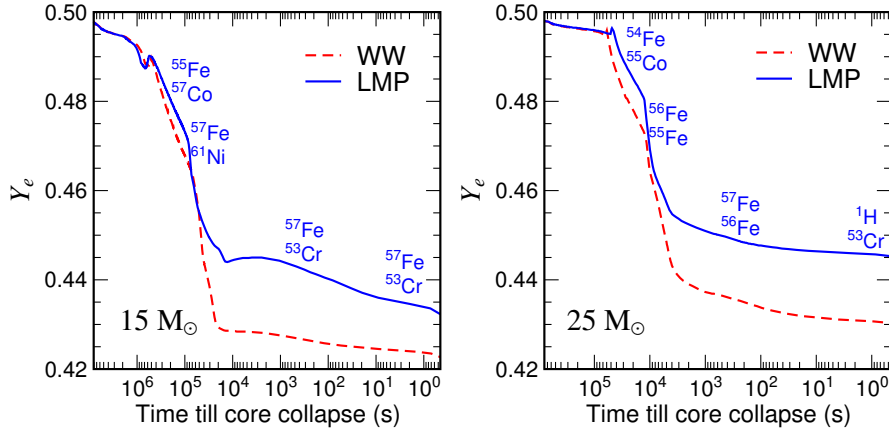


Fig. 4.7 Evolution of the Y_e value in the center of a $15 M_\odot$ star (left panel) and a $25 M_\odot$ star (right panel) as a function of time until bounce. The dashed line shows the evolution in the Woosley and Weaver models (WW) (Woosley and Weaver, 1995), while the solid line shows the results using the shell-model based weak-interaction rates of Langanke and Martínez-Pinedo (LMP). The two most important nuclei in the determination of the total electron-capture rate, for the calculations adopting the shell model rates, are displayed as a function of stellar evolution time.

Initially electron captures occur much more rapidly than beta-decays. As the shell model rates are generally smaller, the initial reduction of Y_e is smaller in the new models. The temperature in these models is correspondingly larger as less energy is radiated away by neutrino emission. An important feature of the new models is shown in the left panel of Fig. 4.7. For times between 10^4 and 10^3 s before core collapse, Y_e increases due to the fact that β -decay becomes competitive with electron capture after Si-depletion in the core and during shell Si-burning. The presence of an important β -decay contribution has two effects (Aufderheide et al, 1994). Obviously it counteracts the reduction of Y_e in the core, but also acts as an additional neutrino source, causing a stronger cooling of the core and a reduction in entropy. This cooling can be quite efficient, as often the average neutrino energy from the β -decays involved is larger than for the competing electron captures. As a consequence the new models have significantly lower core temperatures. At later stages of the collapse β -decay becomes unimportant again as an increased electron Fermi energy blocks/reduces its role. The shell model weak interaction rates predict the presupernova evolution to proceed along a temperature-density- Y_e trajectory where the weak processes involve nuclei rather close to stability which will permit to test these effects in the next-generation radioactive ion-beam facilities.

Fig. 4.7 identifies the two most important nuclei (the ones with the largest value for the product of abundance times rate) for the electron capture during various stages of the final evolution of $15 M_\odot$ and $25 M_\odot$ stars. An exhaustive list of the most important nuclei for both electron capture and beta-decay during the final stages of stellar evolution for stars of different masses is given in Heger et al (2001b). In total, the weak interaction processes shift the matter composition to

smaller Y_e values and hence more neutron-rich nuclei, subsequently affecting the nucleosynthesis. Its importance for the elemental abundance distribution, however, strongly depends on the location of the mass cut in the supernova explosion. It is currently assumed that the remnant will have a larger baryonic mass than the Fe-core, but smaller than the mass enclosed by the O-shell (Woosley et al, 2002). As the reduction of Y_e occurs mainly during Si-burning, it is essential to determine how much of this material will be ejected.

4.4 Supernovae from Massive Stars and the Role of Radioactivity

4.4.1 *The Explosion Mechanism*

Supernova explosions are an application of numerical astrophysical modelling that has a long tradition. Continued improvements of the models are motivated by the following points: (i) open questions regarding the explosion mechanism; (ii) availability of observations for individual supernova explosions; (iii) interesting input physics that tests matter under conditions that are not accessible on earth; (iv) visibility in light and other photon wavelengths, cosmic rays, neutrino emission, decay gamma-rays of radioactive products, perhaps gravitational wave emission; (v) visibility on cosmological distances with improving statistical information on the events and (vi) their impact on the interstellar matter (e.g. abundances of metal-poor stars) and Galactic evolution.

As discussed in the previous sections, the death of massive stars $\approx 8 - 40 M_\odot$ proceeds through several evolutionary and dynamical phases. At first, the modeling of a star must include the evolution through all nuclear burning stages until the resulting inner iron core grows beyond the maximum mass which can be supported by the dominant pressure of the degenerate electron gas. At this point, the inner stellar core enters a dynamical phase of gravitational collapse, during which it compactifies by ~ 5 orders of magnitude. The nuclear saturation density (i.e. the density of stable nuclei $\approx 2 \times 10^{14} \text{ g cm}^{-3}$) is exceeded at the center of the collapse and a protoneutron star (PNS) is formed. The dynamical time scale reduces from a few hundreds of milliseconds at the onset of collapse to a few milliseconds after the core has bounced back at nuclear densities (see Fig. 4.8 from Liebendörfer et al (2003)).

The ensuing accretion phase onto the protoneutron star with fluid instabilities and radiative transfer phenomena, like the transport of neutrinos, is not well understood. It may last $0.5 - 10$ seconds and can therefore be interpreted as a second evolutionary stage (much longer than the dynamical or transport time scale). Eventually it will lead to the observed vigorous supernova explosion, a dynamic phase where heavy elements are produced by explosive nucleosynthesis in an outward propagating shock wave. The processed matter is mixed by fluid instabilities and ejected into the interstellar medium, where it contributes to Galactic evolution. The remaining PNS at the center enters another evolutionary phase during which it cools by neu-

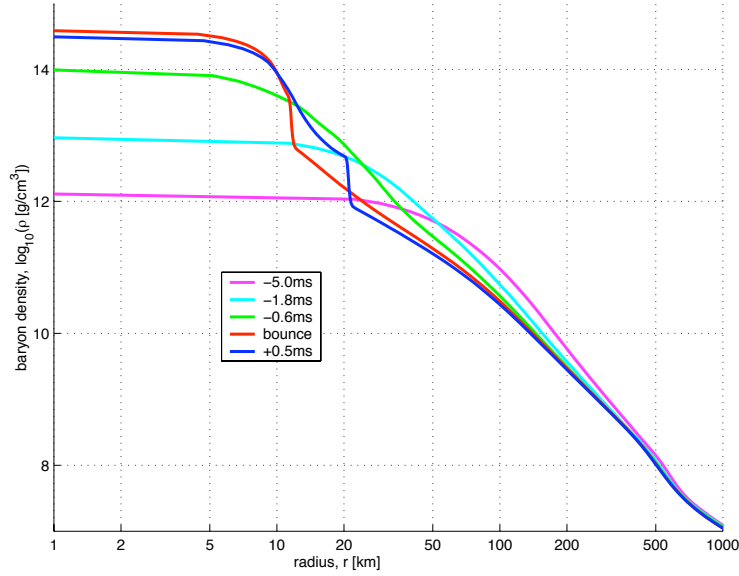


Fig. 4.8 A sequence of density profiles of a $13 M_{\odot}$ star before and after core bounce. For such a relatively low mass supernova with a small Fe-core the bounce occurs at a maximum density of less than twice nuclear matter density. At the bounce one recognizes the size of the homologous core (with roughly constant density). Thereafter the emergence of an outward moving density (shock) wave can be witnessed.

trino emission and contracts or even collapses to a black hole in a last dynamical phase.

While initially such calculations were performed in spherical symmetry and therefore lacked the consistent treatment of turbulent motion, presently performed research is done with multidimensional supernova models (Hix et al, 2003; Liebendörfer et al, 2005; Marek et al, 2005; Burrows et al, 2006a; Sumiyoshi et al, 2007; Langanke et al, 2008; Marek and Janka, 2009). The main ingredients are radiation (neutrino) transport, (relativistic) hydrodynamics, and the nuclear equation of state at such high densities. Recent progress has been made in the exploration of multidimensional hydrodynamics with idealized input physics. A refreshing view on the supernova mechanism has recently been suggested by pointing out that in certain axisymmetric simulations vibrational (so called PNS g-)modes are excited so that sound waves are emitted into the heating region. These sound waves are postulated to revive the stalled shock by dissipation of sound energy (Burrows et al, 2006a). Other efforts explore the role of magnetic fields and rotation in two-dimensional simulations with simplified input physics. One kind of proof-of-principle models is carried out in spherically symmetric approaches. The assumption of spherical symmetry is for many supernovae not compatible with observational constraints. However, one important advantage of spherically symmetric models is that sophisticated treatments of the neutrino-matter interactions can be included and that the neutrino

spectra and transport are correctly treated in general relativistic space-time. Models of this kind try to address the question of how many neutrinos are emerging from the compactification of an inner stellar core, how is their emission distributed as a function of time and how do these neutrino fluxes generically affect the cooling, heating, or nucleosynthesis in the outer layers of the star without the complication of 3D dynamical fluid instabilities (Liebendörfer et al, 2003, 2004; Fischer et al, 2009b,a). The attempt to combine all these aspects with forefront methods is ongoing in order to achieve the final goal of understanding the multi-D explosion mechanism with up to date microphysics from the equation of state to all neutrino and nuclear interactions¹³.

The phase of stellar core collapse has intensively been studied in spherically symmetric simulations with neutrino transport. The crucial weak processes during the collapse and postbounce evolution are $\nu + (A, Z) \leftrightarrow \nu + (A, Z)$, $\nu + e^\pm \leftrightarrow \nu + e^\pm$, $p + e^- \leftrightarrow n + \nu_e$, $(A, Z) + e^- \leftrightarrow (A, Z - 1) + \nu_e$, $\nu + N \leftrightarrow \nu + N$, $n + e^+ \leftrightarrow p + \bar{\nu}_e$, $(A, Z) + e^+ \leftrightarrow (A, Z + 1) + \bar{\nu}_e$, $\nu + (A, Z) \leftrightarrow \nu + (A, Z)^*$, $(A, Z)^* \leftrightarrow (A, Z) + \nu + \bar{\nu}$, $N + N \leftrightarrow N + N + \nu + \bar{\nu}$, $\nu_e + \bar{\nu}_e \leftrightarrow \nu_{\mu, \tau} + \nu_{\mu, \tau}^-$, $e^+ + e^- \leftrightarrow \nu + \bar{\nu}$. Here, a nucleus is symbolized by its mass number A and charge Z , N denotes either a neutron or a proton and ν represents any neutrino or antineutrino. We note that, according to the generally accepted collapse picture (Bethe 1990; Bethe et al (1979)), elastic scattering of neutrinos on nuclei is mainly responsible for the trapping, as it determines the diffusion time scale of the outwards streaming neutrinos. Shortly after trapping, the neutrinos are thermalized by energy downscattering, experienced mainly in inelastic scattering off electrons. The relevant cross sections for these processes are discussed in Martínez-Pinedo et al (2006). The basic neutrino opacity in core collapse is provided by neutrino scattering off nucleons. Depending on the distribution of the nucleons in space and the wavelength of the neutrinos, various important coherence effects can occur: Most important during collapse is the binding of nucleons into nuclei with a density contrast of several orders of magnitude to the surrounding nucleon gas. Coherent scattering off nuclei dominates the scattering opacity of neutrinos (and scales with A^2). Moreover, these neutrino opacities should be corrected by an ion-ion correlation function, this occurs if the neutrino wavelength is comparable to the distances of scattering nuclei and quantum mechanical interference effects appear (Sawyer, 2005; Burrows et al, 2006b). Even if current core collapse models include a full ensemble of nuclei in place of the traditional approach with one representative heavy nucleus, it remains non-trivial to adequately determine correlation effects in the ion mixture. Depending on the Q -value of an electron-capturing nucleus, neutrinos are emitted with a high energy of the order of the electron chemical potential/Fermi energy. As the neutrino opacities scale with the squared neutrino energy, the initially trapped neutrinos will downscatter to lower energies until the diffusion time scale becomes comparable to the thermalization time scale. The thermalization in current collapse models occurs through neutrino-electron scattering because the energy transfer per collision with the light electron is more efficient than with the heavier nucleons. The contribution of inelastic scattering of neutrinos

¹³ For a review of the corresponding tools see Ch. 8.)

off heavy nuclei depends on the individual nuclei and affects only the high-energy tail of the neutrino spectrum.

Goldreich and Weber (1980) have shown that only the inner $M_{Ch}(Y_e)$ (see the definition in Eq. 4.3) undergo a homologous collapse ($v_{collapse}(r) \propto r$), while at the edge of this core the velocity becomes supersonic and a fraction of the free-fall velocity. The inner core, falling at subsonic velocities where matter can communicate with sound speed, cannot communicate with the free-falling envelope. After the neutrinos are trapped, electron captures and neutrino captures are in equilibrium ($e^- + p \leftrightarrow n + \nu_e$) and the total lepton fraction $Y_L = Y_e + Y_\nu$ stays constant. Y_e stops to decrease and M_{Ch} stops shrinking. Typical values (with the most recent electron capture rates (Langanke et al, 2003) of $Y_L \approx 0.3$ are found in numerical collapse calculations (Hix et al, 2003; Marek et al, 2005) which correspond to $M_{Ch} \approx 0.5 M_\odot$. As soon as nuclear densities are reached at the center of the collapsing core, repulsive nuclear forces dominate the pressure in the equation of state. The collapse comes to a halt and matter bounces back to launch an outgoing pressure wave through the core. It travels through the subsonic inner core and steepens to a shock wave as soon as it faces supersonic infall velocities. Hence the matter in the PNS remains at low entropy $\sim 1.4 k_B$ per baryon while the supersonically accreting layers become shock-heated and dissociated at entropies larger than $\sim 6 k_B$ per baryon. Numerical simulations based on standard input physics and accurate neutrino transport exclude the possibility that the kinetic energy of the hydrodynamical bounce at nuclear densities drives a prompt supernova explosion because of dissociation and neutrino losses.

This can be seen in Fig. 4.8 presenting spherically symmetric calculations of a $13 M_\odot$ star. The inner core contains about $0.6 M_\odot$ of the initial Fe-core. The transition to free nucleons occurred only in this inner, homologous core and the outward moving shock runs through material consisting of Fe-group nuclei. The dissociation takes 8.7 MeV/nucleon or $8 \times 10^{18} \text{ erg g}^{-1}$. Based on initial shock energies of $(4 - 8) \times 10^{51} \text{ erg}$, this is sufficient for passing through $0.25\text{-}0.5 M_\odot$ and leads in essentially all cases to a stalling of the prompt shock. Only recently a possible exception was found (Sagert et al, 2009). If a hadron-quark phase transition occurs in the collapsed core at the appropriate time, releasing additional gravitational binding energy in the form of neutrinos from this second collapse, prompt explosions can be attained.

While core collapse determines the state of the *cold* nuclear matter inside the PNS, the mass of the hot mantle around the PNS grows by continued accretion. The infalling matter is heated and dissociated by the impact at the accretion front and continues to drift inward. At first, it can still increase its entropy by the absorption of a small fraction of outstreaming neutrinos (heating region). Further in, where the matter settles on the surface of the PNS, neutrino emission dominates absorption and the electron fraction and entropy decrease significantly (cooling region). The tight non-local feedback between the accretion rate and the luminosity is well captured in computer simulations in spherical symmetry that accurately solve the Boltzmann neutrino transport equation for the three neutrino flavors. All progenitor stars between main sequence masses of 13 and $40 M_\odot$ showed no explosions in simulations

of the postbounce evolution phase (Liebendörfer et al, 2003). This indicates that the neutrino flux from the PNS does not have the fundamental strength to blow off the surrounding layers for a vigorous explosion.

Improved electron capture rates on heavy nuclei overcame the idealized blocking of Gamow-Teller transitions in the traditionally applied single-particle model. In the single-particle picture of nuclei the so-called *pf*-shell is filled for $Z = 40$ or $N = 40$ for protons or neutrons respectively. Neutron numbers beyond $N = 40$ require a filling of the *gd*-orbits. If during core collapse nuclei (Y_e) become so neutron-rich that nuclei with $Z < 40$ and $N > 40$ dominate the NSE composition, electron capture would require the conversion of an *fp* proton to a *gd* neutron as all *pf* neutron orbits are filled. This Pauli-blocked transition would lead to the dominance of electron capture on free protons rather than nuclei and under such conditions. The recent finding, that configuration mixing and finite temperature effects result in unfilled *pf* neutron orbits, removes this Pauli-blocking and results in the fact that under these condition electron capture rates on nuclei dominate those on free protons (Langanke et al, 2003). Thus, there are two effects due to the new set of electron capture rates: 1. at low densities for less neutron-rich nuclei the total amount of electron capture is reduced with an improved description of Gamow-Teller transitions (see the discussion of the early collapse phase in Sect. 4.3), 2. at high densities in the late collapse phase the total amount of electron capture is enhanced, leading to smaller Y_e and Y_L values than before. Such changes caused a reduction of homologous core sizes down to $M_{Ch} = 0.5 M_\odot$ (see discussion above and Hix et al (2003)). This faster deleptonization in the collapse phase in comparison to captures on free protons alone thus resulted in a 20% smaller inner core at bounce.

Taking all this improved physics into account leads in the entire simulations (i.e. all mass zones involved) to conditions in densities ρ , electron abundance Y_e and entropy s per baryon, where properties like the equation of state or other microscopic physics is needed in current supernova simulations. Fig. 4.9 provides this information for a simulation of a $20 M_\odot$ star (Liebendörfer et al, 2009).

Moreover, a comparison of the effects of the only two publicly available equations of state by Lattimer and Douglas Swesty (1991) and Shen et al (1998b,a) is required. In simulations of massive progenitors that do not explode and exceed the maximum stable mass of the accreting neutron star in the postbounce phase, it was demonstrated that the neutrino signal changes dramatically when the PNS collapses to a black hole (Fischer et al, 2009b). Depending on the stiffness of the equation of state or the accretion rate from the external layers of the progenitor star, this can happen at very different time after bounce. Hence, the neutrino signal carries a clear imprint of the stiffness of the equation of state and the accretion rate to the observer of neutrinos.

The detailed treatment of the neutrino transport and interactions is of great importance for the nucleosynthesis. This has been shown in several recent studies (Fröhlich et al, 2006a,b; Pruet et al, 2005, 2006; Wanajo, 2006). This also opens an opportunity to investigate neutrino flavor oscillations among electron, muon and tau neutrinos. On the one hand side the long term explosion runs achieve (low) density structures that allow for MSW (Mikheyev-Smirnov-Wolfenstein effect) neutrino

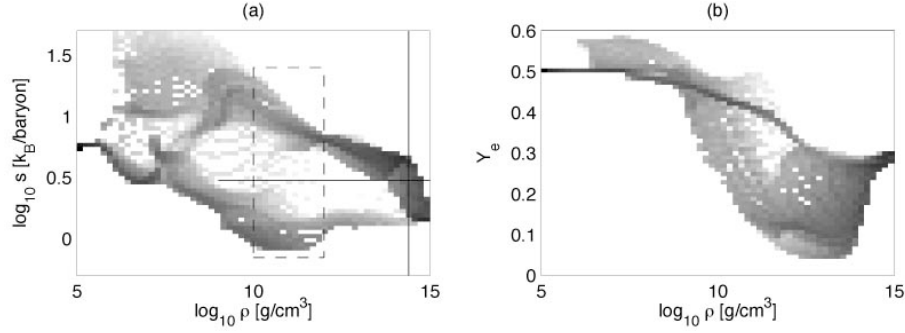


Fig. 4.9 Overview of the conditions attained in a simulation of the collapse, bounce, and explosion (artificially induced) of a $20 M_{\odot}$ star. Shown are two histograms of the occurrence of conditions as a function of density ρ , specific entropy s and electron fraction Y_e . The shading of a given bin corresponds to $\log_{10}(\int dm dt)$ in arbitrary units, where the integral over mass is performed over the mass dm of matter whose thermodynamic state at a given time falls into the bin. The integral over time extends over the duration of a simulation. Hence, regions of dark shading correspond to states that are experienced by considerable mass for an extended time, while light or absent shading corresponds to conditions that are rarely assumed in the supernova simulation. The vertical black line indicates the nuclear density. The horizontal black line indicates an entropy of $3 k_B$ /baryon beyond which ions are dissociated. It clearly separates the conditions of cold infalling matter on the lower branch from the conditions of hot shocked matter on the upper branch.

flavor oscillations in the outer layers (Wolfenstein, 1978; Mikheyev and Smirnov, 1985). These may give additional hints on the expansion velocity and density distribution in case that the neutrinos can be observed from a near-by supernova. On the other hand, collective flavor transitions have recently been postulated in regions where the neutrino density exceeds the electron density (Duan et al, 2006, 2007; Fogli et al, 2007). This condition will be achieved in the evacuated zone that surrounds the PNS after the onset of an explosion. The impact of these collective neutrino flavor oscillations on the neutrino heating during the shock expansion, the neutrino wind, and the nucleosynthesis are important open points that require a detailed investigation under consideration of accurate neutrino transport and spectra.

The difficulty to reproduce explosions in spherically symmetric models of core-collapse and postbounce evolution stimulated the consideration of numerous modifications and alternatives to this basic scenario, mostly relying on multi-dimensional effects that could not be treated in spherical symmetry. It was discussed whether convection inside the PNS could accelerate the deleptonization and increase the neutrino luminosity (Wilson and Mayle, 1993). The convective overturn between the PNS and shock front was shown to increase the efficiency of neutrino energy deposition (Herant et al, 1994). Asymmetric instabilities of the standing accretion shock (Blondin et al, 2003; Foglizzo, 2009) may help to push the shock to larger radii and g-mode oscillations of the PNS may contribute to neutrino heating by the dissipation of sound waves between the PNS and the shock (Burrows et al, 2006a). Moreover, it has been suggested that magnetic fields have an impact on the explosion mechanism (Kotake et al, 2006). Most of the above-mentioned modifications of

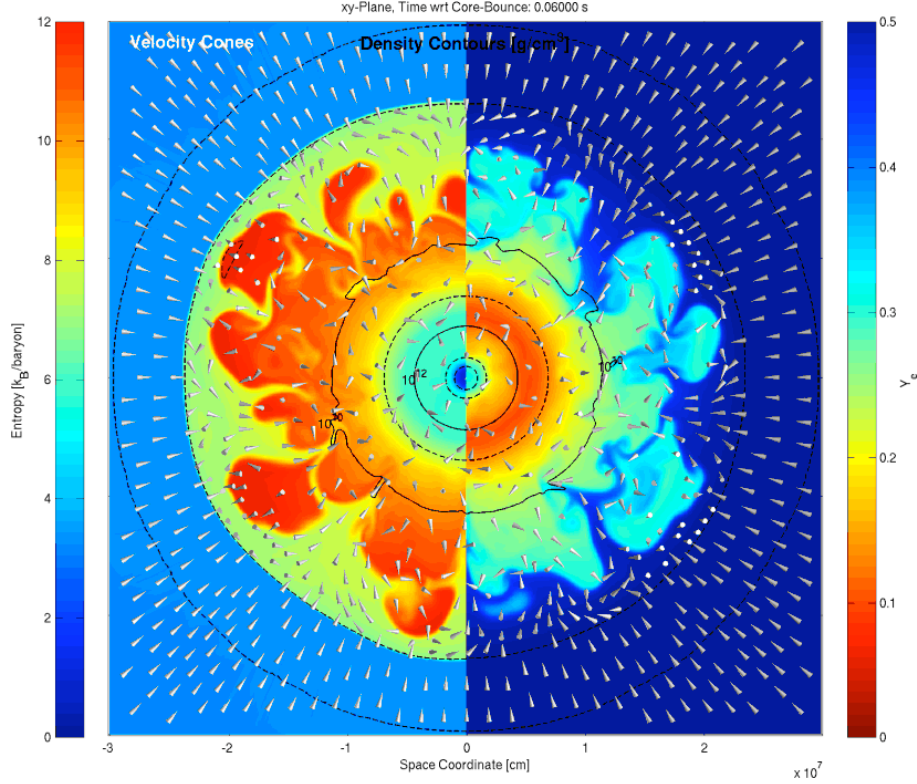


Fig. 4.10 Illustration of the early accretion phase in a three-dimensional simulation with a resolution of 600^3 zones and the isotropic diffusion source approximation for 3D neutrino transport (Liebendörfer et al, 2009). Shown are density contours as black lines for a $15 M_{\odot}$ star from Woosley and Weaver (1995). *Left:* The color indicates the specific entropy and the cones the direction of the velocity. *Right:* The color refers to the magnetic field strength and the cones to its direction. The cool high-density interior of the PNS and the hot low-density accreted matter behind the standing accretion front are clearly distinguishable.

the explosion mechanism are essentially of a three-dimensional nature. In order to illustrate the complexity of the crucial accretion phase we show in Fig. 4.10 a slice through a three-dimensional simulation of core-collapse and postbounce evolution of a recent run (Liebendörfer et al, 2008). Its input physics uses the Lattimer-Swesty equation of state (Lattimer and Douglas Swesty, 1991) and a parameterization of the neutrino physics for the collapse phase (Liebendörfer et al, 2005). The treatment of neutrino cooling and heating in the postbounce phase is based on multi-group diffusion (the isotropic diffusion source approximation of Liebendörfer et al (2009)).

Initially, spherically symmetric supernova models were the most realistic among all feasible computer representations of the event. With increasing observational evidence for the complexity of the explosions (Hamuy, 2003) their primary purpose shifted from a realistic representation to the identification and understanding of the

basic principles of the explosion mechanism. After the emergence of axisymmetric simulations with sophisticated and computationally intensive spectral neutrino transport (Buras et al, 2003; Walder et al, 2005) spherically symmetric models still have several assets. In the following subsection we will first describe purely phenomenological calculations based on artificially induced explosions via a “piston” or energy deposition in terms of a “thermal bomb”, purely in order to discuss nucleosynthesis effects. We will then also discuss still artificial explosions in spherical symmetry, however resulting from a “self-consistent” treatment including neutrino transport, which permits to analyse the effect of neutrinos on the nucleosynthesis of the innermost ejecta.

4.4.2 Nucleosynthesis in Explosions

Major Explosive Burning Processes

Despite considerable improvements of stellar models and numerical simulations in recent years, some fundamental problems remain in nucleosynthesis predictions. It has become evident that certain evolution aspects can only be followed in models going beyond one-dimensional simulations, such as convection, rotation, and the explosion mechanism. However, it is still not feasible to directly couple full reaction networks, containing several thousand nuclei, to multi-dimensional hydrodynamic calculations due to the lack of required computing power, even in modern computers. Thus, postprocessing after explosion models with parameterized networks still remains an important approach. One-dimensional models can directly accommodate increasingly larger networks but they cannot capture all of the necessary physics. As outlined in the previous subsection, it has become apparent that a self-consistent treatment of core collapse supernovae in 1D does not lead to successful explosions when using presently known input physics while 2D models show some promise. There are strong indications that the delayed neutrino mechanism works combined with a multi-D convection treatment for unstable layers (possibly with the aid of rotation, magnetic fields and/or still existent uncertainties in neutrino opacities). Therefore, hybrid approaches using certain parameterizations or approximations have been and are still necessary when predicting the nucleosynthetic yields required for the application described above.

Supernova nucleosynthesis predictions have a long tradition. All of these predictions relied on an artificially introduced explosion, either via a piston or a thermal bomb introduced into the progenitor star model. The mass cut between the ejecta and the remnant does not emerge from this kind of simulations but has to be determined from additional conditions. While the usage of artificially introduced explosions is justifiable for the outer stellar layers, provided we know the correct explosion energy to be dumped into the shock front (on the order of 10^{51} erg seen in observations), it clearly is incorrect for the innermost ejected layers which should be directly related to the physical processes causing the explosion. This affects the Fe-group composi-

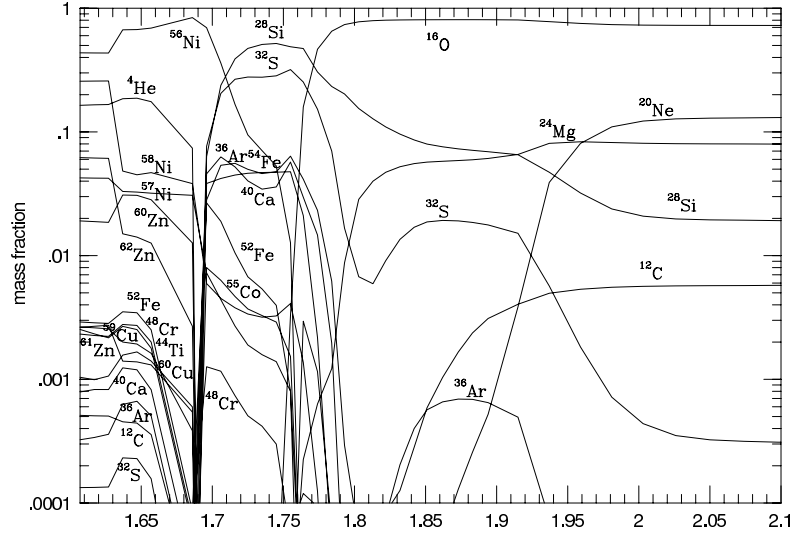


Fig. 4.11 Mass fractions of a few major nuclei after passage of the supernova shockfront through a star with an initial mass of $20 M_{\odot}$. Matter outside $2M_{\odot}$ is essentially unaltered. Mass zones further in experience explosive Si, O, Ne, and C-burning. For ejecting $0.07M_{\odot}$ of ^{56}Ni the mass cut between neutron star and ejecta is required to be located at $1.6M_{\odot}$.

tion, which has been recognized as a clear problem by many groups (Woosley and Weaver, 1995; Thielemann et al, 1990, 1996; Nakamura et al, 1999, 2001; Nomoto et al, 2006). The problem is also linked to the so-called neutrino wind, emitted seconds after the supernova explosion, and considered as a possible source of the r process to produce the heaviest elements via neutron captures (Qian and Woosley, 1996), as will be discussed below.

Given the above detailed discussion of the physics, problems and options regarding core collapse supernovae, we will adopt the following approach in order to predict the most reliable nucleosynthesis predictions for the ejecta in a 1D spherically symmetric treatment. The multiplication of neutrino capture cross sections on nucleons with a free parameter in 1D spherically symmetric calculations can mimic the enhanced energy deposition which multi-D models show. The free parameter is tuned to give correct explosion energies and ^{56}Ni yields for a number of well known supernovae. This approach provides clear predictions for the mass cut between the remaining neutron star and the ejecta. It also includes the effect neutrinos can have on the correct Y_e in the ejecta and the related nucleosynthesis. In the outer explosively burning layers, essentially only the energy in the shock front matters. The behavior of these zones can be easily understood from the maximum tempera-

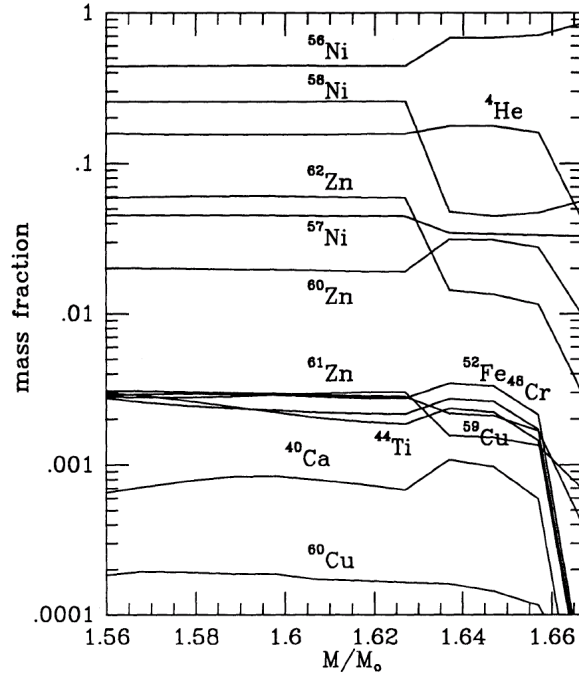


Fig. 4.12 Mass fractions of the dominant nuclei in zones which experience α -rich freeze-out. Notice the relatively large amounts of Zn and Cu nuclei, which originate from α -captures on Ni and Co. One can recognize their strong decrease beyond $1.66M_{\odot}$, which goes parallel with the decrease of the ${}^4\text{He}$ -abundance and other α -nuclei such as ${}^{40}\text{Ca}$, ${}^{44}\text{Ti}$, ${}^{48}\text{Cr}$, and ${}^{52}\text{Fe}$. Nuclei which would dominate in a nuclear statistical equilibrium like ${}^{56,57,58}\text{Ni}$ stay constant or increase even slightly. The increase of all nuclei with $N = Z$ at $1.63M_{\odot}$ and the decrease of nuclei with $N > Z$ is due to the change in Y_e in the original stellar model before collapse (see also Fig. 4.11)

tures attained in the radiation bubble and for a first discussion we will just focus on these features, which can also be obtained with an artificially induced thermal bomb treatment.

For a given/known Y_e and density ρ , the most significant parameter in explosive nucleosynthesis is the temperature, and a good prediction for the composition can already be made by only knowing T_{\max} , without having to perform complex nucleosynthesis calculations. Weaver and Woosley (1980) already recognized, that matter behind the shock front is strongly radiation dominated. Assuming an almost homogeneous density and temperature distribution behind the shock (which is approximately correct, one can equate the supernove energy with the radiation energy inside the radius r of the shock front

$$E_{\text{SN}} = \frac{4\pi}{3} r^3 a T^4(r). \quad (4.4)$$

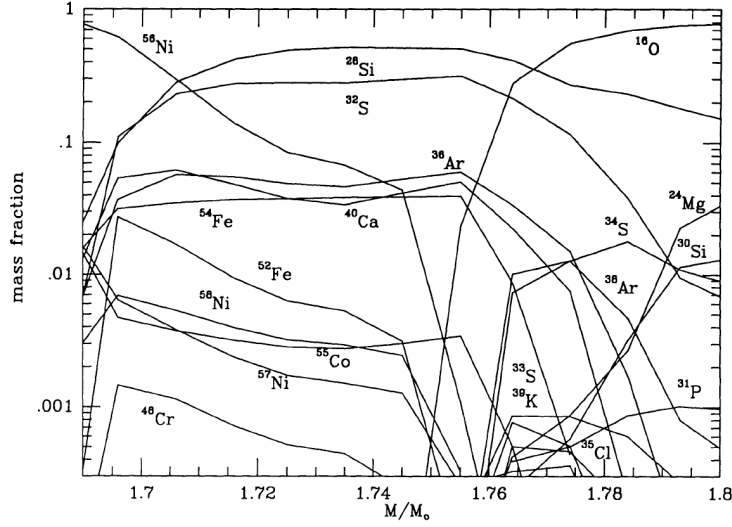


Fig. 4.13 Mass fractions of nuclei in the zones of incomplete Si-burning $M < 1.74M_{\odot}$ and explosive O-burning $M < 1.8M_{\odot}$. The Si-burning zones are characterized by important quantities of Fe-group nuclei besides ^{28}Si , ^{32}S , ^{36}Ar , and ^{40}Ca . Explosive O-burning produces mostly the latter, together with more neutron-rich nuclei like ^{30}Si , ^{34}S , ^{38}Ar etc.

This equation can be solved for r . With $T = 5 \times 10^9 \text{ K}$, the lower bound for explosive Si-burning with complete Si-exhaustion, and an induced thermal bomb energy of $E_{\text{SN}} = 10^{51} \text{ erg}$, the result is $r \approx 3700 \text{ km}$. For the evolutionary model by Nomoto and Hashimoto (1988) of a $20M_{\odot}$ star this radius corresponds to $1.7M_{\odot}$, in excellent agreement with the exact hydrodynamic calculation. Temperatures which characterize the edge of the other explosive burning zones correspond to the following radii: incomplete Si-burning ($T_9=4$, $r=4980 \text{ km}$), explosive O-burning (3.3, 6430), and explosive Ne/C-burning (2.1, 11750). This relates to masses of 1.75, 1.81, and $2.05M_{\odot}$ in case of the $20M_{\odot}$ star. The radii mentioned are model independent and vary only with the supernova energy. In the following we present a number of plots which show the different mass fractions $X_i = A_i Y_i$ as a function of radial mass $M(r)/M_{\odot}$, passing outwards through a $20M_{\odot}$ star through all explosive burning regions.

Matter between the mass cut $M(r)=M_{\text{cut}}$ and the mass enclosed in the radius corresponding to explosive Si-burning with complete Si-exhaustion is indicated with $M(\text{ex Si-c})$. Then follows the zone of incomplete Si-burning until $M(\text{ex Si-i})$, explosive O-burning until $M(\text{ex O})$, explosive Ne/C-burning until $M(\text{ex Ne})$, and unprocessed matter from the C/Ne-core is ejected until $M(\text{C-core})$. The zones beyond explosive Ne/C-burning ($T_{\text{max}} < 2.1 \times 10^9 \text{ K}$) are essentially unaltered and the composition is almost identical to the pre-explosive one. When performing such calculations for a variety of progenitors over a range of initial stellar masses, one can analyze the dependence of the mass involved in these different burning regimes as a function initial stellar mass (see Sect. 4.5).

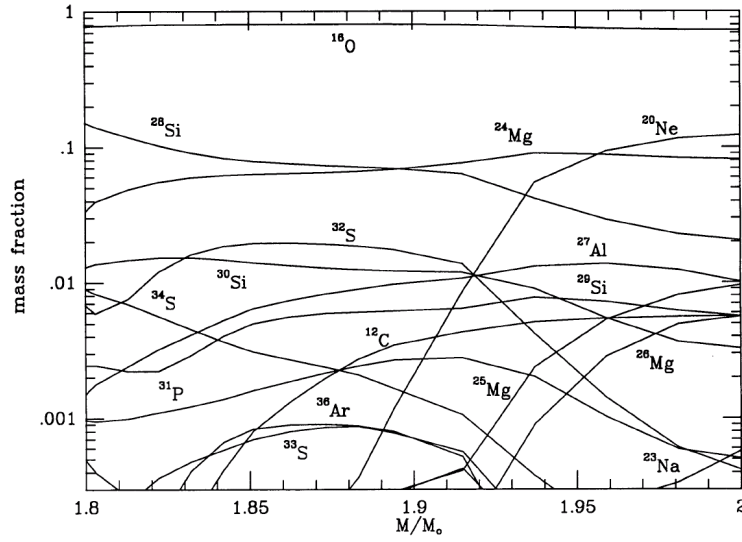


Fig. 4.14 Composition in mass zones of explosive Ne and C-burning. The dominant products are ^{16}O , ^{24}Mg , and ^{28}Si . Besides the major abundances, mentioned above, explosive Ne-burning supplies also substantial amounts of ^{27}Al , ^{29}Si , ^{32}S , ^{30}Si , and ^{31}P . Explosive C-burning contributes in addition the nuclei ^{20}Ne , ^{23}Na , ^{24}Mg , ^{25}Mg , and ^{26}Mg .

Results for a $20M_{\odot}$ star (Nomoto and Hashimoto, 1988) are given as examples for the abundance behavior in a series of Figs 4.11, 4.12, 4.13, 4.14. It should be mentioned here that this still uses a simplified thermal bomb treatment for the pre-collapse model rather than the results from a 1D spherically symmetric simulation with enhanced neutrino capture rates, which insures an explosion also in 1D. The explosion energy used corresponds to a supernova energy of 10^{51} erg. As mentioned before, this treatment cannot predict a self-consistent explosion and the position of the mass cut between neutron star and ejecta. Only the observation of $0.07 \pm 0.01M_{\odot}$ of ^{56}Ni in SN1987A (a $20M_{\odot}$ star) gives an important constraint, because ^{56}Ni is produced in the innermost ejected zones. The explosive nucleosynthesis due to burning in the shock front is shown in Fig. 4.11 for a few major nuclei. Inside $1.7M_{\odot}$ all Fe-group nuclei are produced in *explosive* Si-burning during the SN II event. At $1.63M_{\odot}$ Y_e changes from 0.494 to 0.499 and leads to a smaller ^{56}Ni abundance further inside, where more neutron-rich Ni-isotopes share the abundance with ^{56}Ni . This is an artifact of the Y_e gradient in the pre-collapse model which can be changed in a consistent explosion treatment via neutrino interactions with this matter.

In explosive Si-burning only α -rich freeze-out and incomplete Si-burning are encountered. Contrary to SNe Ia, densities in excess of 10^8gcm^{-3} , which would result in a normal freeze-out, are not attained in the ejecta of this $20M_{\odot}$ star (see also Fig.4.2). The most abundant nucleus in the α -rich freeze-out is ^{56}Ni . For the less abundant nuclei the final α -capture plays a dominant role transforming nuclei like ^{56}Ni , ^{57}Ni , and ^{58}Ni into ^{60}Zn , ^{61}Zn , and ^{62}Zn (see Fig.4.12).

The region which experiences incomplete Si-burning starts at $1.69M_{\odot}$ and extends out to $1.74M_{\odot}$. In the innermost zones with temperatures close to $4 \times 10^9 \text{K}$ there exists still a contamination by the Fe-group nuclei ^{54}Fe , ^{56}Ni , ^{52}Fe , ^{58}Ni , ^{55}Co , and ^{57}Ni . Explosive O-burning occurs in the mass zones up to $1.8M_{\odot}$ (see Fig.4.13). The main burning products are ^{28}Si , ^{32}S , ^{36}Ar , ^{40}Ca , ^{38}Ar , and ^{34}S . With mass fractions less than 10^{-2} also ^{33}S , ^{39}K , ^{35}Cl , ^{42}Ca , and ^{37}Ar are produced. Explosive Ne-burning leads to an ^{16}O -enhancement over its hydrostatic value in the mass zones up to $2M_{\odot}$ (see Fig.4.14).

Explosive Burning off Stability

The p-Process

Up to now we discussed the production of heavy nuclei beyond the Fe-group only via slow neutron captures (the *s* process) in hydrostatic stellar evolution. A number of proton-rich (p-)isotopes of naturally occurring stable heavy nuclei cannot be produced by neutron captures along the line of stability. The currently most favored production mechanism for those 35 p-isotopes between Se and Hg is photodisintegration (γ process) of intermediate and heavy elements at high temperatures in late (explosive) evolution stages of massive stars (Woosley and Howard, 1978; Rayet et al, 1990). However, not all p-nuclides can be produced satisfactorily, yet. A well-known deficiency in the model is the underproduction of the Mo-Ru region, but the region $151 < A < 167$ is also underproduced, even in recent calculations (Rauscher et al, 2002; Arnould and Goriely, 2003; Rapp et al, 2006; Dillmann et al, 2008). There exist deficiencies in astrophysical modeling and the employed nuclear physics. Recent investigations have shown that there are still considerable uncertainties in the description of nuclear properties governing the relevant photodisintegration rates. This has triggered a number of experimental efforts to directly or indirectly determine reaction rates and nuclear properties for the p/γ process (Rauscher, 2006). Here it is important to investigate the sensitivity of the location of the γ -process path with respect to reaction rate uncertainties.

Concerning the astrophysical modeling, only a range of temperatures has to be considered which are related to the explosive Ne/O-burning zones of a supernova explosion (see Figs.4.13 and 4.14), where partial (but not complete) photodisintegration of pre-existing nuclei occurs (from prior hydrostatic evolution or inherited metallicity), i.e. at $\approx 2 - 3 \times 10^9 \text{K}$. The γ process starts with the photodisintegration of stable seed nuclei that are present in the stellar plasma. During the photodisintegration period, neutron, proton, and α -emission channels compete with each other and with beta-decays further away from stability. In general, the process, acting like “spallation” of pre-existing nuclei, commences with a sequence of (γ, n) -reactions, moves the abundances to the proton-rich side. At some point in a chain of isotopes, (γ, p) and/or (γ, α) -reactions become faster than neutron emissions, and the flow branches and feeds other isotopic chains. At late times photodisintegrations become less effective, when decreasing temperatures shift the branching points and make beta-decays more important. Finally the remaining unstable nuclei decay back to

stability. The branchings established by the dominance of proton and/or α -emission over neutron emission are crucial in determining the radioactive progenitors of the stable p -nuclei and depend on the ratios of the involved reaction rates. Numerous experimental and theoretical efforts have been undertaken to improve the reaction input, especially with respect to open questions in optical potentials for α particles and protons (Gyürky et al, 2006; Kiss et al, 2007, 2008; Yalçın et al, 2009).

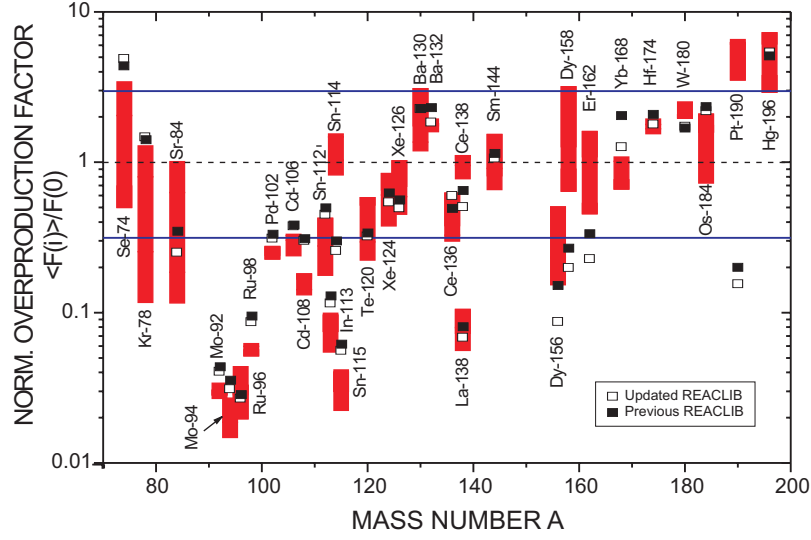


Fig. 4.15 Normalized overproduction factors of p -process nuclei derived with the Rapp et al (2006) (open squares) and Dillmann et al (2008) (full squares) reaction library. In addition, the results from a range of stellar models (10-25 M_{\odot}) from Rayet et al (1995) are given for comparison. A value equal to unity corresponds to relative solar abundances.

Applications of p -process network calculations to the temperature profiles of initiated explosions have been performed by Rayet et al (1995); Rapp et al (2006); Dillmann et al (2008). Here, in Fig. 4.15 we present the results of a 25 M_{\odot} mass model (Dillmann et al, 2008) with two reaction rate libraries without and with inclusion of all experimental improvements, existing at that point. It is noticed that the nuclear uncertainties cannot change the underproduction of especially the light p -nuclei. Another process seems to be required to supply these missing abundances.

The vp -Process

Neutron-deficient nuclei can also be produced by two other astrophysical nucleosynthesis processes: the rp process in X-ray bursts (which, however, does not eject matter into the interstellar medium (Wallace and Woosley, 1981; Schatz et al, 1998; Fisker et al, 2008) and the recently discovered vp process in core collapse supernovae (Fröhlich et al, 2006a,b; Pruet et al, 2006; Wanajo, 2006). The vp process

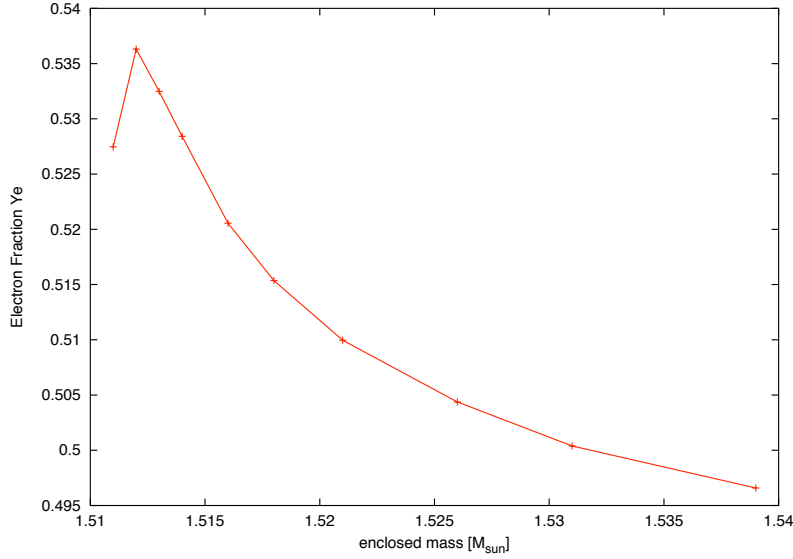


Fig. 4.16 Y_e of the innermost ejecta due to neutrino interactions with matter. At high temperatures electrons are not degenerate, thus the reduction of Y_e due to electron captures is ineffective. For similar neutrino and antineutrino spectra the neutron-proton mass difference favors $\nu_e + n \leftrightarrow p + e^-$ over $\bar{\nu}_e + p \leftrightarrow n + e^+$.

occurs in explosive environments when proton-rich matter is ejected under the influence of strong neutrino fluxes. This includes the innermost ejecta of core-collapse supernova (Buras et al, 2006; Thompson et al, 2005; Liebendörfer et al, 2008) and possible ejecta from black hole accretion disks in the collapsar model of gamma-ray bursts (Surman et al, 2006). The discussion of these innermost ejected mass zones has been skipped above, when discussing the results for explosive nucleosynthesis in a $20 M_{\odot}$ star, utilizing a thermal bomb but the pre-collapse stellar conditions with the corresponding Y_e . Here, as discussed in the beginning of this subsection, we have boosted the energy deposition efficiencies by enhancing the neutrino and anti-neutrino captures on neutrons and protons in a 1D simulation. While this is not a fully self-consistent treatment, no external (artificial) energy is required to produce a successful explosion with a consistently emerging mass cut between neutron star and ejecta. Moreover, this treatment guarantees provides a Y_e that is consistently determined by all weak interactions processes. The result is that explosions are obtained and the neutrino interaction with matter leads to a Y_e enhanced beyond 0.5 (see Fig. 4.16) which overcomes nucleosynthesis problems for the Fe-group encountered previously.

The matter in these ejecta is heated to temperatures well above 10^{10} and becomes fully dissociated into protons and neutrons. The ratio of protons to neutrons is mainly determined by neutrino and antineutrino absorptions on neutrons and protons, respectively. Similar neutrino and antineutrino energy spectra and fluxes produce proton-dominated matter in the reactions $\nu_e + n \leftrightarrow p + e^-$ and $\bar{\nu}_e + p \leftrightarrow n + e^+$, due to the n-p mass difference. When the matter expands and cools, the free neutrons and protons combine into α -particles. Later, at temperatures around 5×10^9 K, α -particles assemble into heavier nuclei via unstable intermediate nuclei, e.g. the triple- α reaction via unstable ^8Be , but - depending on the entropy and the expansion of matter - only a fraction of those form iron-group nuclei (α -rich freeze-out). In case of a proton-rich environment, there are also still free protons available at the time of the alpha freeze-out. Once the temperature drops to about 2×10^9 K, the composition of the ejecta consists mostly of ^4He , protons, and iron group nuclei with $N \approx Z$ (mainly ^{56}Ni) in order of decreasing abundance. Without neutrinos, synthesis of nuclei beyond the iron peak becomes very inefficient due to bottleneck (mainly even-even $N = Z$) nuclei with long beta-decay half-lives and small proton-capture cross sections. Such a nucleus is ^{64}Ge . Thus, with the Y_e determined by neutrino interactions with free neutrons and protons in the early very hot phase of dissociated nuclei, the nucleosynthesis leads to an α - and proton-rich freeze-out which does not stop at ^{56}Ni but continues up to ^{64}Ge (which later decays to ^{64}Zn). This part of the story enables core collapse yeasts which produce Fe-group nuclei up to essentially ^{64}Zn . The effect is seen in the upper portion Fig. 4.17.

However, the matter is subject to a large neutrino/antineutrino flux from the proto-neutron star. While neutrons are bound in neutron-deficient $N = Z$ nuclei and neutrino captures on these nuclei are negligible due to energetics, antineutrinos are readily captured both on free protons and on heavy nuclei on a timescale of a few seconds. As protons are more abundant than heavy nuclei, antineutrino captures occur predominantly on protons, leading to residual neutron densities of $10^{14} - 10^{15} \text{ cm}^{-3}$ for several seconds. These neutrons are easily captured by heavy neutron-deficient nuclei, for example ^{64}Ge , inducing (n, p) reactions with time scales much shorter than the beta-decay half-life. This permits further proton captures and allows the nucleosynthesis flow to continue to heavier nuclei (see lower part of Fig. 4.17). The νp process (Fröhlich et al, 2006b) is this sequence of (p, γ) -reactions, followed by (n, p) -reactions or beta-decays, where the neutrons are supplied by antineutrino captures on free protons.

In Fig.4.18 we also show νp process nucleosynthesis results from the innermost early neutrino wind ejecta produced in the explosion of a $15M_{\odot}$ star (Janka et al, 2003), also utilized in (Pruet et al, 2006; Fisker et al, 2009), which synthesizes efficiently nuclei even for $A > 90$. Two sets of astrophysical reaction rates were used in the reaction network, both based on theoretical rates from the NON-SMOKER code (Rauscher and Thielemann, 2000, 2004), but once with the latest excited state information and masses from the AME2003 compilation (Audi et al, 2003) and another set also with the latest mass measurements (Weber et al, 2008). Fig.4.18 shows the final abundances normalized to solar abundances after decay to stability for these two sets of thermonuclear reaction rates. Only nuclei produced in the p-rich ejecta

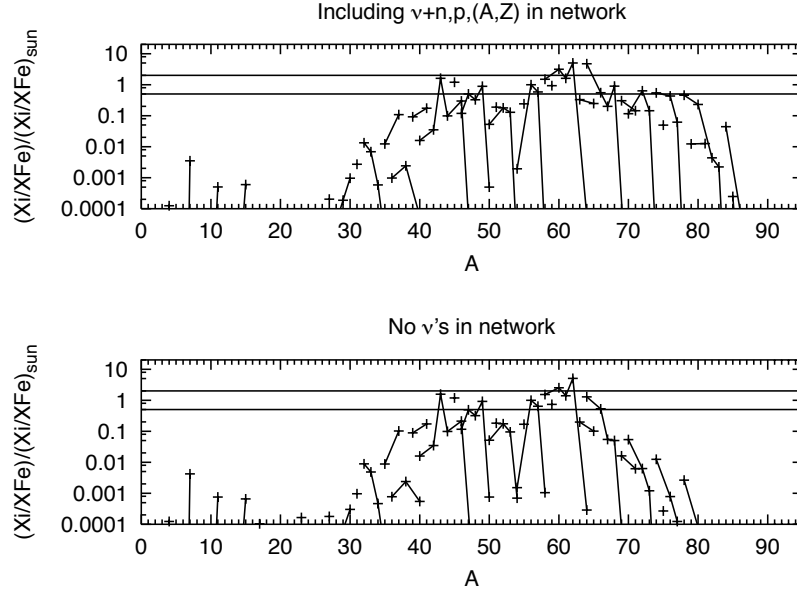


Fig. 4.17 Final abundances in mass zones in the innermost ejecta which experienced neutrino irradiation, leading to proton-rich conditions ($Y_e > 0.5$). The upper part of the figure shows the nucleosynthesis results in the innermost ejecta of explosive, after α -rich and proton-rich freeze-out from Si-burning, normalized to solar after decay. The bottom part of the figure also includes the interaction of anti-electron neutrinos with protons ($\bar{\nu}_e + p \rightarrow n + e^+$) which produces neutrons, permitting the late change of ^{64}Ge via $^{64}\text{Ge}(n, p)^{64}\text{Ga}$. This feature permits further proton captures to produce heavier nuclei (the so-called νp process. Here matter up to $A = 85$ is produced.

are shown. As is clearly seen, there is no difference in the yields for the two different sets of rates except for a few nuclei in the mass range $85 < A < 95$, namely $^{87,88}\text{Sr}$, ^{89}Y , and $^{90,91}\text{Zr}$. This can be directly traced back to the large change in the mass of ^{88}Tc ($\Delta M = -1031$ keV). This change in mass leads to an increase in the reaction rate for $^{88}\text{Tc}(\gamma, p)^{87}\text{Mo}$ at the relevant temperatures and therefore a relative suppression of the opposite capture rate. These results show that the νp process can easily produce the light p-nuclei of Mo and Ru, which are deficient in p -process calculations. Further processing depends on the expansion (speed) of matter and the overlying mass of ejecta.

The r-Process

A rapid neutron-capture process (r process) in an explosive environment is traditionally believed to be responsible for the nucleosynthesis of about half of the heavy elements above Fe. While in recent years the high entropy (neutrino) wind (HEW) of core-collapse supernovae has been considered to be one of the most promising sites, hydrodynamical simulations still encounter difficulties to reproduce the astrophysical conditions under which this process occurs. The classical *waiting-point*

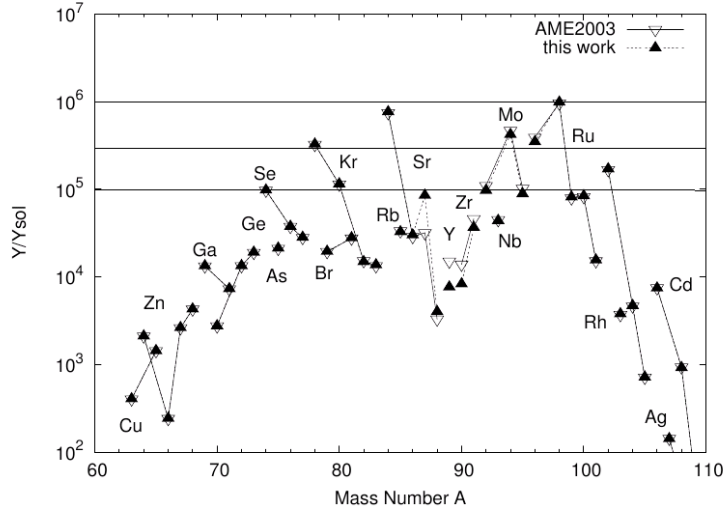


Fig. 4.18 Final abundances in mass zones experiencing the νp process, i.e. the innermost ejecta of explosive, α -rich freeze-out Si-burning, normalized to solar after decay for two sets of thermonuclear reaction rates/masses. Matter up to $A = 100$ can be produced easily.

approximation, with the basic assumptions of an Fe-group seed, an $(n, \gamma) - (\gamma, n)$ -equilibrium for constant neutron densities n_n at a chosen temperature T , over a process duration τ , and an instantaneous freezeout, has helped to gain improved insight into the systematics of an r process in terms of its dependence on nuclear-physics input and astrophysical conditions (Cowan et al, 1991; Kratz et al, 1993, 2007). This corresponds to a set of quasi-equilibria with each QSE group being represented by an isotopic chain. Taking a specific seed nucleus, the solar r -process pattern peaks can be reproduced by a variation/superposition of neutron number densities n_n and durations τ . Whether the solar r -process abundances are fully reproduced in each astrophysical event, i.e., whether each such event encounters the full superposition of conditions required, is a matter of debate (Wasserburg et al, 1996; Pfeiffer et al, 2001; Sneden et al, 2003; Honda et al, 2006; Qian and Wasserburg, 2007; Farouqi et al, 2009, 2010). In realistic astrophysical environments with time variations in n_n and T , it has to be investigated whether at all and for which time duration τ the supposed $(n, \gamma) - (\gamma, n)$ -equilibrium of the classical approach will hold and how freeze-out effects change this behavior. In general, late neutron captures may alter the final abundance distribution. In this case neutron capture reactions will be important. Also β -delayed neutrons can play a role in forming and displacing the peaks after freeze-out.

For many years since Woosley et al (1994); Takahashi et al (1994); Qian and Woosley (1996) the high entropy wind has been considered as the most promising (realistic?) environment, expelled from newly formed (hot) neutron stars in

core-collapse supernovae, which continue to release neutrinos after the supernova shock wave is launched. These neutrinos interact with matter of the outermost proto-neutron star layers which are heated and ejected in a continuous wind. The late neutrino flux also leads to moderately neutron-rich matter (Qian and Woosley, 1996) via interactions with neutrons and protons and causes matter ejection with high entropies. (However, there are recent studies (Fischer et al, 2009a) from collapse calculations which predict a proton-rich wind composition for more than the first 10s after collapse.) Problems were encountered to attain entropies sufficiently high in order to obtain high neutron/seed ratios which can produce the heaviest r process nuclei (Thompson et al, 2001; Wanajo et al, 2001; Terasawa et al, 2002). Recent hydrodynamic simulations for core-collapse supernovae support the idea that these entropy constraints can be fulfilled in the late phase (after the initial explosion) when a reverse shock is forming (Fryer et al, 2006; Arcones et al, 2007; Burrows et al, 2007; Janka et al, 2007; Panov and Janka, 2009).

The question is whether such high entropies occur at times with sufficiently high temperatures when an r process is still underway (Kuroda et al, 2008). Exploratory calculations to obtain the necessary conditions for an r process in expanding high-entropy matter have been undertaken by a number of groups (Hoffman et al, 1997; Meyer and Brown, 1997; Otsuki et al, 2000; Wanajo et al, 2001; Terasawa et al, 2002; Wanajo et al, 2004; Yoshida et al, 2004; Wanajo, 2007; Kuroda et al, 2008). Recent investigations (Farouqi et al, 2009, 2010) focussed (a) on the effects of varying nuclear physics input [mass models FRDM (Finite Range Droplet Model, Möller et al (1995)), ETFSI-1 (Extended Thomas-Fermi with Strutinsky Integral) (Abousir et al, 1995), ETFS-Q with quenching of shell closures far from stability (Pearson et al, 1996), the mass formula by Duflo & Zuker (DUFLO-ZUKER, Duflo and Zuker (1995)) and HFB-17 (a recent Hartree-Fock-Bogoliubov approach) (Goriely et al, 2009a)] and (b) the detailed understanding of the nuclear flow through the chart of nuclides, testing equilibria, freeze-out and delayed neutron capture. To investigate these effects we have applied a full network containing up to 6500 nuclei and the corresponding nuclear masses, cross sections and β -decay properties.

The calculations presented here are based on trajectories for densities and temperatures originating from expansions with a complete parameter study in terms of entropy S , electron fraction Y_e and expansion velocity V_{exp} , the latter being related to the expansion timescale τ_{exp} (Freiburghaus et al, 1999a; Farouqi et al, 2010). Here we only show the results utilizing the Duflo-Zuker mass model for a range of entropies. It is assumed that in the late phases of the neutrino wind of a deleptonized neutron star conditions with $Y_e < 0.5$ prevail (but see the discussion above).

Either higher entropies than obtained by the simulations discussed above or conditions with intrinsically high neutron densities (like expanding neutron star matter with $Y_e \approx 0.1 - 0.2$) can lead to neutron/seed ratios which are sufficiently high to reach fissionable nuclei in the r process. The fission fragments can again capture neutrons and produce fissionable nuclei, leading to an r process with fission recycling (Rauscher et al, 1994; Martínez-Pinedo et al, 2007). This requires reliable fission barriers (and fission fragment distributions) to test the possibility for the production of superheavy elements. It was shown recently that neutron-induced fission

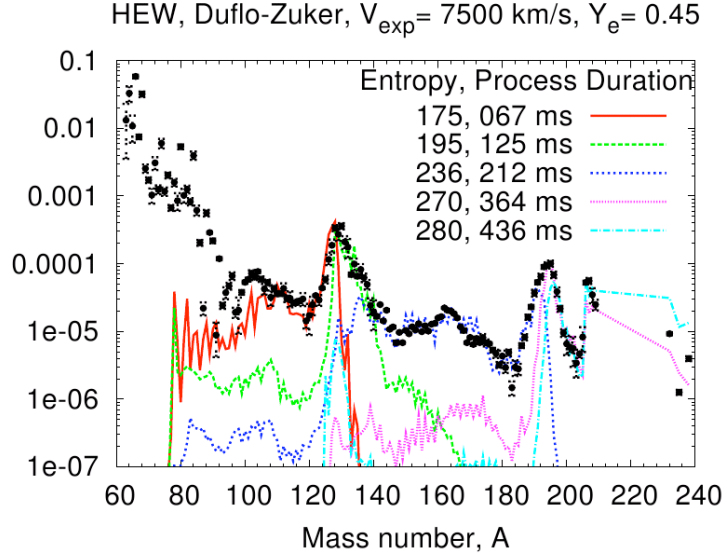


Fig. 4.19 High entropy neutrino wind results for the mass model by Duflo and Zuker (1995), expansion parameters and proton/nucleon ratio Y_e as given in the label, for a variation in entropies per baryon and k_B . (Farouqi et al, 2010)

is more important in r -process nucleosynthesis than beta-delayed fission (Panov and Thielemann, 2003; Martínez-Pinedo et al, 2007). Thus, the need to provide a compilation of neutron-induced fission rates is obvious and has been performed recently (Panov et al, 2005; Goriely et al, 2009b; Panov et al, 2009). Comparison of rates obtained with different sets for mass and fission barrier predictions give a measure of the uncertainties involved.

4.4.3 Exotic SN Types: Hypernovae and GRBs

As was outlined in various parts of the preceding sections, massive stars in the range of 8 to $\sim 130M_{\odot}$ undergo core-collapse at the end of their evolution and become Type II and Ib/c supernovae unless the entire star collapses into a black hole with no mass ejection (Heger et al, 2003). These Type II and Ib/c supernovae (as well as Type Ia supernovae, see Ch. 5) release large explosion energies and eject matter which underwent explosive nucleosynthesis, thus having strong dynamical, thermal, and chemical influences on the evolution of interstellar matter and galaxies. They have been the main focus of the present chapter up to now. The explosion energies of core-collapse supernovae are fundamentally important quantities, and an estimate of $E \sim 1 \times 10^{51} \text{ erg}$ has often been used in calculating nucleosynthesis and the impact on the interstellar medium. (Here we use the explosion energy E for

the final kinetic energy of the explosion.) A good example is SN1987A in the Large Magellanic Cloud, whose energy is estimated to be $E = (1.0 - 1.5) \times 10^{51}$ ergs from its early light curve

One of the most interesting recent developments in the study of supernovae (SNe) is the discovery of some very energetic supernovae (see e.g. Nomoto et al (2006), whose kinetic energy (KE) (in spherically symmetric analysis, see also Piran (2004)) exceeds 10^{52} erg, about 10 times the KE of normal core-collapse SNe (hereafter $E_{51} = E/10^{51}$ erg). The most luminous and powerful of these objects, the Type Ic supernova (SN Ic) 1998bw, was probably linked to the gamma-ray burst GRB 980425, thus establishing for the first time a connection between gamma-ray bursts (GRBs) and the well-studied phenomenon of core-collapse SNe. However, SN 1998bw was exceptional for a SN Ic: it was as luminous at peak as a SN Ia, indicating that it synthesized $\sim 0.5M_{\odot}$ of ^{56}Ni , and its KE was estimated at $E \sim 3 \times 10^{52}$ erg.

There is another class of supernovae which appears to be rather faint with apparently almost vanishing ^{56}Ni ejection. Thus, the question emerges how these different objects are related, whether they correspond to different initial masses and how the explosion mechanism changes. The questions to be answered are the following:

- do 8-10 M_{\odot} stars which produce an Fe-core in a collapse initiated via electron capture after core He-burning (electron capture supernovae) have a different explosion mechanism after core collapse than more massive stars? Is here only a small amount of material involved outside the collapsing C-core and little Ni-ejection occurring?
- for which stellar progenitor masses do we have a transition from the formation of neutron stars to the formation of black holes after collapse?
- to which extent is this transition region shifted by the nuclear equation of state?
- for which transition region are initially neutron stars formed, causing a regular supernova explosion, and only fall back by the reverse shock swallows inner matter, leading to a small final Ni-ejection and faint light curves?
- for which progenitor masses are black holes formed directly during collapse and how can this be observed?
- what is the role of rotation and magnetic fields to cause gamma-ray bursts?
- can we give reliable nucleosynthesis yields for such events?

Before going into a too involved discussion of the causes of these events, let us first consider the possible effect which higher energy explosions have on the ejecta, i.e. nucleosynthesis products. Here we use the term 'hypernova' to describe an extremely energetic supernova with $E \geq 10^{52}$ erg without specifying the explosion mechanism (Nomoto et al, 2001). Following SN 1998bw, other *hypernovae* of Type Ic have been discovered or recognised. Nucleosynthesis features in such hyper-energetic supernovae must show some important differences in comparison to normal supernova explosions. The higher explosion energies could lead to larger ejected ^{56}Ni masses, as observed in such explosions. They also cause higher entropies in the innermost ejecta, which result in a more extreme α -rich freeze-out from explosive Si-burning. Such conditions permit the sizable production of Fe-group nuclei beyond ^{56}Ni , up to ^{64}Ge which decays to ^{64}Zn (Nakamura et al, 2001).

This feature could have an influence on abundance patterns observed in extremely metal-poor halo stars. In fact, the observational finding that Zn behaves like an Fe-group element in galactic evolution - and was underproduced in existing supernova models (which were not including the νp process) - was used as a strong argument that a large fraction of massive stars explode as hypernovae (Nomoto et al, 2006; Kobayashi et al, 2006).

The observed frequency of type Ib supernovae is about 20% of SNe II at solar metallicity (Cappellaro et al, 1999). In four cases the typical spectrum of type Ic supernovae has been observed, associated with long soft gamma-ray bursts (Woosley and Bloom, 2006), indicating a link between SNe Ic and long soft GRBs. Prantzos and Boissier (2003) found an increase in the ratio of SNe Ibc / SNe II with metallicity. In order to understand this trend one has to understand stellar models as a function of metallicity, from the first stars in the Universe, i.e., metal-free, Population III (Pop III) stars which were born in a primordial hydrogen-helium gas cloud to present metallicities. This is one of the important challenges of current astronomy and relates to Sect. 4.2, where we have discussed the evolution of massive stars from lowest metallicities to solar values, including rotation and metallicity-dependent winds. In fact Meynet and Maeder (2003) could reproduce this observed trend metallicity trend. On the other hand different groups (Podsiadlowski et al, 1992; Vanbeveren et al, 2007; Eldridge et al, 2008) provide models from binary evolution with mass transfer (removing the H-rich envelope) which seems to reproduce this trend as well. Recent observations (Prieto et al, 2008) provide for the first time the individual ratios of SNe Ib / SNe II and SNe Ic / SNe II, rather than only the combined SNe Ibc / SNe II ratio. Georgy et al (2009) have studied stellar evolution in detail as a function of initial mass, metallicity and rotation, based on the Geneva evolution models. As a full understanding of the GRB mechanism is pending, two options have been considered for the cases where the Fe-core is massive enough that the formation of a black hole in the collapse is expected: (i) nevertheless a supernova-type explosion is assumed, (ii) a black hole forms without a supernovae. They find that current models of stellar evolution can account for the observed number ratios of SNe Ib / SNe II and SNe Ic / SNe II and their variation with metallicity. In case (ii), i.e. when no supernova occurs after black holes are formed, single-star models can still account for more than one half of the combined SNe Ibc / SNe II ratio for metallicities above solar, however, low metallicity SNe Ic events have to come from binary evolution. If black hole formation is identified with the occurrence of GRBs, the resulting number is too large, indicating that only a fraction of such events, most probably very rapid rotators, result in GRBs after collapse (MacFadyen and Woosley, 1999).

As mentioned earlier in this subsection, the explanation of SN Ic SN1998bw is based on a very large progenitor mass M and explosion energy E . The type Ic hypernovae 1998bw and 2003dh were clearly linked to the gamma-ray bursts GRB 980425 and GRB 030329, thus establishing the connection between long GRBs and core-collapse supernovae (SNe). SNe 1998bw and 2003dh were exceptional for SNe Ic: they were as luminous at peak as a SN Ia, indicating that they synthesized 0.3 - 0.5 M_{\odot} of ^{56}Ni , and their kinetic energies (KE) were estimated in the

range $E_{51} = E/10^{51} \text{ erg} \sim 30 - 50$. Other *hypernovae* have been recognized, such as SN 1997ef and SN 2002ap. These hypernovae span a wide range of properties, although they all appear to be highly energetic compared to normal core-collapse SNe. The mass estimates, obtained from fitting the optical light curves and spectra, place hypernovae at the high-mass end of SN progenitors.

In contrast, SNe II 1997D and 1999br were very faint SNe with very low kinetic energy. This leads to a diagram with the explosion energy E or the ejected ^{56}Ni mass $M(^{56}\text{Ni})$ as a function of the main-sequence mass M_{ms} of the progenitor star which shows two branches. Therefore, one is led to the conclusion that SNe from stars with $M_{\text{ms}} \gtrsim 20\text{-}25 M_{\odot}$ have different E and $M(^{56}\text{Ni})$, show a bright, energetic *hypernova branch* at one extreme and a faint, low-energy SN branch at the other extreme. For the faint SNe, the explosion energy was so small that most ^{56}Ni fell back onto the compact remnant. Thus the faint SN branch may become a *failed* SN branch at larger M_{ms} . Between the two branches, there may be a variety of SNe.

This trend could be interpreted as follows. Stars more massive than $\sim 25 M_{\odot}$ form a black hole at the end of their evolution. Stars with non-rotating black holes are likely to collapse *quietly* ejecting a small amount of heavy elements (Faint supernovae). A preceding stage could be the temporary formation of a neutron star and a supernova explosion, but fallback of matter leads to an increase of the neutron star mass beyond its maximum stable value. (The combination of mixing processes in the innermost ejecta and fallback can influence the ejecta composition.) In contrast, stars which formed rotating black holes are likely to give rise to hypernovae. Here disk and jet formation seems to be a necessary ingredient to understand the explosion. (An option is that hypernova progenitors might form from the rapidly rotating cores after spiraling-in of a companion star in a binary system).

4.5 The Aftermath of Explosions

In the preceding sections we have given an overview of hydrostatic and explosive burning processes in massive stars, the individual phases of stellar evolution, the endstages like core collapse, explosive nucleosynthesis products from supernovae explosions and possible variations in outcome if core collapse ends in black hole formation, related possibly to hypernovae or gamma-ray bursts. What remains to be done is to (i) get a complete picture from stellar models and simulations how hydrostatic/wind and explosive contributions add up to the complete yields observed in such events, (ii) verify such models with individual observations, e.g. from lightcurves and from remnants, (iii) finally to integrate all these events/stellar yields over a mass distribution and metallicity evolution of galaxies, in order to make comparisons with overall galactic observations of very long-lived radioisotopes which average over several stellar generations.

4.5.1 Massive Stars and Their Complete Yields

In section 4.4 we have introduced in Eq. (4.4) a simplified rule which determined at which radius certain temperatures are attained in the explosion, assuming that the explosion energy is distributed at all times in a homogenous bubble within the radius of the present shock front position. If one knows the radial mass distribution $M(r)$ in pre-explosion models through which the shock front passes, one knows the amount of matter which encountered certain burning conditions. In table 4.5.1 we provide this information for different initial stellar masses (still based on models from Nomoto and Hashimoto (1988)), at (up to) which radial mass position explosive (complete and incomplete) Si-burning, O-burning, Ne/C-burning are occurring (upper portion) and the size of these regions (in M_{\odot}) involved (lower portion). In addition, we give the size of the CO-core of prior He-burning in stellar evolution. To first order matter between explosive C/Ne-burning and the stellar surface is ejected unchanged. As this simplified treatment does not know anything of the explosion mechanism which produced this explosion energy, the position of the mass cut is not known and therefore also not the total amount of complete Si-burning material. The core sizes given (e.g. CO-core after He-burning) also make no difference whether this matter resulted from initial core burning of this burning stage or subsequent outward propagating shell burning (e.g. shell He-burning of shell C-burning) which produce specific isotopes of interest (e.g. ^{26}Al , ^{60}Fe as discussed in Sect. 4.3).

Initially we want to focus here on the explosive burning phases. We also want to add that table 4.5.1 includes always two values for the radial masses involved, (a) from the simplified Eq.(4.4) applied to the appropriate stellar model ($M(r)$) and (b) resulting from an actual explosion calculation (initiated via a thermal bomb), as obtained in Thielemann et al (1996). When comparing these numbers, we see a quite close agreement, except for the most massive star where non-negligible deviations are encountered.

Table 4.9 Masses and products in explosive and hydrostatic burning

$M(r)$	Burning site	13 M_{\odot}	15 M_{\odot}	20 M_{\odot}	25 M_{\odot}
Fe-core	hydr. Si-burning	1.18	1.28	1.40	1.61
mass cut	(expl. mechanism)	?	?	?	?
ex Si-c	expl. compl. Si-burning	1.42	1.40	1.46	1.44
ex Si-i	expl. incompl. Si-burning	1.70	1.69	1.79	1.80
ex O	expl. O-burning	1.48	1.47	1.52	1.51
ex C/Ne	expl. Ne-burning	1.75	1.75	1.85	1.89
CO-core	hydr. He-burning	1.54	1.54	1.57	1.57
		1.81	1.81	1.92	2.00
		1.66	1.65	1.73	1.70
		2.05	2.05	2.26	2.40
		1.75	2.02	3.70	5.75
ΔM	(Main) products, major radioactivities				
ex. Si-c	"Fe", He; $^{56,57}\text{Ni}$, $^{61,62}\text{Zn}$, ^{59}Cu , ^{52}Fe , ^{48}Cr	?	?	?	?
ex. Si-c	^{44}Ti , νp process, r process?	?	?	?	?
ex. Si-i	Si, S, Fe, Ar, Ca; ^{55}Co , ^{52}Fe , ^{48}Cr	0.06	0.07	0.06	0.07
ex. O	O, Si, S, Ar, Ca	0.05	0.06	0.05	0.06
ex. C/Ne	O, Mg, Si, Ne; ^{26}Al , p process	0.06	0.07	0.05	0.06
hydr. He	O, Ne, Mg, Si, s process	0.07	0.11	0.16	0.13
		0.24	0.24	0.34	0.40
		0.09	0.10	0.29	0.32
		1.65	1.65	3.49	3.35

Based on this information we want to discuss complete nucleosynthesis yields, including explosive processing (also the νp process, affected by neutrinos in the innermost ejecta, as well as the p process in explosive Ne/O-burning), hydrostatic yields from the outer layers (including s process) which are ejected unaltered, and prior wind yields lost during stellar evolution. Then we concentrate on the long-lived radioactivities ^{26}Al , ^{60}Fe , ^{44}Ti , other Fe-group and lightcurve-determining nuclei, including their origin which is e.g. important for ^{26}Al and ^{60}Fe , which have hydrostatic burning as well as explosive origins. The r process in the neutrino wind or possibly polar jets has been presented qualitatively with entropy, Y_e and expansion timescale as free parameters or expansion timescale of neutron star matter as a free parameter. Presently no realistic explosion models are available to discuss this matter in a real stellar context, but a short discussion of long-lived radioactive chronometers is presented.

Table 4.5.1 provides the following conclusions: The amount of ejected mass from the unaltered (essentially only hydrostatically processed) CO-core varies strongly over the progenitor mass range. The variation is still large for the matter from explosive Ne/C-burning, while the amount of mass from explosive O- and Si-burning is almost the same for all massive stars. Therefore, the amount of ejected mass from the unaltered (essentially only hydrostatically processed) CO-core and from explosive Ne/C-burning (C, O, Ne, Mg) varies strongly over the progenitor mass range, while the amount of mass from explosive O- and Si-burning (S, Ar, and Ca) is almost the same for all massive stars. Si has some contribution from hydrostatic burning and varies by a factor of 2-3. The amount of Fe-group nuclei ejected depends directly on the explosion mechanism which also affects the Y_e in these inner zones. Thus, we have essentially three types of elements, which test different aspects of supernovae, when comparing with individual observations. The first set (C, O, Ne, Mg) tests the stellar progenitor models, the second (Si, S, Ar, Ca) the progenitor models and the explosion energy in the shock wave, while the Fe-group (beyond Ti) probes clearly in addition the actual supernova mechanism. Thus, we require that all three aspects of the predicted abundance yields are based on secure modeling (stellar evolution, explosion energy, and explosion mechanism) in order to be secure for their application in lightcurve modeling, radioactivities in remnants as well as the the in chemical evolution of galaxies.

r -process ejecta

The biggest uncertainty exists for the absolutely innermost ejecta, i.e. the possible r process ejection in the neutrino wind. This matter escapes after the supernova explosion shock wave was launched and the continuing neutrino escape from the remaining neutron star leads to its *surface erosion/evaporation*, i.e. a neutron-rich wind which could trigger an r process (Qian and Woosley, 1996). Early modelling seemed to lead to a full r -process abundance distribution (Woosley et al, 1994), which was, however, already then questioned by other investigations (Takahashi et al, 1994), when utilizing the entropies obtained from their calculations. Results with present neutrino physics and detailed transport modeling seem to find the opposite behavior, i.e. proton-rich conditions for more than the first 10s after the explo-

sion (Fischer et al, 2009a; Marek and Janka, 2009), as noticed first by Liebendörfer et al (2003) and discussed in Sect. 4.4 together with the νp process. A major question is if and how this turns to be neutron-rich in later phases, what physics causes this change (the nuclear EoS or neutrino properties?), and how very high entropies can be attained to produce also the heaviest nuclei. Present observations of low metallicity stars show huge variations in heavy r -process content and indicate that in most explosions the latter is not taking place, making the *full* r process a rare event. Then typical supernovae would only provide a weak r -process environment. Whether either high entropies are only attained in exceptional cases or other origins of low entropy, highly neutron-rich matter (neutron star mergers or neutron-rich jets from rotating core collapse supernovae, Freiburghaus et al (1999b); Cameron (2001, 2003)) cause the main r process has to be explored, in parallel with the still remaining challenges of nuclear physics far from stability.

In the preceding sections we have shown that there exists a principle understanding about the nuclear working of the r process and that it is possible to reproduce solar system r -process abundances by superpositions of components with varying environment conditions. What seems not possible, yet, is to clearly identify, without doubt, the responsible astrophysical site. Taking, however, such r process superposition fits as *zero-age* abundances with e.g. production ratios for $^{232}\text{Th}/^{238}\text{U}$ or other actinide (chronometer) nuclei, one can predict such ratios also as a function of decay time (present-age abundances) and identify ages of very metal-poor stars which were born with a fresh pollution of an r process pattern (see e.g. Cowan et al (1991, 1999); Thielemann et al (2002); Kratz et al (2007) and references therein). The typical result is that these chronometers indicate an age of the oldest stars in our Galaxy in the range of 14-15 Gyr with an uncertainty of about 3-4 Gyr. A more complex utilization of long-lived r -process radioactivities in terms of a continuing enrichment in galactic evolution is given in Ch. 2.

Fe-group and beyond

The neutrino wind works via evaporation of the neutron star surface after the supernova shock wave emerged and caused the explosion. The innermost matter which experienced the shock is thus ejected earlier and a typical example for its composition is seen in Fig. 4.12, which shows the zones of complete Si-burning with α -rich freeze-out. The change in abundances at $M = 1.63M_{\odot}$ is due to a change in Y_e in the original stellar model, which was utilized for explosive nucleosynthesis predictions just by introducing a thermal bomb of 10^{51}erg . If one accounts correctly for the neutrino interactions during the collapse and explosion, this turns matter even slightly proton-rich ($Y_e > 0.5$), see the discussion of the νp process in Sect. 4.4 and Figs. 4.16, 4.17 and 4.18 (Fröhlich et al, 2006a,b; Pruet et al, 2005, 2006; Wanajo, 2006). This results also in substantial fractions of ^{64}Ge (decaying to ^{64}Zn via ^{64}Ga , both of short half-life in the minute to second regime and therefore not of interest in terms of radioactivities with long half-lives), but within the νp process also to the production of Sr and heavier nuclei. The isotopic ratios ^{58}Ni , $^{60,61,62}\text{Zn}$ change strongly. Alpha-nuclei such as ^{40}Ca , ^{44}Ti , ^{48}Cr , and ^{52}Fe are affected as well. Higher entropies and Y_e -values close to 0.5 increase the fraction of these α -nuclei (and would in hyper-

novae also cause a substantial production of ^{64}Ge as discussed in Sect. 4.4 in the context of the νp process (see also Arcones and Montes, 2010; Roberts et al, 2010). It was also discussed there that probably only a small fraction of black-hole producing events actually lead to hypernovae (not 50% as assumed in some cases (Nomoto et al, 2006; Kobayashi et al, 2006)). However, this reduction in the ^{64}Ge production can well be balanced by the larger ^{64}Ge production in regular supernovae due to the correct inclusion of neutrino-interactions and their effect on increasing Y_e to values larger than 0.5.

Other explosive burning zones, ^{44}Ti , ^{26}Al

While such a discussion is of general interest for the composition of the Fe-group and filling in of lighter p -process nuclei, which are underproduced in the classical picture (see Sect. 4.4), we would like to concentrate here on long-lived radioactivities. The nucleus which is mainly produced in the complete Si-burning regime with α -rich freeze-out is ^{44}Ti . As discussed above, its total amount depends on the matter experiencing this burning outside the mass cut (which is in principle unknown without successful explosion calculations). Several authors have made assumptions on its position, either based on total ^{56}Ni ejecta in thermal bombs (Thielemann et al, 1996; Nomoto et al, 2006) or entropy jumps in the pre-collapse models in piston-induced explosions (Woosley and Weaver, 1995,?). Based on these assumptions different authors find somewhat different predictions, which are, however, a relatively flat function of the stellar progenitor mass. The values of Thielemann et al (1996) range between 2×10^{-5} and $1.5 \times 10^{-4} M_\odot$. The interesting point here is that variations in the Y_e -structure can lead to changes up to a factor of 2. Here either the initial pre-collapse distribution was assumed (with possible Y_e -dips in the innermost parts from shell O-burning) or a smoothed flat Y_e -distributions closer to 0.5 (which also reproduces the solar $^{56}\text{Fe}/^{57}\text{Fe}$ -ratio). This latter case leads to the higher values and will also be closer to reality when neutrino interactions are taken into account during the explosion (see discussion above on the νp process and Y_e). Rauscher et al (2002) and Tur et al (2009) find smaller values (either $1.5 - 5 \times 10^{-5}$ and $3.5 - 6 \times 10^{-5} M_\odot$). The latter is based on a readjustment of the 3α - and $^{12}\text{C}(\alpha, \gamma)^{16}\text{O}$ -rates to most recent experimental values, which does not have a drastic influence, however. Indirectly, core sizes and other stellar properties, including explosion energies, can enter.

^{44}Ti is only made in the explosive phase of complete Si-burning with α -rich freeze-out from charged particle equilibrium. There have been investigations on the reactions producing ($^{40}\text{Ca}(\alpha, \gamma)^{44}\text{Ti}$) and destroying ($^{44}\text{Ti}(\alpha, p)^{47}\text{V}$) reactions as well as the half-life of ^{44}Ti . Due to the fact, that this is a freeze-out from equilibrium, Hoffman et al (1999) found that even rate changes by a factor of 6 change the ^{44}Ti production only by a factor of 1.3. What is different between both approaches, leading to productions either larger or smaller than $5 \times 10^{-5} M_\odot$, is the introduction of the explosion (i) a thermal bomb, (ii) a piston. This apparently leads to higher entropies in the first case and a more intense α -rich freeze-out. It should also be mentioned that non-spherical explosions can lead to larger ^{44}Ti -production than spher-

ical models (Nagataki et al, 1998; Nagataki, 2000). A comparison to observations from either SN 1987A or the SNR Cas A is discussed in the following subsection.

Complete explosive nucleosynthesis predictions for a range of progenitor stars with induced explosions have been given by a number of authors in recent years (Rauscher et al, 2002; Woosley et al, 2002; Nomoto et al, 2006; Limongi and Chieffi, 2006; Woosley and Heger, 2007; Umeda and Nomoto, 2008), updating some of the discussions made above, based on earlier models (Woosley and Weaver, 1995; Thielemann et al, 1996). Also specific investigations were undertaken for Pop III low metallicity stars (Umeda and Nomoto, 2005; Tominaga et al, 2007). We limit the present discussion to stars below $130 M_{\odot}$ which still undergo core collapse and do not explode via explosive O-burning like the so-called pair-creation supernovae (Heger et al, 2003). While such explosions seem theoretically possible, provided that these massive cores can result from stellar evolution, the apparent absence of predicted abundance patterns in low metallicity stars plus our present understanding of massive stars with rotation (Maeder and Meynet, 2010), seem to exclude this outcome.

Then, the basic pattern given in table 4.5.1 always applies. The abundances from incomplete Si-burning and explosive O-burning can explain Galactic chemical evolution. As mention in Sect. 4.4, the classical p process takes place in explosive Ne-burning via photodisintegrations of pre-existing heavy nuclei, but even with the best nuclear input the underproduction of light p -nuclei cannot be solved. The solution can be obtained by adding a *light (heavy) element primary process* (LEPP, (Travaglio et al, 2004) where the best candidate is the νp process. Thus, the classical p -process isotopes have to be explained by a superposition of the innermost proton-rich complete Si-burning ejecta with those of explosive Ne-burning in outer zones.

The scheme indicated in table 4.5.1 is a bit too simplified when considering the ejecta of outer layers, whose composition was produced during stellar evolution and ejected essentially unaltered during the explosion. However, the *CO-core* scheme is not sufficient to describe massive-star yields. While it includes all matter which underwent He-burning, it does not differentiate between core He-burning and shell He-burning. The latter occurs at higher temperatures and has specific features different from core He-burning. In a similar way, the NeO-core contains all matter which underwent C-burning during stellar evolution, but also here, no difference is made between core C-burning and higher temperature shell C-burning. The same is true for Ne-burning.

^{26}Al production during stellar evolution was discussed in Sect. 4.3; now we include also the explosive production of ^{26}Al . It occurs in the regions of explosive Ne/C-burning. Under these conditions ^{25}Mg is produced via $^{24}\text{Mg}(n, \gamma)^{25}\text{Mg}$ and the protons arise from $^{23}\text{Na}(\alpha, p)^{26}\text{Mg}$, similar to the reaction pattern shown in table 4.4 for hydrostatic Ne-burning (and partially also C-burning). Under explosive conditions at temperatures of the order $2.3 \times 10^9 \text{K}$, these burning stages act explosively in a combined way, and the temperatures are also sufficiently high to utilize the released protons for the $^{25}\text{Mg}(p, \gamma)^{26}\text{Al}$ reaction. However, as also seen from table 4.4, neutrons are abundantly produced. They act as the main destructive

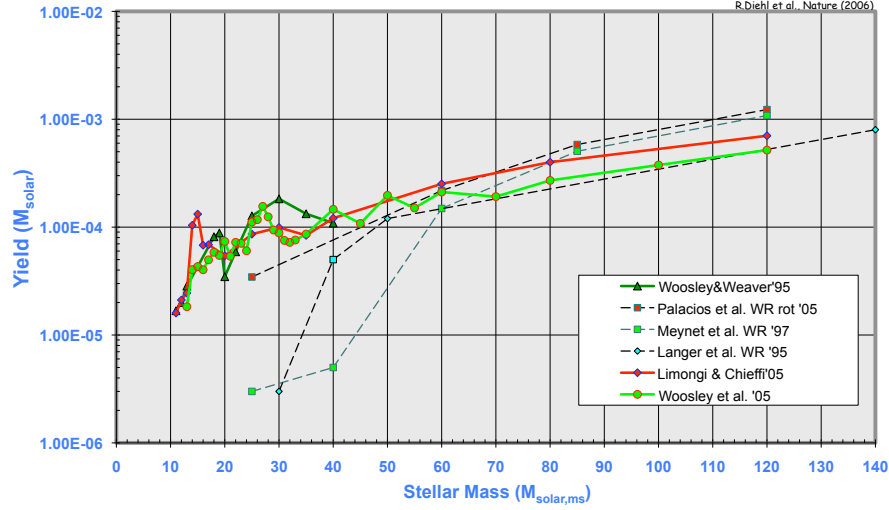


Fig. 4.20 The ^{26}Al yields from wind ejections and from the explosive release in the supernova, as a function of the initial mass of the star (as assembled by Diehl et al, 2006, (in their appenix).

species via (n, p) and (n, α) reactions. As can be seen from table 4.5.1, the mass involved in explosive Ne/C burning is strongly dependent on the progenitor mass. Thus, we expect a dramatic increase with increasing initial stellar masses, which is exactly what we see. Limongi and Chieffi (2006) have analyzed in detail the contributions from (i) wind ejecta during stellar evolution, (ii) hydrostatic burning products ejected during the explosion, and (iii) explosive Ne/C-burning. The latter dominates up to about $60 M_{\odot}$ and increases from initially about $2 \times 10^{-5} M_{\odot}$ per event to $2 - 3 \times 10^{-4} M_{\odot}$. Then wind ejecta start to take over and flatten out close to $10^{-3} M_{\odot}$ at initial stellar masses of 120-140 M_{\odot} . The latter are subject to rotational effects (Langer et al, 1995; Meynet et al, 1997; Palacios et al, 2005) and increase in fact with higher rotation rates (see Sect. 4.3). Tur et al (2009) have reanalyzed this behavior in the lower mass range from 15-25 M_{\odot} and confirmed this trend. They also did not find a strong dependence of the result on the He-burning reactions 3α - and $^{12}\text{C}(\alpha, \gamma)^{16}\text{O}$. They show nicely how ^{26}Al is produced starting in H-burning, but the final explosion produces close to a factor of 10 more of it. Yields from different studies have been assembled in Fig. 4.20.

^{60}Fe

Massive-star yields for ^{60}Fe are summarized in Fig. 4.21 and should only be mentioned here for completeness, although not produced in explosive nucleosynthesis. It is entirely produced in the s process during shell He-burning and thus a pure product of stellar evolution. The explosion only acts to eject the corresponding layers. As ^{60}Fe is produced via neutron capture of beta-unstable ^{59}Fe , a relatively high neutron density of about $3 \times 10^{10} \text{cm}^{-3}$ is required in order for its efficient produc-

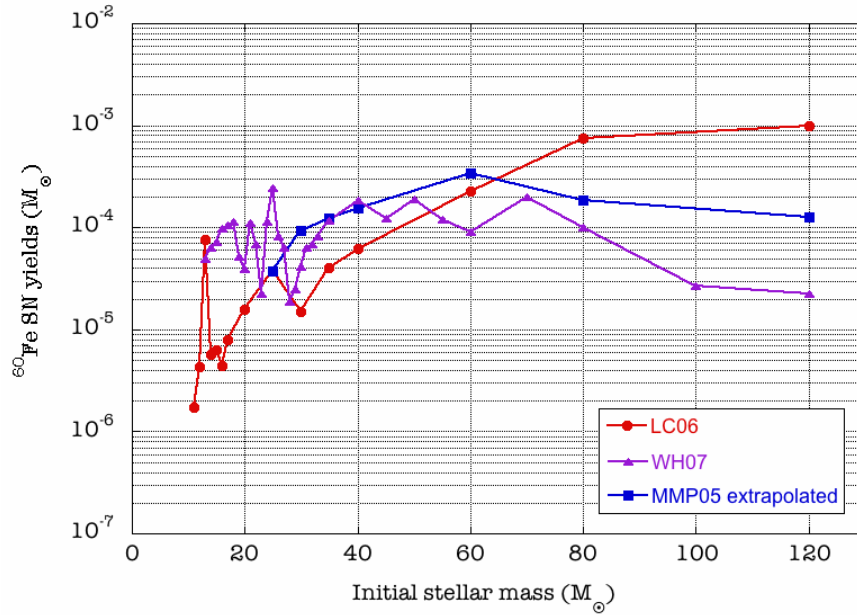


Fig. 4.21 The ^{60}Fe yields from the explosive release in the supernova, as a function of the initial mass of the star (as assembled by ?).

tion. This is only attained in shell He-burning during late evolution stages after core C-burning. The production ranges from 2×10^{-6} to $8 \times 10^{-5} M_{\odot}$ for initial stellar masses between 10 and $40 M_{\odot}$. This result is dependent on the He-burning reactions 3α - and $^{12}\text{C}(\alpha, \gamma)^{16}\text{O}$, as they compete with the neutron producing reaction $^{22}\text{Ne}(\alpha, n)^{25}\text{Mg}$. There exist also uncertainties in $^{59}\text{Fe}(n, \gamma)^{60}\text{Fe}$ and $^{60}\text{Fe}(n, \gamma)^{61}\text{Fe}$, which cause yield uncertainties by a factor of up to 5. If the star experiences strong mass loss, the He-burning shell does not encounter the higher density conditions required for the high neutron density of $3 \times 10^{10} \text{cm}^{-3}$. Thus for initial stellar masses in excess of $40 M_{\odot}$, the mass loss treatment can also lead to variations in predicted yields of more than a factor of 10. Apparently a high mass loss rate is required to not overproduce ^{60}Fe in high mass stars $M > 40 M_{\odot}$ (Limongi and Chieffi, 2006) with respect to γ -ray line constraints (see Wang et al, 2007, and Ch. 7).

4.5.2 Observational Diagnostics: Lightcurves, Spectra and SNR

Lightcurves

Supernova light curves are powered by radioactive decays. Very early interpretations of supernova lightcurves related them to the radioactive decay of ^{254}Cf (Burbidge

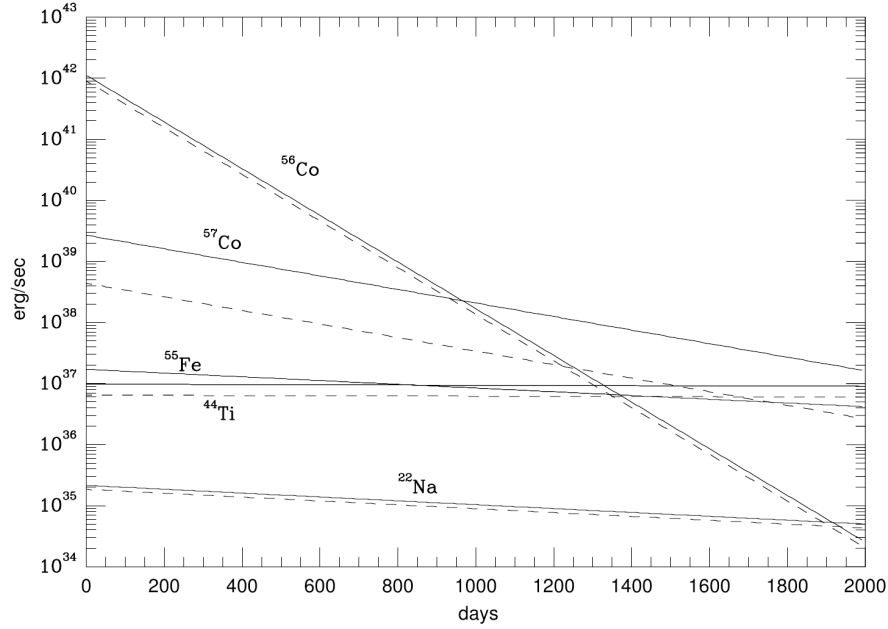


Fig. 4.22 Total energy release due to the decay of long-lived radioactive species (dashed lines) and due to the release in terms of thermalized decay photons (solid lines). The ejected masses of radioactive species are taken from a $20 M_{\odot}$ model for SN 1987A (Thielemann et al, 1990, 1996) .

et al, 1957). In fact, a strong r process (with fission-cycling) would cause observable features based on the decay of heavy radioactive nuclei. (This question was addressed very recently with respect to r -process ejecta from neutron star mergers (Metzger et al, 2010)). Supernova lightcurves, however, are dominated by Fe-group ejecta. In addition to abundant ^{56}Ni , there are a number of radioactive nuclei which will decay on time scales of ms up to 10^7y . Here we only want to concentrate on a few nuclei, which by a combination of their abundances and half-lives, can be of importance. These nuclei are ^{56}Co (^{56}Ni), ^{57}Co (^{57}Ni), ^{55}Fe (^{55}Co), ^{44}Ti , and ^{22}Na . For a $20 M_{\odot}$ star like SN 1987A they were predicted with total masses of 0.07, 3.12×10^{-3} , 3.03×10^{-4} , 1.53×10^{-4} , and $1.33 \times 10^{-7} M_{\odot}$ (Thielemann et al, 1990, 1996).

Observations of light curves in radiation which reflects the thermalized energy of this radioactivity constrained these values to $M(^{56}\text{Ni}) \approx 0.071 M_{\odot}$ (e.g. Suntzeff and Bouchet (1990)) and $M(^{57}\text{Ni}) \approx 3.3 \times 10^{-3} M_{\odot}$ (Fransson and Kozma (1993) and references therein). Only more recently a very careful analysis confirmed an upper limit on ^{44}Ti of the order $1.1 \times 10^{-4} M_{\odot}$ (Lundqvist et al, 2001).

Generally, after beta-decay or electron capture, a daughter nucleus is produced in an excited state (^{55}Fe is a notable exception, see below). The ground state is reached by one or several gamma transitions, observable by current gamma-ray detectors for nearby sources (see Sect. 10.1). Photons, positron-electron annihilations following

β^+ -decays, and the kinetic energy given to the decay products can contribute to the light curve at later times.

The number of photons released for each of the transitions, occurring in the daughter nucleus after beta-decay, is equal to the number of decays N_d , multiplied with the appropriate percentage of the occurrence (*branching ratio*) for the specific transition. The total energy released corresponds to the product of the number of decays with the decay Q-value:

$$N_d(t) = -\frac{dN}{dt}(t) = \lambda N_o \exp(-\lambda t) \quad \frac{dE}{dt}(t) = Q N_d(t) = Q \lambda N_o \exp(-\lambda t), \quad (4.5)$$

where $\lambda = \ln 2 / t_{1/2}$ is the decay rate of the nucleus. The initial number of radioactive nuclei can be calculated from their total mass by $N_o = M / A m_u$, with A being the nucleon number of the nucleus, m_u the atomic mass unit, and M the mass given above. When using the radioactivity half-lives of relevant isotopes expected in supernova ejecta (i.e., 78.76d, 271.3d, 2.7y, 54.2y, and 2.602y, and atomic Q-values of 4.566, 0.835, 0.232, 3.919, and 2.842 MeV) we can estimate radioactive-energy generation rates in erg s^{-1} and the total number of decays per sec. The Q-value used for ^{44}Ti combines the subsequent decays of ^{44}Ti and ^{44}Sc . Q-values include all available energies, i.e. the kinetic energy of the decay products, the energy in photons, the annihilation energy of positron-electron pairs in β^+ -decays, and the neutrino energy. At densities prevailing in the expanding remnant, neutrinos will escape freely and their energy has to be subtracted, which leaves corrected values for the appropriate energy deposits of 3.695, 0.136, 0.0, 2.966, and 2.444 MeV. Because the electron capture on ^{55}Fe does only lead to an energetic neutrino, there is no local energy deposition from this isotope¹⁴. Gamma transitions following the decays of the other isotopes under consideration obtain candidate γ -rays at (rounded to full percent values): ^{56}Co , 847 keV (100%), 1038 keV (14%), 1238 keV (68%), 1772 keV (16%), 2599 keV (17%); ^{57}Co , 122 keV (86%), 136 keV (11%); ^{44}Ti , 78 keV (93%), 68 keV (88%), 147 keV (9%), 1157 keV (100%); ^{22}Na , 1275 keV (100%; branching ratios given as percentages per decay). If positrons from β^+ -decay slow down and annihilate with electrons locally within the supernova envelope, the full neutrino-loss corrected energy corresponding to the reaction Q-value will be deposited in the envelope. Observable signatures include high energy photons such as the ones from the gamma transitions, and their Compton scattered and completely thermalized descendants¹⁵.

¹⁴ This situation was recently re-evaluated by Seitzzahl et al (2009). The electron capture occurs from an electron in an atomic orbit, leaving a hole which can be filled by other electrons cascading down to fill this hole, thus emitting photons - X-rays - or depositing the energy in ejecting outer electrons - Auger electrons. Thus, in cases where only ground-state to ground-state electron capture occurs and the energy is emitted in an escaping neutrino only Auger electrons or X-rays can contribute to local energy deposition.

¹⁵ Deposition of energy from radioactive decay involves absorption of high-energy photons, slowing down of $\sim\text{MeV}$ -type energy electrons and positrons, and proper treatment of temporary energy reservoirs such as ionization and inhibited radioactive decay from completely-ionized nuclei (see, e.g., Sim et al, 2009; Mochizuki et al, 1999; Woosley et al, 2007)

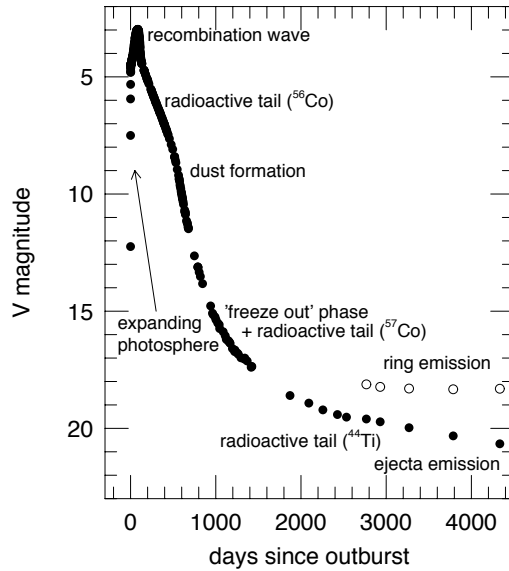


Fig. 4.23 Observed (visual) lightcurve of SN1987A for the first 1500 days from Leibundgut and Suntzeff (2003).

Then the sum of all individual contributions discussed above would make up the bolometric lightcurve of the supernova (see Fig.4.5.2). The *light curve*, i.e. the brightness as a function of time, will be dominated first by the decay of ^{56}Co , and then ^{57}Co and ^{44}Ti , if one neglects possible radiation from a pulsar. ^{22}Na never plays a dominant role for the lightcurve. At lower densities (and later times), escaping high energy photons or positrons lead to a reduction of the brightness of *bolometric* emission. This can be seen in late time observations as shown e.g. in Leibundgut and Suntzeff (2003) (see Fig.4.23). An important consistency check would be to compare this bolometric light curve (which includes only optical, UV and IR emission, hence thermalized gas and dust components) to the high-energy photons more directly reflecting radioactive decays. At late times, those high energy photons escape freely.

The γ -ray detections of SN1987A were the first to identify γ -rays from ^{56}Co decay. Later improved observations by CGRO for ^{56}Co and ^{57}Co were a direct proof of these unstable species in the right amounts. It turned out that Ni decay γ -ray lines were seen with the Gamma-Ray Spectrometer on the Solar Maximum Mission (Matz et al, 1988; Leising and Share, 1990) significantly earlier than expected from a spherically stratified distribution of elements, where the Fe-group nuclei are produced in the center. This is understood from deviations from spherical symmetry in the expanding remnant, bringing Ni-rich clumps to the surface earlier by convective instabilities, mixing $^{56}\text{Ni}/^{56}\text{Co}$ to outer layers at early times. Gamma-ray line profiles measured with high spectral resolution indicated Doppler broadening of the lines from their ejecta motion (Tueller et al, 1990).

Many supernova remnants (such as the 300-year old Cas A remnant) show mixing in their ejecta (Vink, 2005). While there existed some theoretical indications that this is due to instabilities of the propagating shock wave, it is generally and more plausibly associated with the expansion of the supernova into an inhomogeneous medium. SN1987A observations showed clearly that mixing is part of the supernova explosion itself. Several independent reasons lead to such a conclusion. The supernova produces large amounts of unstable long-lived nuclei, the dominant abundance is found in the doubly-magic nucleus ^{56}Ni , which is produced in the innermost part of the ejecta. ^{56}Ni decays with half-lives of 6.1 days to ^{56}Co and 77.8 days to ^{56}Fe . After the beta-transition, deexcitations to the ground state of the daughter nucleus lead to the emission of high energy gamma-rays. While these gamma-rays would escape freely at low densities, Compton scattering will reduce their energies into the X-ray and even thermal regime at higher densities. With decreasing densities during the expansion, initially only thermalized photons will escape, then X-rays and finally gamma-rays. For SN1987A X-ray observations with GINGA, HEXE, and balloons and gamma-ray observations with the SMM-satellite and balloons actually agreed with this general behavior (e.g. Sunyaev et al, 1990; Leising and Share, 1990). The main problem was that the predicted time scales did not agree with the observations, where X-rays and gamma-rays appeared earlier than predicted. An agreement could only be obtained when part of the ^{56}Ni , being produced initially in the inner parts of the ejecta, was mixed out to larger distances (Fu and Arnett, 1989). Mixing is also required to explain the spread of expansion velocities seen in line widths of infrared observations for various elements and in the gamma ray lines of ^{56}Co . The inferred velocities differ strongly from the much smaller ones, expected from an expanding remnant, which maintains the stratified composition from explosive and hydrostatic nuclear burning. Other indications came from the modeling of the optical light curve. The best agreement between calculated and observed light curves were obtained for a composition which mixed a small fraction of Ni all the way into the $10M_{\odot}$ hydrogen envelope and hydrogen into the deeper layers, containing mostly heavy elements (see e.g. Benz and Thielemann (1990)).

The lightcurve from SN1987A could be reproduced with theoretical modelling, including the effects of X-ray and γ -ray escape, as well as mixing of ^{56}Ni . SNe Ib and Ic events, believed to be core collapse events without an overlying hydrogen envelope have to be treated accordingly. The combination of small masses involved (only He-cores or C-cores without H-envelope) and the assumption of mixing can reproduce the steeper decline than found in massive SNe II. A typical case of a type Ic supernova is SN 1998bw, associated with GRB 980425. The straight-forward modeling of the observed lightcurve (Sollerman et al, 2002), similar to the discussion in the beginning of this subsection (Nakamura et al, 2001), led to interpretations of a largely non-solar $^{56}\text{Ni}/\text{Fe}$ to $^{56}\text{Ni}/\text{Fe}$ ratio. The inclusion of internal conversion and Auger electrons, as suggested by Seitenzahl et al (2009) could naturally explain the observed slowdown of the lightcurve without invoking such extreme abundance ratios.

We note that in recent years photon transport calculations have reached major improvements, and are now able to consistently reproduce both light curves and

spectra from SNIa, and also from core collapse supernovae (e.g. Sim et al, 2009, for a description of the method). Presently, systematic uncertainties of the method are being investigated, and appear rather well understood (at least for SNIa (see, e.g., Woosley et al, 2007). As optical-to-IR light curves and spectra will be collected in abundance through large telescope survey programs for cosmological studies, it is likely that those (more indirect) measurements of core-collapse supernova nucleosynthesis will generate the tightest constraints to learn more about these events and their internal nuclear processes.

Optical/IR Spectra and Dust Formation

In the preceding subsection we laid out the framework of understanding supernova lightcurves. What is missing here, is the evolution of supernova spectra. The receding photosphere in terms of radial mass in an expanding, radiation-filled bubble can give clear indications of the element composition (as a function of time equivalent to declining Lagrangian mass). The problem of type II supernovae is that the huge H-envelope does not really contain much information in terms of nucleosynthesis. Type Ib and Ic supernovae, which lost their H- and possibly He-envelope, reveal much more information of the compact inner part, which experienced explosive processing (Matheson et al, 2001; Branch et al, 2002; Sauer et al, 2006). This is similar to type Ia supernovae, originating from exploding white dwarfs, which have been extensively utilized for abundance diagnostics.

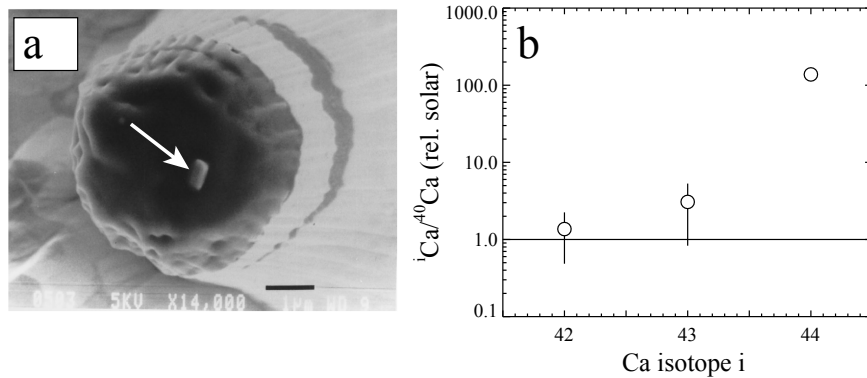


Fig. 4.24 (a) Scanning electron microscope image of a presolar graphite grain following isotopic measurement with an ion microprobe (from Nittler et al, 1996). The arrow indicates TiC sub-grain originally enclosed in graphite but revealed by the ion-probe sputtering. (b) Calcium isotopic composition of graphite grain shown in a. The $^{44}\text{Ca}/^{40}\text{Ca}$ ratio is 137 times the solar ratio, whereas the other Ca-isotopic ratios are normal within $2 - \sigma$ errors (the error bar in the isotope 44 abundance is smaller than the symbol size). This is a clear signature of in situ decay of live ^{44}Ti , originally condensed in the TiC sub-grain, and demonstrates that the grain formed in the ejecta of a supernova.

Another issue, which has been discussed already in the subsection on supernova lightcurves is related to convective instabilities and mixing of nucleosynthesis products. The extent of mixing is responsible for the element mixture in the expanding and cooling remnant when chemical reactions and dust formation set in. For which compositions and conditions does this environment lead to presolar grains with high melting temperatures which can survive the interstellar medium and formation of the solar system in order to be detected today in meteoritic inclusions? When do we form oxides, diamonds, hybonites, carbides ... and how selectively do they include matter from the regions where they form? How can we relate ^{26}Mg and ^{44}Ca excesses in presolar grains to initially embedded ^{26}Al and ^{44}Ti ? Fig. 4.24 shows an example of a grain attributed to supernova condensation. A discussion of these questions can be found in Sect. 10.3.

^{26}Al in the Vela Region

The Vela region appears prominent in several astronomical images of our Galaxy: It includes the Gum nebula and the Vela Supernova Remnant, both prominent agents to form nearby structures of the interstellar gas and bright in X- and radio emissions, and it includes the Vela pulsar where bright gamma-ray pulsations teach us about particle acceleration in neutron star magnetospheres, and furthermore with Vela X-1 a remarkable X-ray source and prototype of a binary system where a neutron star accretes wind material from a high-mass companion star. All those objects are relatively nearby, mostly in the foreground of the Vela molecular ridge which is one of the nearest star-forming regions and located in about 700 (± 200) kpc distance (Massi et al, 2007).

Three prominent sources have been discussed in the context of measuring ^{26}Al production for individual objects – all related to massive star and explosive nucleosynthesis, respectively (^{26}Al observations are discussed in Chap. 7 otherwise): The Vela supernova remnant, a recently-discovered supernova remnant called *Vela Junior*, and a Wolf-Rayet binary system $\gamma^2\text{Velorum}$.

The Vela supernova remnant is relatively nearby at 250 pc, about 10,000 y old, and spans an area of about 8° diameter on the southern sky. It hosts the Vela pulsar and a plerionic pulsar nebula at its center. Such a nearby supernova explosion in the recent past seems a unique opportunity to calibrate the ^{26}Al yield of a core-collapse supernova. With COMPTEL, diffuse and extended emission had been recognized from this direction (Diehl et al, 1995). But possibly-underlying extended ^{26}Al emission limits the precision of this measurement, the ^{26}Al gamma-ray flux attributed to this supernova remnant is $0.5\text{--}2.7 \cdot 10^{-5} \text{ ph cm}^{-2} \text{ s}^{-1}$. This is well within expectations (an ^{26}Al yield of $10^{-4} M_\odot$ would result in a gamma-ray flux of $\sim 2 \cdot 10^{-5} \text{ ph cm}^{-2} \text{ s}^{-1}$). INTEGRAL could not detect the supernova remnant, however, despite sufficient exposure. This may be due to the low surface brightness of this extended source and line broadening from the remaining ejecta motion of this young supernova remnant.

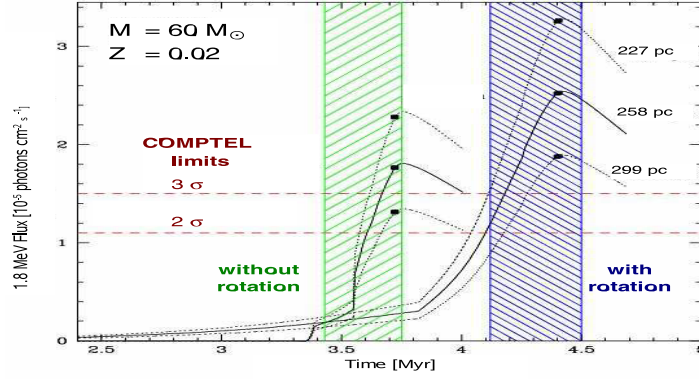


Fig. 4.25 The ^{26}Al gamma-ray flux estimated from ejection of ^{26}Al -rich envelope material during the Wolf-Rayet phase (Mowlavi et al, 2005). Shown are two different stellar models, with and without stellar rotation. In addition to delaying the WR phase, rotation also increases the ^{26}Al production. Shown are gamma-ray fluxes for different distances, not including the more recent and larger distance of 330–390 pc.

In refined X-ray imaging analysis of the Vela supernova remnant, a new supernova remnant was discovered being superimposed with a diameter of $\sim 2^\circ$ and named RXJ0852.0-46.22 or *Vela Junior* for short (Aschenbach, 1998). Early speculations about its ^{26}Al emission were stimulated from hints for ^{44}Ti emission, which would have implied that this supernova remnant would be both young and nearby; these could not be substantiated by additional measurements and studies. Now absence of ^{26}Al emission from Vela Jr. appears plausible, as the supernova remnant is probably older than 1000 y and more distant than 740 pc (Katsuda et al, 2009).

The $\gamma^2\text{Velorum}$ binary system is yet another tantalizing ^{26}Al source: It consists of a Wolf Rayet star (WR11) and an O-star companion. If the binary interactions can be ignored for ^{26}Al production of the WR11 star, this would be *the* opportunity to calibrate the ^{26}Al ejection during the Wolf-Rayet phase of a massive star, as the distance to this object has been derived from Hipparcos measurements as only 258 pc. The Wolf-Rayet star currently has a mass of $\sim 9 M_\odot$, with a $30 M_\odot$ O star companion (De Marco et al, 2000). Modeling the Wolf-Rayet star evolution in detail, and also accounting for possibly rapid rotation as it delays the wind ejection phase, Mowlavi et al (2005) show that the upper limit on ^{26}Al emission from WR11 would be hard to understand (Fig. 4.25). But doubts have appeared on the Hipparcos distance measurement, and current belief is that the system is part of the Vela OB2 association and rather at a distance of 330–390 pc (see Eldridge, 2009, and references therein). Additionally, the system's age may also be somewhat higher than estimated earlier (beyond 5 My, rather than 3–5 My) (Eldridge, 2009), and part of the ^{26}Al ejected in the earlier wind phase may now be spread over a shell extended by up to 6° (Mowlavi and Meynet, 2006), hence of lower surface brightness and still consistent with the non-detection by COMPTEL and INTEGRAL gamma-ray telescopes. Note, however, that binary mass transfer may have altered the evolution of

the Wolf-Rayet star substantially; this mutual impact on stellar evolution in close binaries is still very uncertain, but could lead to orders of magnitude increases of ^{26}Al production in rare cases (de Mink et al, 2009; Langer et al, 1998).

Supernova Remnants

An expanding supernova as it interacts with circumstellar matter gives rise to thermal X-ray line emission, for remnants of ages between \sim hundreds to several 10000 years. Although in principle circumstellar and ejecta materials are both contributing to such emission, and such atomic-shell emission carries uncertainties of ionization degrees and local temperature (to define a local thermodynamic equilibrium), abundance determinations for specific ejecta species can be made, and also have been explored for determinations both of supernova types and of nucleosynthesis yields (Hughes et al, 1995; Nymark et al, 2006). Even an (unsuccessful) search for X-ray line emission of radioactive ^{44}Sc from the decay of ^{44}Ti had been performed for the presumably young and nearby Vela Junior SNR (Hiraga et al, 2009, and references herein). More directly, the very late phases of the expansion into the interstellar medium permits the detection of long-lived radioactivities by detecting its decay photons of specific γ -ray energies, when these can escape freely from the expanding debris. Such detections can then be identified with the amount of matter existing in radioactive isotopes.

The discovery of the 1157 keV ^{44}Ti γ -ray line emission from the youngest Galactic SNR Cas A with COMPTEL (Iyudin et al, 1994) was the first direct proof that this isotope is indeed produced in SNe. This has been strengthened by the BeppoSAX/PDS detection of the two low-energy ^{44}Ti lines (Vink et al, 2001). By combining both observations, Vink et al (2001) deduced a ^{44}Ti yield of $(1.5 \pm 1.0) \times 10^{-4} M_{\odot}$. This value seemed higher than the predictions of most models (see the previous subsection), although it is not outside the error bars. Several aspects have been considered to explain this large value: a large energy of the explosion ($\approx 2 \times 10^{51}$ erg), asymmetries (Nagataki et al, 1998) currently observed in the ejecta expansion, and a strong mass loss of the progenitor consistent with the scenario of a Type Ib SN (Vink, 2004).

If ^{44}Ti ejection as seen in the Cas A event was typical for core-collapse events, the *gamma*-ray surveys made with COMPTEL (Dupraz et al, 1997; Iyudin et al, 1999) and with INTEGRAL (Renaud et al, 2006) should have seen several objects along the plane of the Galaxy through their ^{44}Ti decay emission (see Sect. 7.6 for a detailed discussion of Galactic supernovae and ^{44}Ti). From this, it had been concluded that ^{44}Ti ejection is rather a characteristic of a rare subclass of core-collapse supernovae (The et al, 2006).

From the three different γ -ray lines resulting from the ^{44}Ti decay chain, constraints for kinematic Doppler broadening can be derived: The Doppler broadening being a linear function of energy, it would broaden the 1157 keV line to values in the few to tens of keV range, which can be measured with Ge spectrometers; the lower-energy lines at 68 and 78 keV would not show significant kinematic broaden-

ing. Martin et al (2009) have exploited INTEGRAL/SPI spectrometer data to show that ^{44}Ti ejecta as seen by above measurements need to be faster than 500 km s^{-1} , as the 1157 keV line is not found with SPI and assumed to be broadened such as to disappear in instrumental background.

Ejecta from a Supernova Remnant on Earth



Fig. 4.26 Ocean crust sample as analyzed by Knie et al (2004) for ^{60}Fe content. The insert graph shows their result, i.e. the number of ^{60}Fe nuclei versus age as determined from cosmic-ray produced Be radioactivity.

^{60}Fe has been discovered through accelerator-mass spectroscopy (AMS) analyses of ocean crust material (Knie et al, 2004) (Fig. 4.26). If taken from places on Earth which are remote from any anthropogeneous contamination, such as in deep parts of the Pacific ocean, they provide a record of past composition of ocean water. Manganese crusts grow very slowly from sedimentation. Therefore, a rather small sample will cover tens of My of sedimentation history within a few cm of depth. ^{60}Fe production from cosmic ray irradiation in the atmosphere is unlikely, other systematic contaminations also seem low. The age of each depth layer can be determined from Be isotopes produced by cosmic rays in the atmosphere of the Earth, also ingested into ocean water with other atmospheric gas and dust. The AMS method is one of the most-sensitive techniques to detect small amounts of specific isotopes, reaching a sensitivity of 10^{-16} . Evaporization of chemically-prepared Fe-enriched crust samples and successive ion acceleration and mass spectrometry obtained the result shown in Fig. 4.26. This discovery was taken as evidence that debris from a very nearby supernova event must have been deposited on Earth about 3 million years ago. Unclear remain the deposition and crust uptake efficiencies, such that the quantitative estimation of interstellar ^{60}Fe flux or supernova distance is uncertain; distances in the 10–30 pc range have been discussed. Studies of other sediment

samples are underway to estimate these effects, and to confirm this exciting record of nearby supernova activity. Supernova nucleosynthesis of radioactivities appears close to our lives, indeed.

Acknowledgements

Many colleagues have contributed to the subject of this chapter. We would like to acknowledge specifically our discussions with Alessandro Chieffi, John Cowan, Iris Dillmann, Khalil Farouqi, Claes Fransson, Carla Fröhlich, Alexander Heger, Wolfgang Hillebrandt, Thomas Janka, Gunther Korschinek, Karl-Ludwig Kratz, Karlheinz Langanke, Bruno Leibundgut, Marco Limongi, Gabriel Martinez-Pinedo, Bradley Meyer, Georges Meynet, Yuko Mochizuki, Ewald Müller, Ken'ichi Nomoto, Igor Panov, Thomas Rauscher, Lih-Sin The, James Truran, Jacco Vink, Stan Woosley, and Hans Zinnecker.

References

- Aboussir Y, Pearson JM, Dutta AK, Tondeur F (1995) Nuclear Mass Formula via an Approximation to the Hartree-Fock Method. *Atomic Data and Nuclear Data Tables* 61:127–+, DOI 10.1016/S0092-640X(95)90014-4
- Arcones A, Montes F (2010) Production of Light Element Primary Process nuclei in neutrino-driven winds. *ArXiv e-prints* 1007.1275
- Arcones A, Janka H, Scheck L (2007) Nucleosynthesis-relevant conditions in neutrino-driven supernova outflows. I. Spherically symmetric hydrodynamic simulations. *A&A* 467:1227–1248, DOI 10.1051/0004-6361:20066983, *arXiv:astro-ph/0612582*
- Arnett D (1996) Supernovae and nucleosynthesis. an investigation of the history of matter, from the Big Bang to the present
- Arnett D, Meakin C, Young PA (2009) Turbulent Convection in Stellar Interiors. II. The Velocity Field. *ApJ* 690:1715–1729, DOI 10.1088/0004-637X/690/2/1715, 0809.1625
- Arnould M, Goriely S (2003) The p-process of stellar nucleosynthesis: astrophysics and nuclear physics status. *Phys. Rep.* 384:1–84, DOI 10.1016/S0370-1573(03)00242-4
- Aschenbach B (1998) Discovery of a young nearby supernova remnant. *Nature* 396:141–142, DOI 10.1038/24103
- Audi G, Wapstra AH, Thibault C (2003) The Ame2003 atomic mass evaluation (II). Tables, graphs and references. *Nuclear Physics A* 729:337–676, DOI 10.1016/S0375-9474(03)01809-8
- Aufderheide MB, Fushiki I, Woosley SE, Hartmann DH (1994) Search for important weak interaction nuclei in presupernova evolution. *ApJS* 91:389–417, DOI 10.1086/191942
- Benz W, Thielemann F (1990) Convective instabilities in SN 1987A. *ApJ* 348:L17–L20, DOI 10.1086/185620
- Bethe HA (1990) Supernova mechanisms. *Reviews of Modern Physics* 62:801–866, DOI 10.1103/RevModPhys.62.801
- Bethe HA, Brown GE, Applegate J, Lattimer JM (1979) Equation of state in the gravitational collapse of stars. *Nuclear Physics A* 324:487–533, DOI 10.1016/0375-9474(79)90596-7
- Blondin JM, Mezzacappa A, DeMarino C (2003) Stability of Standing Accretion Shocks, with an Eye toward Core-Collapse Supernovae. *ApJ* 584:971–980, DOI 10.1086/345812, *arXiv:astro-ph/0210634*

- Branch D, Benetti S, Kasen D, Baron E, Jeffery DJ, Hatano K, Stathakis RA, Filippenko AV, Matheson T, Pastorello A, Altavilla G, Cappellaro E, Rizzi L, Turatto M, Li W, Leonard DC, Shields JC (2002) Direct Analysis of Spectra of Type Ib Supernovae. *ApJ*566:1005–1017, DOI 10.1086/338127, [arXiv:astro-ph/0106367](#)
- Buchmann LR, Barnes CA (2006) Nuclear reactions in stellar helium burning and later hydrostatic burning stages. *Nuclear Physics A* 777:254–290, DOI 10.1016/j.nuclphysa.2005.01.005
- Buras R, Rampp M, Janka H, Kifonidis K (2003) Improved Models of Stellar Core Collapse and Still No Explosions: What Is Missing? *Physical Review Letters* 90(24):241,101–+, DOI 10.1103/PhysRevLett.90.241101, [arXiv:astro-ph/0303171](#)
- Buras R, Janka H, Rampp M, Kifonidis K (2006) Two-dimensional hydrodynamic core-collapse supernova simulations with spectral neutrino transport. II. Models for different progenitor stars. *A&A*457:281–308, DOI 10.1051/0004-6361:20054654, [arXiv:astro-ph/0512189](#)
- Burbidge EM, Burbidge GR, Fowler WA, Hoyle F (1957) Synthesis of the Elements in Stars. *Reviews of Modern Physics* 29:547–650, DOI 10.1103/RevModPhys.29.547
- Burrows A, Livne E, Dessart L, Ott CD, Murphy J (2006a) A New Mechanism for Core-Collapse Supernova Explosions. *ApJ*640:878–890, DOI 10.1086/500174, [arXiv:astro-ph/0510687](#)
- Burrows A, Reddy S, Thompson TA (2006b) Neutrino opacities in nuclear matter. *Nuclear Physics A* 777:356–394, DOI 10.1016/j.nuclphysa.2004.06.012, [arXiv:astro-ph/0404432](#)
- Burrows A, Dessart L, Ott CD, Livne E (2007) Multi-dimensional explorations in supernova theory. *Phys. Rep.*442:23–37, DOI 10.1016/j.physrep.2007.02.001, [arXiv:astro-ph/0612460](#)
- Cameron AGW (2001) Some Properties of r-Process Accretion Disks and Jets. *ApJ*562:456–469, DOI 10.1086/323869
- Cameron AGW (2003) Some Nucleosynthesis Effects Associated with r-Process Jets. *ApJ*587:327–340, DOI 10.1086/368110
- Cappellaro E, Evans R, Turatto M (1999) A new determination of supernova rates and a comparison with indicators for galactic star formation. *A&A*351:459–466, [arXiv:astro-ph/9904225](#)
- Chiappini C, Hirschi R, Meynet G, Ekström S, Maeder A, Matteucci F (2006) A strong case for fast stellar rotation at very low metallicities. *A&A*449:L27–L30, DOI 10.1051/0004-6361:20064866, [arXiv:astro-ph/0602459](#)
- Chieffi A, Limongi M (2004) Explosive Yields of Massive Stars from $Z = 0$ to $Z = Z_{\text{solar}}$. *ApJ*608:405–410, DOI 10.1086/392523, [arXiv:astro-ph/0402625](#)
- Costantini H, Formicola A, Imbriani G, Junker M, Rolfs C, Strieder F (2009) LUNA: a laboratory for underground nuclear astrophysics. *Reports on Progress in Physics* 72(8):086,301–+, DOI 10.1088/0034-4885/72/8/086301, 0906.1097
- Cowan JJ, Thielemann F, Truran JW (1991) The R-process and nucleochronology. *Phys. Rep.*208:267–394, DOI 10.1016/0370-1573(91)90070-3
- Cowan JJ, Pfeiffer B, Kratz K, Thielemann F, Sneden C, Burles S, Tytler D, Beers TC (1999) R-Process Abundances and Chronometers in Metal-poor Stars. *ApJ*521:194–205, DOI 10.1086/307512, [arXiv:astro-ph/9808272](#)
- De Marco O, Schmutz W, Crowther PA, Hillier DJ, Dessart L, de Koter A, Schweickhardt J (2000) The gamma Velorum binary system. II. WR stellar parameters and the photon loss mechanism. *A&A*358:187–200, [arXiv:astro-ph/0004081](#)
- de Mink SE, Pols OR, Langer N, Izzard RG (2009) Massive binaries as the source of abundance anomalies in globular clusters. *A&A*507:L1–L4, DOI 10.1051/0004-6361/200913205, 0910.1086
- Diehl R, Bennett K, Bloemen H, Dupraz C, Hermsen W, Knoedlseder J, Lichti G, Morris D, Oberlack U, Ryan J, Schoenfelder V, Steinle H, Varendorff M, Winkler C (1995) 1.809 MeV gamma-rays from the VELA region. *A&A*298:L25+
- Diehl R, Halloin H, Kretschmer K, Lichti GG, Schönfelder V, Strong AW, von Kienlin A, Wang W, Jean P, Knödseder J, Roques JP, Weidenspointner G, Schanne S, Hartmann DH, Winkler

- C, Wunderer C (2006) Radioactive ^{26}Al from massive stars in the Galaxy. *Nature* 439:45–47, DOI 10.1038/nature04364, arXiv:astro-ph/0601015
- Dillmann I, Rauscher T, Heil M, Käppeler F, Rapp W, Thielemann F (2008) p-Process simulations with a modified reaction library. *Journal of Physics G Nuclear Physics* 35(1):014,029–+, DOI 10.1088/0954-3899/35/1/014029, 0805.4756
- Duan H, Fuller GM, Qian Y (2006) Collective neutrino flavor transformation in supernovae. *Phys. Rev. D* 74(12):123,004–+, DOI 10.1103/PhysRevD.74.123004, arXiv:astro-ph/0511275
- Duan H, Fuller GM, Carlson J, Qian Y (2007) Neutrino Mass Hierarchy and Stepwise Spectral Swapping of Supernova Neutrino Flavors. *Physical Review Letters* 99(24):241,802–+, DOI 10.1103/PhysRevLett.99.241802, 0707.0290
- Duflo J, Zuker AP (1995) Microscopic mass formulas. *Phys. Rev. C* 52:23–+, DOI 10.1103/PhysRevC.52.R23, arXiv:nucl-th/9505011
- Dupraz C, Bloemen H, Bennett K, Diehl R, Hermsen W, Iyudin AF, Ryan J, Schoenfelder V (1997) COMPTEL three-year search for galactic sources of ^{44}Ti gamma-ray line emission at 1.157 MeV. *A&A* 324:683–689
- Ekström S, Meynet G, Chiappini C, Hirschi R, Maeder A (2008) Effects of rotation on the evolution of primordial stars. *A&A* 489:685–698, DOI 10.1051/0004-6361/200809633, 0807.0573
- El Eid MF, The L, Meyer BS (2009) Massive Stars: Input Physics and Stellar Models. *Space Science Reviews* 147:1–29, DOI 10.1007/s11214-009-9517-6
- Eldridge JJ (2009) A new-age determination for $\gamma^2\text{Velorum}$ from binary stellar evolution models. *MNRAS* 400:L20–L23, DOI 10.1111/j.1745-3933.2009.00753.x, 0909.0504
- Eldridge JJ, Izzard RG, Tout CA (2008) The effect of massive binaries on stellar populations and supernova progenitors. *MNRAS* 384:1109–1118, DOI 10.1111/j.1365-2966.2007.12738.x, 0711.3079
- Fabbian D, Nissen PE, Asplund M, Pettini M, Akerman C (2009) The C/O ratio at low metallicity: constraints on early chemical evolution from observations of Galactic halo stars. *A&A* 500:1143–1155, DOI 10.1051/0004-6361/200810095, 0810.0281
- Farouqi K, Kratz K, Mashonkina LI, Pfeiffer B, Cowan JJ, Thielemann F, Truran JW (2009) Nucleosynthesis Modes in The High-Entropy Wind of Type II Supernovae: Comparison of Calculations With Halo-Star Observations. *ApJ* 694:L49–L53, DOI 10.1088/0004-637X/694/L49, 0901.2541
- Farouqi K, Kratz K, Pfeiffer B, Rauscher T, Thielemann F, Truran JW (2010) Charged-particle and Neutron-capture Processes in the High-entropy Wind of Core-collapse Supernovae. *ApJ* 712:1359–1377, DOI 10.1088/0004-637X/712/2/1359, 1002.2346
- Fischer T, Whitehouse SC, Mezzacappa A, Thielemann F, Liebendörfer M (2009a) Protoneutron star evolution and the neutrino driven wind in general relativistic neutrino radiation hydrodynamics simulations. *ArXiv e-prints* 0908.1871
- Fischer T, Whitehouse SC, Mezzacappa A, Thielemann F, Liebendörfer M (2009b) The neutrino signal from protoneutron star accretion and black hole formation. *A&A* 499:1–15, DOI 10.1051/0004-6361/200811055, 0809.5129
- Fisker JL, Schatz H, Thielemann F (2008) Explosive Hydrogen Burning during Type I X-Ray Bursts. *ApJS* 174:261–276, DOI 10.1086/521104
- Fisker JL, Hoffman RD, Pruet J (2009) On the Origin of the Lightest Molybdenum Isotopes. *ApJ* 690:L135–L139, DOI 10.1088/0004-637X/690/2/L135, 0711.1502
- Fogli G, Lisi E, Marrone A, Mirizzi A (2007) Collective neutrino flavor transitions in supernovae and the role of trajectory averaging. *Journal of Cosmology and Astro-Particle Physics* 12:10–+, DOI 10.1088/1475-7516/2007/12/010, 0707.1998
- Foglizzo T (2009) A Simple Toy Model of the Advective-Acoustic Instability. I. Perturbative Approach. *ApJ* 694:820–832, DOI 10.1088/0004-637X/694/2/820, 0809.2302
- Fransson C, Kozma C (1993) The freeze-out phase of SN 1987A - Implications for the light curve. *ApJ* 408:L25–L28, DOI 10.1086/186822
- Freiburghaus C, Rembges J, Rauscher T, Kolbe E, Thielemann F, Kratz K, Pfeiffer B, Cowan JJ (1999a) The Astrophysical r-Process: A Comparison of Calculations following Adia-

- batic Expansion with Classical Calculations Based on Neutron Densities and Temperatures. *ApJ*516:381–398, DOI 10.1086/307072
- Freiburghaus C, Rosswog S, Thielemann F (1999b) R-Process in Neutron Star Mergers. *ApJ*525:L121–L124, DOI 10.1086/312343
- Fröhlich C, Hauser P, Liebendörfer M, Martínez-Pinedo G, Thielemann F, Bravo E, Zinner NT, Hix WR, Langanke K, Mezzacappa A, Nomoto K (2006a) Composition of the Innermost Core-Collapse Supernova Ejecta. *ApJ*637:415–426, DOI 10.1086/498224, [arXiv:astro-ph/0410208](#)
- Fröhlich C, Martínez-Pinedo G, Liebendörfer M, Thielemann F, Bravo E, Hix WR, Langanke K, Zinner NT (2006b) Neutrino-Induced Nucleosynthesis of A greater 64 Nuclei: The vp Process. *Physical Review Letters* 96(14):142,502–+, DOI 10.1103/PhysRevLett.96.142502, [arXiv:astro-ph/0511376](#)
- Fryer CL, Herwig F, Hungerford A, Timmes FX (2006) Supernova Fallback: A Possible Site for the r-Process. *ApJ*646:L131–L134, DOI 10.1086/507071, [arXiv:astro-ph/0606450](#)
- Fu A, Arnett WD (1989) The Late Behavior of Supernova 1987A. II. Gamma-Ray Transparency of the Ejecta. *ApJ*340:414–+, DOI 10.1086/167403
- Fukuda I (1982) A statistical study of rotational velocities of the stars. *PASP*94:271–284, DOI 10.1086/130977
- Fuller GM, Fowler WA, Newman MJ (1980) Stellar weak-interaction rates for sd-shell nuclei. I - Nuclear matrix element systematics with application to Al-26 and selected nuclei of importance to the supernova problem. *ApJS*42:447–473, DOI 10.1086/190657
- Fuller GM, Fowler WA, Newman MJ (1982) Stellar weak interaction rates for intermediate-mass nuclei. II - A = 21 to A = 60. *ApJ*252:715–740, DOI 10.1086/159597
- Fuller GM, Fowler WA, Newman MJ (1985) Stellar weak interaction rates for intermediate-mass nuclei. IV - Interpolation procedures for rapidly varying lepton capture rates using effective log (ft)-values. *ApJ*293:1–16, DOI 10.1086/163208
- Georgy C, Meynet G, Walder R, Folini D, Maeder A (2009) The different progenitors of type Ib, Ic SNe, and of GRB. *A&A*502:611–622, DOI 10.1051/0004-6361/200811339, 0906.2284
- Giron S, Hammache F, de Séréville N, Beaumel D, Burgunder J, Caceres L, Clement E, Duchene G, Flavigny F, de France G, Franchoo S, Fernandez B, Galaviz-Redondo D, Gasques L, Gibelin J, Gillibert A, Grevy S, Guillot J, Heil M, Kiener J, Lapoux V, Maréchal F, Matta A, Matea Y, Moukaddam M, Nalpas L, Obertelli A, Perrot L, Raabe R, Scarpaci JA, Sorlin O, Stefan I, Stoedel C, Takechi M, Thomas JC, Togano Y (2010) Study of $^{60}\text{Fe}(n,\gamma)^{61}\text{Fe}$ reaction of astrophysical interest via $d(^{60}\text{Fe},p\gamma)$ indirect reaction. In: C Spitaleri, C Rolfs, & R G Pizzone (ed) American Institute of Physics Conference Series, American Institute of Physics Conference Series, vol 1213, pp 201–204, DOI 10.1063/1.3362577
- Goldreich P, Weber SV (1980) Homologously collapsing stellar cores. *ApJ*238:991–997, DOI 10.1086/158065
- Goriely S, Hilaire S, Girod M, Péru S (2009a) First Gogny-Hartree-Fock-Bogoliubov Nuclear Mass Model. *Physical Review Letters* 102(24):242,501–+, DOI 10.1103/PhysRevLett.102.242501
- Goriely S, Hilaire S, Koning AJ, Sin M, Capote R (2009b) Towards a prediction of fission cross sections on the basis of microscopic nuclear inputs. *Phys. Rev. C*79(2):024,612–+, DOI 10.1103/PhysRevC.79.024612
- Gyürky G, Kiss GG, Elekes Z, Fülöp Z, Somorjai E, Palumbo A, Görres J, Lee HY, Rapp W, Wiescher M, Özkan N, Güray RT, Efe G, Rauscher T (2006) α -induced cross sections of Cd106 for the astrophysical p process. *Phys. Rev. C*74(2):025,805–+, DOI 10.1103/PhysRevC.74.025805, [arXiv:nucl-ex/0605034](#)
- Hamuy M (2003) Observed and Physical Properties of Core-Collapse Supernovae. *ApJ*582:905–914, DOI 10.1086/344689, [arXiv:astro-ph/0209174](#)
- Haxton WC, Parker PD, Rolfs CE (2006) Solar hydrogen burning and neutrinos. *Nuclear Physics A* 777:226–253, DOI 10.1016/j.nuclphysa.2005.02.088, [arXiv:nucl-th/0501020](#)

- Heger A, Langer N (2000) Presupernova Evolution of Rotating Massive Stars. II. Evolution of the Surface Properties. *ApJ*544:1016–1035, DOI 10.1086/317239, arXiv:astro-ph/0005110
- Heger A, Woosley SE (2002) The Nucleosynthetic Signature of Population III. *ApJ*567:532–543, DOI 10.1086/338487, arXiv:astro-ph/0107037
- Heger A, Langanke K, Martínez-Pinedo G, Woosley SE (2001a) Presupernova Collapse Models with Improved Weak-Interaction Rates. *Physical Review Letters* 86:1678–1681, DOI 10.1103/PhysRevLett.86.1678, arXiv:astro-ph/0007412
- Heger A, Woosley SE, Martínez-Pinedo G, Langanke K (2001b) Presupernova Evolution with Improved Rates for Weak Interactions. *ApJ*560:307–325, DOI 10.1086/324092, arXiv:astro-ph/0011507
- Heger A, Fryer CL, Woosley SE, Langer N, Hartmann DH (2003) How Massive Single Stars End Their Life. *ApJ*591:288–300, DOI 10.1086/375341, arXiv:astro-ph/0212469
- Herant M, Benz W, Hix WR, Fryer CL, Colgate SA (1994) Inside the supernova: A powerful convective engine. *ApJ*435:339–361, DOI 10.1086/174817, arXiv:astro-ph/9404024
- Hiraga JS, Kobayashi Y, Tamagawa T, Hayato A, Bamba A, Terada Y, Petre R, Katagiri H, Tsunemi H (2009) Search for Sc-K Line Emission from RX J0852.0-4622 Supernova Remnant with Suzaku. *PASJ*61:275–, 0906.0216
- Hirschi R (2007) Very low-metallicity massive stars: Pre-SN evolution models and primary nitrogen production. *A&A*461:571–583, DOI 10.1051/0004-6361:20065356, arXiv:astro-ph/0608170
- Hirschi R, Meynet G, Maeder A (2005) Stellar evolution with rotation. XIII. Predicted GRB rates at various Z. *A&A*443:581–591, DOI 10.1051/0004-6361:20053329, arXiv:astro-ph/0507343
- Hirschi R, Frischknecht U, Thielemann F, Pignatari M, Chiappini C, Ekström S, Meynet G, Maeder A (2008) Stellar Evolution in the Early Universe. In: L K Hunt, S Madden, & R Schneider (ed) *IAU Symposium, IAU Symposium*, vol 255, pp 297–304, DOI 10.1017/S1743921308024976
- Hix WR, Thielemann F (1996) Silicon Burning. I. Neutronization and the Physics of Quasi-Equilibrium. *ApJ*460:869–+, DOI 10.1086/177016, arXiv:astro-ph/9511088
- Hix WR, Thielemann F (1999a) Computational methods for nucleosynthesis and nuclear energy generation. *Journal of Computational and Applied Mathematics* 109:321–351, arXiv:astro-ph/9906478
- Hix WR, Thielemann F (1999b) Silicon Burning. II. Quasi-Equilibrium and Explosive Burning. *ApJ*511:862–875, DOI 10.1086/306692, arXiv:astro-ph/9808203
- Hix WR, Messer OE, Mezzacappa A, Liebendörfer M, Sampaio J, Langanke K, Dean DJ, Martínez-Pinedo G (2003) Consequences of Nuclear Electron Capture in Core Collapse Supernovae. *Physical Review Letters* 91(20):201,102–+, DOI 10.1103/PhysRevLett.91.201102, arXiv:astro-ph/0310883
- Hix WR, Parete-Koon ST, Freiburghaus C, Thielemann F (2007) The QSE-Reduced Nuclear Reaction Network for Silicon Burning. *ApJ*667:476–488, DOI 10.1086/520672
- Hoffman RD, Woosley SE, Qian Y (1997) Nucleosynthesis in Neutrino-driven Winds. II. Implications for Heavy Element Synthesis. *ApJ*482:951–+, DOI 10.1086/304181, arXiv:astro-ph/9611097
- Hoffman RD, Woosley SE, Weaver TA, Rauscher T, Thielemann F (1999) The Reaction Rate Sensitivity of Nucleosynthesis in Type II Supernovae. *ApJ*521:735–752, DOI 10.1086/307568, arXiv:astro-ph/9809240
- Honda S, Aoki W, Ishimaru Y, Wanajo S, Ryan SG (2006) Neutron-Capture Elements in the Very Metal Poor Star HD 122563. *ApJ*643:1180–1189, DOI 10.1086/503195, arXiv:astro-ph/0602107
- Hughes JP, Hayashi I, Helfand D, Hwang U, Itoh M, Kirshner R, Koyama K, Markert T, Tsunemi H, Woo J (1995) ASCA observations of the Large Magellanic Cloud supernova remnant sample: Typing supernovae from their remnants. *ApJ*444:L81–L84, DOI 10.1086/187865
- Iliadis C (2007) *Nuclear Physics of Stars*. Wiley-VCH Verlag

- Iyudin AF, Diehl R, Bloemen H, Hermsen W, Lichti GG, Morris D, Ryan J, Schoenfelder V, Steinle H, Varendorff M, de Vries C, Winkler C (1994) COMPTEL observations of Ti-44 gamma-ray line emission from CAS A. *A&A*284:L1–L4
- Iyudin AF, Schönfelder V, Bennett K, Bloemen H, Diehl R, Hermsen W, Knödlseider J, Lichti GG, Oberlack U, Ryan J, Strong AW, Winkler C (1999) COMPTEL All-Sky Survey in ^{44}Ti Line Emission. *Astrophysical Letters Communications* 38:383–+
- Janka H, Buras R, Rampp M (2003) The mechanism of core-collapse supernovae and the ejection of heavy elements. *Nuclear Physics A* 718:269–276, DOI 10.1016/S0375-9474(03)00727-9, [arXiv:astro-ph/0212317](#)
- Janka H, Langanke K, Marek A, Martínez-Pinedo G, Müller B (2007) Theory of core-collapse supernovae. *Phys. Rep.*442:38–74, DOI 10.1016/j.physrep.2007.02.002, [arXiv:astro-ph/0612072](#)
- Käppeler F, Mengoni A (2006) Nuclear input for the s process: progress with experiments and theory. *Nuclear Physics A* 777:291–310, DOI 10.1016/j.nuclphysa.2005.01.028
- Katsuda S, Tsunemi H, Mori K (2009) Is Vela Jr. a young supernova remnant? *Advances in Space Research* 43:895–899, DOI 10.1016/j.asr.2009.01.004
- Kippenhahn R, Weigert A (1994) *Stellar Structure and Evolution*
- Kiss GG, Gyürky G, Elekes Z, Fülöp Z, Somorjai E, Rauscher T, Wiescher M (2007) $\text{Ge70}(p,\gamma)\text{As71}$ and $\text{Ge76}(p,n)\text{As76}$ cross sections for the astrophysical p process: Sensitivity of the optical proton potential at low energies. *Phys. Rev. C*76(5):055807–+, DOI 10.1103/PhysRevC.76.055807, 0711.1079
- Kiss GG, Rauscher T, Gyürky G, Simon A, Fülöp Z, Somorjai E (2008) Coulomb Suppression of the Stellar Enhancement Factor. *Physical Review Letters* 101(19):191101–+, DOI 10.1103/PhysRevLett.101.191101, 0809.2676
- Knie K, Korschinek G, Faestermann T, Dorfi EA, Rugel G, Wallner A (2004) ^{60}Fe Anomaly in a Deep-Sea Manganese Crust and Implications for a Nearby Supernova Source. *Physical Review Letters* 93(17):171103–+, DOI 10.1103/PhysRevLett.93.171103
- Kobayashi C, Umeda H, Nomoto K, Tominaga N, Ohkubo T (2006) Galactic Chemical Evolution: Carbon through Zinc. *ApJ*653:1145–1171, DOI 10.1086/508914, [arXiv:astro-ph/0608688](#)
- Kotake K, Sato K, Takahashi K (2006) Explosion mechanism, neutrino burst and gravitational wave in core-collapse supernovae. *Reports on Progress in Physics* 69:971–1143, DOI 10.1088/0034-4885/69/4/R03, [arXiv:astro-ph/0509456](#)
- Kratz K, Bitouzet J, Thielemann F, Moeller P, Pfeiffer B (1993) Isotopic r-process abundances and nuclear structure far from stability - Implications for the r-process mechanism. *ApJ*403:216–238, DOI 10.1086/172196
- Kratz K, Farouqi K, Pfeiffer B, Truran JW, Sneden C, Cowan JJ (2007) Explorations of the r-Processes: Comparisons between Calculations and Observations of Low-Metallicity Stars. *ApJ*662:39–52, DOI 10.1086/517495, [arXiv:astro-ph/0703091](#)
- Kuroda T, Wanajo S, Nomoto K (2008) The r-Process in Supersonic Neutrino-driven Winds: The Role of the Wind Termination Shock. *ApJ*672:1068–1078, DOI 10.1086/523795
- Langanke K, Martínez-Pinedo G (2000) Shell-model calculations of stellar weak interaction rates: II. Weak rates for nuclei in the mass range $A=45-65$ in supernovae environments. *Nuclear Physics A* 673:481–508, DOI 10.1016/S0375-9474(00)00131-7, [arXiv:nucl-th/0001018](#)
- Langanke K, Martínez-Pinedo G, Sampaio JM, Dean DJ, Hix WR, Messer OE, Mezzacappa A, Liebendörfer M, Janka H, Rampp M (2003) Electron Capture Rates on Nuclei and Implications for Stellar Core Collapse. *Physical Review Letters* 90(24):241102–+, DOI 10.1103/PhysRevLett.90.241102, [arXiv:astro-ph/0302459](#)
- Langanke K, Martínez-Pinedo G, Müller B, Janka H, Marek A, Hix WR, Juodagalvis A, Sampaio JM (2008) Effects of Inelastic Neutrino-Nucleus Scattering on Supernova Dynamics and Radiated Neutrino Spectra. *Physical Review Letters* 100(1):011101–+, DOI 10.1103/PhysRevLett.100.011101, 0706.1687

- Langer N, Braun H, Fliegner J (1995) The production of circumstellar ^{26}Al by massive stars. *Ap&SS*224:275–278, DOI 10.1007/BF00667858
- Langer N, Braun H, Wellstein S (1998) Massive Close Binaries as Source of Galactic ^{26}Al . In: W Hillebrandt & E Muller (ed) *Nuclear Astrophysics*, pp 18–+
- Lattimer JM, Douglas Swesty F (1991) A generalized equation of state for hot, dense matter. *Nuclear Physics A* 535:331–376, DOI 10.1016/0375-9474(91)90452-C
- Leibundgut B, Suntzeff NB (2003) Optical Light Curves of Supernovae. In: K Weiler (ed) *Supernovae and Gamma-Ray Bursters, Lecture Notes in Physics*, Berlin Springer Verlag, vol 598, pp 77–90
- Leising MD, Share GH (1990) The gamma-ray light curves of SN 1987A. *ApJ*357:638–648, DOI 10.1086/168952
- Liebendörfer M, Mezzacappa A, Messer OEB, Martinez-Pinedo G, Hix WR, Thielemann F (2003) The neutrino signal in stellar core collapse and postbounce evolution. *Nuclear Physics A* 719:144–+, DOI 10.1016/S0375-9474(03)00984-9, arXiv:astro-ph/0211329
- Liebendörfer M, Messer OEB, Mezzacappa A, Bruenn SW, Cardall CY, Thielemann F (2004) A Finite Difference Representation of Neutrino Radiation Hydrodynamics in Spherically Symmetric General Relativistic Spacetime. *ApJS*150:263–316, DOI 10.1086/380191, arXiv:astro-ph/0207036
- Liebendörfer M, Rampp M, Janka H, Mezzacappa A (2005) Supernova Simulations with Boltzmann Neutrino Transport: A Comparison of Methods. *ApJ*620:840–860, DOI 10.1086/427203, arXiv:astro-ph/0310662
- Liebendörfer M, Fischer T, Fröhlich C, Thielemann F, Whitehouse S (2008) Nuclear physics with spherically symmetric supernova models. *Journal of Physics G Nuclear Physics* 35(1):014,056–+, DOI 10.1088/0954-3899/35/1/014056, 0708.4296
- Liebendörfer M, Whitehouse SC, Fischer T (2009) The Isotropic Diffusion Source Approximation for Supernova Neutrino Transport. *ApJ*698:1174–1190, DOI 10.1088/0004-637X/698/2/1174, 0711.2929
- Limongi M, Chieffi A (2003) Evolution, Explosion, and Nucleosynthesis of Core-Collapse Supernovae. *ApJ*592:404–433, DOI 10.1086/375703, arXiv:astro-ph/0304185
- Limongi M, Chieffi A (2006) The Nucleosynthesis of ^{26}Al and ^{60}Fe in Solar Metallicity Stars Extending in Mass from 11 to 120 M_{solar} : The Hydrostatic and Explosive Contributions. *ApJ*647:483–500, DOI 10.1086/505164, arXiv:astro-ph/0604297
- Limongi M, Straniero O, Chieffi A (2000) Massive Stars in the Range 13–25 M_{solar} : Evolution and Nucleosynthesis. II. The Solar Metallicity Models. *ApJS*129:625–664, DOI 10.1086/313424, arXiv:astro-ph/0003401
- Lundqvist P, Kozma C, Sollerman J, Fransson C (2001) ISO/SWS observations of SN 1987A. II. A refined upper limit on the mass of ^{44}Ti in the ejecta of SN 1987A. *A&A*374:629–637, DOI 10.1051/0004-6361:20010725, arXiv:astro-ph/0105402
- MacFadyen AI, Woosley SE (1999) Collapsars: Gamma-Ray Bursts and Explosions in “Failed Supernovae”. *ApJ*524:262–289, DOI 10.1086/307790, arXiv:astro-ph/9810274
- Maeder A (2009) *Physics, Formation and Evolution of Rotating Stars*. DOI 10.1007/978-3-540-76949-1
- Maeder A, Meynet G (2010) Massive Stars through the ages: evolution and wind composition. *Reviews of Modern Physics* ((in press)):???–???, DOI 10.1103/RevModPhys.62.801
- Maeder A, Grebel EK, Mermilliod J (1999) Differences in the fractions of Be stars in galaxies. *A&A*346:459–464, arXiv:astro-ph/9904008
- Marek A, Janka H (2009) Delayed Neutrino-Driven Supernova Explosions Aided by the Standing Accretion-Shock Instability. *ApJ*694:664–696, DOI 10.1088/0004-637X/694/1/664, 0708.3372
- Marek A, Janka H, Buras R, Liebendörfer M, Rampp M (2005) On ion-ion correlation effects during stellar core collapse. *A&A*443:201–210, DOI 10.1051/0004-6361:20053236, arXiv:astro-ph/0504291
- Martayan C, Frémat Y, Hubert A, Floquet M, Zorec J, Neiner C (2007) Effects of metallicity, star-formation conditions, and evolution in B and Be stars. II. Small Magellanic Cloud, field

- of NGC330. *A&A*462:683–694, DOI 10.1051/0004-6361:20065076, arXiv:astro-ph/0609677
- Martin P, Knödlseeder J, Vink J, Decourchelle A, Renaud M (2009) Constraints on the kinematics of the ^{44}Ti ejecta of Cassiopeia A from INTEGRAL/SPI. *A&A*502:131–137, DOI 10.1051/0004-6361/200809735
- Martínez-Pinedo G, Liebendörfer M, Frekers D (2006) Nuclear input for core-collapse models. *Nuclear Physics A* 777:395–423, DOI 10.1016/j.nuclphysa.2006.02.014, arXiv:astro-ph/0412091
- Martínez-Pinedo G, Mocelj D, Zinner NT, Kelić A, Langanke K, Panov I, Pfeiffer B, Rauscher T, Schmidt K, Thielemann F (2007) The role of fission in the r-process. *Progress in Particle and Nuclear Physics* 59:199–205, DOI 10.1016/j.pnpnp.2007.01.018
- Massi F, de Luca M, Elia D, Giannini T, Lorenzetti D, Nisini B (2007) Star formation in the Vela molecular ridge. Large scale mapping of cloud D in the mm continuum. *A&A*466:1013–1023, DOI 10.1051/0004-6361:20066438, arXiv:astro-ph/0702687
- Matheson T, Filippenko AV, Li W, Leonard DC, Shields JC (2001) Optical Spectroscopy of Type IB/C Supernovae. *AJ*121:1648–1675, DOI 10.1086/319390, arXiv:astro-ph/0101119
- Matz SM, Share GH, Leising MD, Chupp EL, Vestrand WT (1988) Gamma-ray line emission from SN1987A. *Nature*331:416–418, DOI 10.1038/331416a0
- Meakin CA, Arnett D (2007) Turbulent Convection in Stellar Interiors. I. Hydrodynamic Simulation. *ApJ*667:448–475, DOI 10.1086/520318, arXiv:astro-ph/0611315
- Metzger BD, Martínez-Pinedo G, Darbha S, Quataert E, Arcones A, Kasen D, Thomas R, Nugent P, Panov IV, Zinner NT (2010) Electromagnetic counterparts of compact object mergers powered by the radioactive decay of r-process nuclei. *MNRAS*406:2650–2662, DOI 10.1111/j.1365-2966.2010.16864.x, 1001.5029
- Meyer BS, Brown JS (1997) Survey of r-Process Models. *ApJS*112:199–+, DOI 10.1086/313032
- Meynet G, Maeder A (2000) Stellar evolution with rotation. V. Changes in all the outputs of massive star models. *A&A*361:101–120, arXiv:astro-ph/0006404
- Meynet G, Maeder A (2003) Stellar evolution with rotation. X. Wolf-Rayet star populations at solar metallicity. *A&A*404:975–990, DOI 10.1051/0004-6361:20030512, arXiv:astro-ph/0304069
- Meynet G, Maeder A (2005) Stellar evolution with rotation. XI. Wolf-Rayet star populations at different metallicities. *A&A*429:581–598, DOI 10.1051/0004-6361:20047106, arXiv:astro-ph/0408319
- Meynet G, Arnould M, Prantzos N, Paulus G (1997) Contribution of Wolf-Rayet stars to the synthesis of ^{26}Al . I. The γ -ray connection. *A&A*320:460–468
- Meynet G, Ekström S, Maeder A (2006) The early star generations: the dominant effect of rotation on the CNO yields. *A&A*447:623–639, DOI 10.1051/0004-6361:20053070, arXiv:astro-ph/0510560
- Meynet G, Ekström S, Georgy C, Maeder A, Hirschi R (2008) Massive star evolution: from the early to the present day Universe. In: L Deng & K L Chan (ed) *IAU Symposium, IAU Symposium*, vol 252, pp 317–327, DOI 10.1017/S1743921308023119
- Mikheyev SP, Smirnov AY (1985) Resonance enhancement of oscillations in matter and solar neutrino spectroscopy. *Yadernaya Fizika, Sov J Nucl Phys* 42:1441–1448, 913
- Mochizuki Y, Takahashi K, Janka HT, Hillebrandt W, Diehl R (1999) ^{44}Ti : its effective decay rate in young supernova remnants, and its abundance in Cassiopeia A. *A&A*346:831–842, arXiv:astro-ph/9904378
- Möller P, Nix JR, Myers WD, Swiatecki WJ (1995) Nuclear Ground-State Masses and Deformations. *Atomic Data and Nuclear Data Tables* 59:185–+, DOI 10.1006/adnd.1995.1002, arXiv:nucl-th/9308022
- Mowlavi N, Meynet G (2006) ^{26}Al production from γ^2 – *Velorum*: Point source or diffuse emission at 1.8 MeV? *New Astronomy Review* 50:484–486, DOI 10.1016/j.newar.2006.06.060
- Mowlavi N, Knödlseeder J, Meynet G, Dubath P, Diehl R, Lichti G, Schanne S, Winkler C (2005) ^{26}Al production in γ^2 Velorum. *Nuclear Physics A* 758:320–323, DOI 10.1016/j.nuclphysa.2005.05.177

- Nagataki S (2000) Effects of Jetlike Explosion in SN 1987A. *ApJS*127:141–157, DOI 10.1086/313317, [arXiv:astro-ph/9907109](#)
- Nagataki S, Hashimoto M, Sato K, Yamada S, Mochizuki YS (1998) The High Ratio of $^{44}\text{Ti}/^{56}\text{Ni}$ in Cassiopeia A and the Axisymmetric Collapse-driven Supernova Explosion. *ApJ*492:L45+, DOI 10.1086/311089, [arXiv:astro-ph/9807015](#)
- Nakamura T, Umeda H, Nomoto K, Thielemann F, Burrows A (1999) Nucleosynthesis in Type II Supernovae and the Abundances in Metal-poor Stars. *ApJ*517:193–208, DOI 10.1086/307167, [arXiv:astro-ph/9809307](#)
- Nakamura T, Umeda H, Iwamoto K, Nomoto K, Hashimoto M, Hix WR, Thielemann F (2001) Explosive Nucleosynthesis in Hypernovae. *ApJ*555:880–899, DOI 10.1086/321495, [arXiv:astro-ph/0011184](#)
- Nittler LR, Amari S, Zinner E, Woosley SE, Lewis RS (1996) Extinct ^{44}Ti in Presolar Graphite and SiC: Proof of a Supernova Origin. *ApJ*462:L31+, DOI 10.1086/310021
- Nomoto K (1987) Evolution of 8–10 solar mass stars toward electron capture supernovae. II - Collapse of an O + NE + MG core. *ApJ*322:206–214, DOI 10.1086/165716
- Nomoto K, Hashimoto M (1988) Presupernova evolution of massive stars. *Phys. Rep.*163:13–36, DOI 10.1016/0370-1573(88)90032-4
- Nomoto K, Thielemann F, Miyaji S (1985) The triple alpha reaction at low temperatures in accreting white dwarfs and neutron stars. *A&A*149:239–245
- Nomoto K, Mazzali PA, Nakamura T, Iwamoto K, Danziger IJ, Patat F (2001) The properties of hypernovae: SNe Ic 1998bw, 1997ef, and SN IIn 1997cy. In: M Livio, N Panagia, & K Sahu (ed) *Supernovae and Gamma-Ray Bursts: the Greatest Explosions since the Big Bang*, pp 144–170
- Nomoto K, Tominaga N, Umeda H, Kobayashi C, Maeda K (2006) Nucleosynthesis yields of core-collapse supernovae and hypernovae, and galactic chemical evolution. *Nuclear Physics A* 777:424–458, DOI 10.1016/j.nuclphysa.2006.05.008, [arXiv:astro-ph/0605725](#)
- Nymark TK, Fransson C, Kozma C (2006) X-ray emission from radiative shocks in type II supernovae. *A&A*449:171–192, DOI 10.1051/0004-6361:20054169, [arXiv:astro-ph/0510792](#)
- Oberlack U, Wessolowski U, Diehl R, Bennett K, Bloemen H, Hermsen W, Knödlseider J, Morris D, Schönfelder V, von Ballmoos P (2000) COMPTEL limits on ^{26}Al 1.809 MeV line emission from gamma² Velorum. *A&A*353:715–721, [arXiv:astro-ph/9910555](#)
- Ohkubo T, Umeda H, Maeda K, Nomoto K, Suzuki T, Tsuruta S, J Rees M (2008) Evolution of Core-Collapse Very Massive Population III Stars. In: B W O'Shea & A Heger (ed) *First Stars III*, American Institute of Physics Conference Series, vol 990, pp 244–246, DOI 10.1063/1.2905553
- Otsuki K, Tagoshi H, Kajino T, Wanajo S (2000) General Relativistic Effects on Neutrino-driven Winds from Young, Hot Neutron Stars and r-Process Nucleosynthesis. *ApJ*533:424–439, DOI 10.1086/308632, [arXiv:astro-ph/9911164](#)
- Palacios A, Meynet G, Vuissoz C, Knödlseider J, Schaerer D, Cerviño M, Mowlavi N (2005) New estimates of the contribution of Wolf-Rayet stellar winds to the Galactic ^{26}Al . *A&A*429:613–624, DOI 10.1051/0004-6361:20041757, [arXiv:astro-ph/0409580](#)
- Panov IV, Janka H (2009) On the dynamics of proto-neutron star winds and r-process nucleosynthesis. *A&A*494:829–844, DOI 10.1051/0004-6361:200810292, 0805.1848
- Panov IV, Thielemann F (2003) Final r-process yields and the influence of fission: The competition between neutron-induced and β -delayed fission. *Nuclear Physics A* 718:647–649, DOI 10.1016/S0375-9474(03)00875-3
- Panov IV, Kolbe E, Pfeiffer B, Rauscher T, Kratz K, Thielemann F (2005) Calculations of fission rates for r-process nucleosynthesis. *Nuclear Physics A* 747:633–654, DOI 10.1016/j.nuclphysa.2004.09.115, [arXiv:astro-ph/0412654](#)
- Panov IV, Korneev IY, Rauscher T, Martínez-Pinedo G, Kelić-Heil A, Zinner NT, Thielemann F (2009) Neutron-induced astrophysical reaction rates for translead nuclei. *ArXiv e-prints* 0911.2181

- Pearson JM, Nayak RC, Goriely S (1996) Nuclear mass formula with Bogolyubov-enhanced shell-quenching: application to r-process. *Physics Letters B* 387:455–459, DOI 10.1016/0370-2693(96)01071-4
- Pettini M, Zych BJ, Steidel CC, Chaffee FH (2008) C, N, O abundances in the most metal-poor damped Lyman alpha systems. *MNRAS* 385:2011–2024, DOI 10.1111/j.1365-2966.2008.12951.x, 0712.1829
- Pfeiffer B, Kratz K, Thielemann F, Walters WB (2001) Nuclear structure studies for the astrophysical r-process. *Nuclear Physics A* 693:282–324, DOI 10.1016/S0375-9474(01)01141-1
- Piran T (2004) The physics of gamma-ray bursts. *Reviews of Modern Physics* 76:1143–1210, DOI 10.1103/RevModPhys.76.1143, arXiv:astro-ph/0405503
- Podsiadlowski P, Joss PC, Hsu JYL (1992) Presupernova evolution in massive interacting binaries. *ApJ* 391:246–264, DOI 10.1086/171341
- Prantzos N, Boissier S (2003) On the relative frequencies of core-collapse supernovae sub-types: The role of progenitor metallicity. *A&A* 406:259–264, DOI 10.1051/0004-6361:20030717, arXiv:astro-ph/0305376
- Prieto JL, Stanek KZ, Beacom JF (2008) Characterizing Supernova Progenitors via the Metallicities of their Host Galaxies, from Poor Dwarfs to Rich Spirals. *ApJ* 673:999–1008, DOI 10.1086/524654, 0707.0690
- Pruet J, Woosley SE, Buras R, Janka H, Hoffman RD (2005) Nucleosynthesis in the Hot Convective Bubble in Core-Collapse Supernovae. *ApJ* 623:325–336, DOI 10.1086/428281, arXiv:astro-ph/0409446
- Pruet J, Hoffman RD, Woosley SE, Janka H, Buras R (2006) Nucleosynthesis in Early Supernova Winds. II. The Role of Neutrinos. *ApJ* 644:1028–1039, DOI 10.1086/503891, arXiv:astro-ph/0511194
- Qian Y, Wasserburg GJ (2007) Where, oh where has the r-process gone? *Phys. Rep.* 442:237–268, DOI 10.1016/j.physrep.2007.02.006, 0708.1767
- Qian Y, Woosley SE (1996) Nucleosynthesis in Neutrino-driven Winds. I. The Physical Conditions. *ApJ* 471:331–+, DOI 10.1086/177973, arXiv:astro-ph/9611094
- Rapp W, Görres J, Wiescher M, Schatz H, Käppeler F (2006) Sensitivity of p-Process Nucleosynthesis to Nuclear Reaction Rates in a 25 M_{solar} Supernova Model. *ApJ* 653:474–489, DOI 10.1086/508402, arXiv:astro-ph/0608341
- Rauscher T (2006) Branchings in the γ process path revisited. *Phys. Rev. C* 73(1):015,804–+, DOI 10.1103/PhysRevC.73.015804, arXiv:astro-ph/0510710
- Rauscher T, Thielemann F (2000) Astrophysical Reaction Rates From Statistical Model Calculations. *Atomic Data and Nuclear Data Tables* 75:1–351, DOI 10.1006/adnd.2000.0834, arXiv:astro-ph/0004059
- Rauscher T, Thielemann F (2004) Predicted cross-sections for photon-induced particle emission. *Atomic Data and Nuclear Data Tables* 88:1–81, DOI 10.1016/j.adt.2004.07.001, arXiv:nucl-th/0403084
- Rauscher T, Applegate JH, Cowan JJ, Thielemann F, Wiescher M (1994) Production of heavy elements in inhomogeneous cosmologies. *ApJ* 429:499–530, DOI 10.1086/174339
- Rauscher T, Heger A, Hoffman RD, Woosley SE (2002) Nucleosynthesis in Massive Stars with Improved Nuclear and Stellar Physics. *ApJ* 576:323–348, DOI 10.1086/341728, arXiv:astro-ph/0112478
- Rayet M, Arnould M, Prantzos N (1990) The p-process revisited. *A&A* 227:271–281
- Rayet M, Arnould M, Hashimoto M, Prantzos N, Nomoto K (1995) The p-process in Type II supernovae. *A&A* 298:517–+
- Renaud M, Vink J, Decourchelle A, Lebrun F, Terrier R, Ballet J (2006) An INTEGRAL/IBIS view of young Galactic SNRs through the ^{44}Ti gamma-ray lines. *New Astronomy Review* 50:540–543, DOI 10.1016/j.newar.2006.06.061, arXiv:astro-ph/0602304
- Roberts LF, Woosley SE, Hoffman RD (2010) Integrated Nucleosynthesis in Neutrino Driven Winds. *ArXiv e-prints* 1004.4916

- Rugel G, Faestermann T, Knie K, Korschinek G, Poutivtsev M, Schumann D, Kivel N, Günther-Leopold I, Weinreich R, Wohlmuther M (2009) New Measurement of the Fe60 Half-Life. *Physical Review Letters* 103(7):072,502–+, DOI 10.1103/PhysRevLett.103.072502
- Sagert I, Fischer T, Hempel M, Pagliara G, Schaffner-Bielich J, Mezzacappa A, Thielemann F, Liebendörfer M (2009) Signals of the QCD Phase Transition in Core-Collapse Supernovae. *Physical Review Letters* 102(8):081,101–+, DOI 10.1103/PhysRevLett.102.081101, 0809.4225
- Sauer DN, Mazzali PA, Deng J, Valenti S, Nomoto K, Filippenko AV (2006) The properties of the ‘standard’ Type Ic supernova 1994I from spectral models. *MNRAS* 369:1939–1948, DOI 10.1111/j.1365-2966.2006.10438.x, arXiv:astro-ph/0604293
- Sawyer RF (2005) Effects of ion and electron correlations on neutrino scattering in the infall phase of a supernova. *Physics Letters B* 630:1–6, DOI 10.1016/j.physletb.2005.09.032, arXiv:astro-ph/0505520
- Schatz H, Aprahamian A, Goerres J, Wiescher M, Rauscher T, Rembges JF, Thielemann F, Pfeiffer B, Moeller P, Kratz K, Herndl H, Brown BA, Rebel H (1998) rp-Process Nucleosynthesis at Extreme Temperature and Density Conditions. *Phys. Rep.* 294:167–264, DOI 10.1016/S0370-1573(97)00048-3
- Seitenzahl IR, Taubenberger S, Sim SA (2009) Late-time supernova light curves: the effect of internal conversion and Auger electrons. *MNRAS* 400:531–535, DOI 10.1111/j.1365-2966.2009.15478.x, 0908.0247
- Shen H, Toki H, Oyamatsu K, Sumiyoshi K (1998a) Relativistic equation of state of nuclear matter for supernova and neutron star. *Nuclear Physics A* 637:435–450, DOI 10.1016/S0375-9474(98)00236-X, arXiv:nucl-th/9805035
- Shen H, Toki H, Oyamatsu K, Sumiyoshi K (1998b) Relativistic Equation of State of Nuclear Matter for Supernova Explosion. *Progress of Theoretical Physics* 100:1013–1031, DOI 10.1143/PTP.100.1013, arXiv:nucl-th/9806095
- Sim SA, Kromer M, Roepke FK, Sorokina EI, Blinnikov SI, Kasen D, Hillebrandt W (2009) Monte Carlo Radiative Transfer Simulations: Applications to Astrophysical Outflows and Explosions. *ArXiv e-prints* 0911.1549
- Snedden C, Cowan JJ, Lawler JE, Ivans II, Burles S, Beers TC, Primas F, Hill V, Truran JW, Fuller GM, Pfeiffer B, Kratz K (2003) The Extremely Metal-poor, Neutron Capture-rich Star CS 22892-052: A Comprehensive Abundance Analysis. *ApJ* 591:936–953, DOI 10.1086/375491, arXiv:astro-ph/0303542
- Sollerman J, Holland ST, Challis P, Fransson C, Garnavich P, Kirshner RP, Kozma C, Leibundgut B, Lundqvist P, Patat F, Filippenko AV, Panagia N, Wheeler JC (2002) Supernova 1998bw - the final phases. *A&A* 386:944–956, DOI 10.1051/0004-6361:20020326, arXiv:astro-ph/0204498
- Spite M, Cayrel R, Plez B, Hill V, Spite F, Depagne E, François P, Bonifacio P, Barbuy B, Beers T, Andersen J, Molaro P, Nordström B, Primas F (2005) First stars VI - Abundances of C, N, O, Li, and mixing in extremely metal-poor giants. Galactic evolution of the light elements. *A&A* 430:655–668, DOI 10.1051/0004-6361:20041274, arXiv:astro-ph/0409536
- Sumiyoshi K, Yamada S, Suzuki H (2007) Dynamics and Neutrino Signal of Black Hole Formation in Nonrotating Failed Supernovae. I. Equation of State Dependence. *ApJ* 667:382–394, DOI 10.1086/520876, 0706.3762
- Suntzeff NB, Bouchet P (1990) The bolometric light curve of SN 1987A. I - Results from ESO and CTIO U to Q0 photometry. *AJ* 99:650–663, DOI 10.1086/115358
- Sunyaev RA, Kaniovsky AS, Efremov VV, Grebenev SA, Kuznetsov AV, Englhauser J, Doebereiner S, Pietsch W, Reppin C, Truemper J, Kendziorra E, Maisack M, Mony B, Staubert R (1990) Hard X-rays from supernova 1987A - Results of observations performed with the Roentgen observatory onboard the KVANT module during 1987-1989. *Pis ma Astronomicheskii Zhurnal* 16:403–415
- Surman R, McLaughlin GC, Hix WR (2006) Nucleosynthesis in the Outflow from Gamma-Ray Burst Accretion Disks. *ApJ* 643:1057–1064, DOI 10.1086/501116, arXiv:astro-ph/0509365

- Takahashi K, Witt J, Janka H (1994) Nucleosynthesis in neutrino-driven winds from protoneutron stars II. The r-process. *A&A*286:857–869
- Terasawa M, Sumiyoshi K, Yamada S, Suzuki H, Kajino T (2002) r-Process Nucleosynthesis in Neutrino-driven Winds from a Typical Neutron Star with $M=1.4 M_{\text{solar}}$. *ApJ*578:L137–L140, DOI 10.1086/344698, [arXiv:astro-ph/0206322](#)
- The L, El Eid MF, Meyer BS (2007) s-Process Nucleosynthesis in Advanced Burning Phases of Massive Stars. *ApJ*655:1058–1078, DOI 10.1086/509753, [arXiv:astro-ph/0609788](#)
- The LS, Clayton DD, Diehl R, Hartmann DH, Iyudin AF, Leising MD, Meyer BS, Motizuki Y, Schönfelder V (2006) Are ^{44}Ti -producing supernovae exceptional? *A&A*450:1037–1050, DOI 10.1051/0004-6361:20054626, [arXiv:astro-ph/0601039](#)
- Thielemann F, Hashimoto M, Nomoto K (1990) Explosive nucleosynthesis in SN 1987A. II - Composition, radioactivities, and the neutron star mass. *ApJ*349:222–240, DOI 10.1086/168308
- Thielemann F, Nomoto K, Hashimoto M (1996) Core-Collapse Supernovae and Their Ejecta. *ApJ*460:408–+, DOI 10.1086/176980
- Thielemann F, Hauser P, Kolbe E, Martinez-Pinedo G, Panov I, Rauscher T, Kratz K, Pfeiffer B, Rosswog S, Liebendörfer M, Mezzacappa A (2002) Heavy Elements and Age Determinations. *Space Science Reviews* 100:277–296
- Thompson TA, Burrows A, Meyer BS (2001) The Physics of Proto-Neutron Star Winds: Implications for r-Process Nucleosynthesis. *ApJ*562:887–908, DOI 10.1086/323861, [arXiv:astro-ph/0105004](#)
- Thompson TA, Quataert E, Burrows A (2005) Viscosity and Rotation in Core-Collapse Supernovae. *ApJ*620:861–877, DOI 10.1086/427177, [arXiv:astro-ph/0403224](#)
- Timmes FX (1999) Integration of Nuclear Reaction Networks for Stellar Hydrodynamics. *ApJS*124:241–263, DOI 10.1086/313257
- Tominaga N, Umeda H, Nomoto K (2007) Supernova Nucleosynthesis in Population III 13-50 M_{solar} Stars and Abundance Patterns of Extremely Metal-poor Stars. *ApJ*660:516–540, DOI 10.1086/513063
- Travaglio C, Gallino R, Arnone E, Cowan J, Jordan F, Sneden C (2004) Galactic Evolution of Sr, Y, And Zr: A Multiplicity of Nucleosynthetic Processes. *ApJ*601:864–884, DOI 10.1086/380507, [arXiv:astro-ph/0310189](#)
- Tueller J, Barthelmy S, Gehrels N, Teegarden BJ, Leventhal M, MacCallum CJ (1990) Observations of gamma-ray line profiles from SN 1987A. *ApJ*351:L41–L44, DOI 10.1086/185675
- Tur C, Heger A, Austin SM (2009) Production of ^{26}Al , ^{44}Ti , and ^{60}Fe in Core-Collapse Supernovae: Sensitivity to the Rates of the Triple Alpha and $^{12}\text{C}(\alpha, n)^{16}\text{O}$ Reactions. *ArXiv e-prints* 0908.4283
- Uberseder E, Reifarh R, Schumann D, Dillmann I, Pardo CD, Görres J, Heil M, Käppeler F, Marganiec J, Neuhausen J, Pignatari M, Voss F, Walter S, Wiescher M (2009) Measurement of the $\text{Fe}60(n, \gamma)^{61}\text{Fe}$ Cross Section at Stellar Temperatures. *Physical Review Letters* 102(15):151101–+, DOI 10.1103/PhysRevLett.102.151101
- Umeda H, Nomoto K (2005) Variations in the Abundance Pattern of Extremely Metal-Poor Stars and Nucleosynthesis in Population III Supernovae. *ApJ*619:427–445, DOI 10.1086/426097, [arXiv:astro-ph/0308029](#)
- Umeda H, Nomoto K (2008) How Much ^{56}Ni Can Be Produced in Core-Collapse Supernovae? Evolution and Explosions of 30-100 M_{solar} Stars. *ApJ*673:1014–1022, DOI 10.1086/524767, 0707.2598
- Vanbeveren D, Van Bever J, Belkus H (2007) The Wolf-Rayet Population Predicted by Massive Single Star and Massive Binary Evolution. *ApJ*662:L107–L110, DOI 10.1086/519454, [arXiv:astro-ph/0703796](#)
- Vink J (2004) Revealing the Obscured Supernova Remnant Kesteven 32 with Chandra. *ApJ*604:693–699, DOI 10.1086/381930, [arXiv:astro-ph/0312328](#)
- Vink J (2005) Gamma-ray observations of explosive nucleosynthesis products. *Advances in Space Research* 35:976–986, DOI 10.1016/j.asr.2005.01.097, [arXiv:astro-ph/0501645](#)

- Vink J, Laming JM, Kaastra JS, Bleeker JAM, Bloemen H, Oberlack U (2001) Detection of the 67.9 and 78.4 keV Lines Associated with the Radioactive Decay of ^{44}Ti in Cassiopeia A. *ApJ*560:L79–L82, DOI 10.1086/324172, *arXiv:astro-ph/0107468*
- Walder R, Burrows A, Ott CD, Livne E, Lichtenstadt I, Jarrah M (2005) Anisotropies in the Neutrino Fluxes and Heating Profiles in Two-dimensional, Time-dependent, Multigroup Radiation Hydrodynamics Simulations of Rotating Core-Collapse Supernovae. *ApJ*626:317–332, DOI 10.1086/429816, *arXiv:astro-ph/0412187*
- Wallace RK, Woosley SE (1981) Explosive hydrogen burning. *ApJS*45:389–420, DOI 10.1086/190717
- Wanajo S (2006) The rp-Process in Neutrino-driven Winds. *ApJ*647:1323–1340, DOI 10.1086/505483, *arXiv:astro-ph/0602488*
- Wanajo S (2007) Cold r-Process in Neutrino-driven Winds. *ApJ*666:L77–L80, DOI 10.1086/521724, 0706.4360
- Wanajo S, Kajino T, Mathews GJ, Otsuki K (2001) The r-Process in Neutrino-driven Winds from Nascent, “Compact” Neutron Stars of Core-Collapse Supernovae. *ApJ*554:578–586, DOI 10.1086/321339, *arXiv:astro-ph/0102261*
- Wanajo S, Goriely S, Samyn M, Itoh N (2004) The r-Process in Supernovae: Impact of New Microscopic Mass Formulae. *ApJ*606:1057–1069, DOI 10.1086/383140, *arXiv:astro-ph/0401412*
- Wang W, Harris MJ, Diehl R, Halloin H, Cordier B, Strong AW, Kretschmer K, Knödseder J, Jean P, Lichti GG, Roques JP, Schanne S, von Kienlin A, Weidenspointner G, Wunderer C (2007) SPI observations of the diffuse ^{60}Fe emission in the Galaxy. *A&A*469:1005–1012, DOI 10.1051/0004-6361:20066982, 0704.3895
- Wasserburg GJ, Busso M, Gallino R (1996) Abundances of Actinides and Short-lived Nonactinides in the Interstellar Medium: Diverse Supernova Sources for the r-Processes. *ApJ*466:L109+, DOI 10.1086/310177
- Weaver TA, Woosley SE (1980) Evolution and explosion of massive stars. In: J Ehlers, J J Perry, & M Walker (ed) Ninth Texas Symposium on Relativistic Astrophysics, New York Academy Sciences Annals, vol 336, pp 335–357, DOI 10.1111/j.1749-6632.1980.tb15942.x
- Weaver TA, Woosley SE (1993) Nucleosynthesis in massive stars and the $^{12}\text{C}(\alpha, \gamma)^{16}\text{O}$ reaction rate. *Phys. Rep.*227:65–96, DOI 10.1016/0370-1573(93)90058-L
- Weber C, Elomaa V, Ferrer R, Fröhlich C, Ackermann D, Äystö J, Audi G, Batist L, Blaum K, Block M, Chaudhuri A, Dworschak M, Eliseev S, Eronen T, Hager U, Hakala J, Herfurth F, Heßberger FP, Hofmann S, Jokinen A, Kankainen A, Kluge H, Langanke K, Martín A, Martínez-Pinedo G, Mazzocco M, Moore ID, Neumayr JB, Novikov YN, Penttilä H, Pläß WR, Popov AV, Rahaman S, Rauscher T, Rauth C, Rissanen J, Rodríguez D, Saastamoinen A, Scheidenberger C, Schweikhard L, Seliverstov DM, Sonoda T, Thielemann F, Thierolf PG, Vorobjev GK (2008) Mass measurements in the vicinity of the rp-process and the vp-process paths with the Penning trap facilities JYFLTRAP and SHIPTRAP. *Phys. Rev. C*78(5):054,310–+, DOI 10.1103/PhysRevC.78.054310, 0808.4065
- Wiescher M, Görres J, Pignatari M (2010) Experimental Status of Reactions in H- and He-Burning. *Annual Review of Nuclear and Particle Science* 60:175–251, DOI 10.1146/annurev.nucl.60.1.175
- Wilson JR, Mayle RW (1993) Report on the progress of supernova research by the Livermore group. *Phys. Rep.*227:97–111, DOI 10.1016/0370-1573(93)90059-M
- Wolfenstein L (1978) Neutrino oscillations in matter. *Phys. Rev. D*17:2369–2374, DOI 10.1103/PhysRevD.17.2369
- Woosley SE, Bloom JS (2006) The Supernova Gamma-Ray Burst Connection. *ARA&A*44:507–556, DOI 10.1146/annurev.astro.43.072103.150558, *arXiv:astro-ph/0609142*
- Woosley SE, Heger A (2007) Nucleosynthesis and remnants in massive stars of solar metallicity. *Phys. Rep.*442:269–283, DOI 10.1016/j.physrep.2007.02.009, *arXiv:astro-ph/0702176*
- Woosley SE, Howard WM (1978) The p-process in supernovae. *ApJS*36:285–304, DOI 10.1086/190501

- Woosley SE, Weaver TA (1995) The Evolution and Explosion of Massive Stars. II. Explosive Hydrodynamics and Nucleosynthesis. *ApJS*101:181–+, DOI 10.1086/192237
- Woosley SE, Wilson JR, Mathews GJ, Hoffman RD, Meyer BS (1994) The r-process and neutrino-heated supernova ejecta. *ApJ*433:229–246, DOI 10.1086/174638
- Woosley SE, Heger A, Weaver TA (2002) The evolution and explosion of massive stars. *Reviews of Modern Physics* 74:1015–1071, DOI 10.1103/RevModPhys.74.1015
- Woosley SE, Kasen D, Blinnikov S, Sorokina E (2007) Type Ia Supernova Light Curves. *ApJ*662:487–503, DOI 10.1086/513732, [arXiv:astro-ph/0609562](#)
- Yalçın C, Güray RT, Özkan N, Kutlu S, Gyürky G, Farkas J, Kiss GG, Fülöp Z, Simon A, Somorjai E, Rauscher T (2009) Odd p isotope In113: Measurement of α -induced reactions. *Phys. Rev. C*79(6):065,801–+, DOI 10.1103/PhysRevC.79.065801, 0906.4041
- Yoshida T, Terasawa M, Kajino T, Sumiyoshi K (2004) Nucleosynthesis of Light Elements and Heavy r-Process Elements through the v-Process in Supernova Explosions. *ApJ*600:204–213, DOI 10.1086/379766, [arXiv:astro-ph/0305555](#)